

**SUPERPARAMAGNETIC LANTHANIDE ( $La^{3+}$ ,  $Gd^{3+}$ ,  
 $Nd^{3+}$ ) DOPED *Mn-Zn* FERRITE NANOPARTICLES:  
EFFECT OF DOPANT CONTENT**

*Thesis submitted in fulfillment of the requirements for the Degree of*

**DOCTOR OF PHILOSOPHY**

By

**PRASHANT THAKUR**



DEPARTMENT OF PHYSICS AND MATERIALS SCIENCE  
JAYPEE UNIVERSITY OF INFORMATION TECHNOLOGY  
WAKNAGHAT, DISTRICT SOLAN, H.P., INDIA

NOVEMBER 2018

Copyright

@

JAYPEE UNIVERSITY OF INFORMATION TECHNOLOGY

WAKNAGHAT

NOVEMBER 2018

ALL RIGHTS RESERVED

# CONTENTS

	<i>Page No.</i>
<b>Cover page</b>	<i>i</i>
<b>Copyright</b>	<i>ii</i>
<b>Table of contents</b>	<i>iii-vi</i>
<b>Declaration by the Scholar</b>	<i>vii</i>
<b>Supervisor's certificate</b>	<i>ix</i>
<b>Acknowledgement</b>	<i>xi-xiv</i>
<b>Abstract</b>	<i>xv</i>
<b>List of abbreviations</b>	<i>xvii</i>
<b>List of figures</b>	<i>xix-xxii</i>
<b>List of tables</b>	<i>xxiii-xiv</i>
<b>List of publications</b>	<i>xv</i>
<b>CHAPTER-1</b>	
<b>Introduction</b>	<b>1-28</b>
1.1 Magnetic materials	
1.2 Ferrites: history and development	
1.3 Types of ferrites	
1.3.1 Soft ferrites	
1.3.2 Hard ferrites	
1.4 Classification of ferrites based on crystal structure	
1.5 Structure of spinel ferrite	
1.6 Classification of spinel ferrites	
1.7 Literature survey of spinel ferrites	
1.7.1 Lithium ferrites	
1.7.2 Magnesium ferrites	
1.7.3. Magnesium – Manganese ferrites	
1.7.4 Nickel-Zinc ferrites	
1.8 Mn-Zn spinel ferrites and their applications	
1.9 Motivation of thesis work	
1.10 Outline of thesis	
<b>CHAPTER-2</b>	
<b>Experimental details</b>	<b>29-40</b>
2.1. Synthesis Techniques	

	2.1.1. Conventional Mixed Oxide Synthesis Technique	
	2.1.2. Sol Gel Synthesis Technique	
	2.1.3. Sol Gel Auto Combustion Synthesis Technique	
	2.1.4. Hydrothermal Synthesis Technique	
	2.1.5 Co-precipitation Synthesis Technique	
	2.2. Characterization Techniques	
	2.2.1. X-Ray Diffraction	
	2.2.2. Fourier Transform Infrared Spectroscopy	
	2.2.3. Field Emission - Scanning Electron Microscopy and Electron Dispersion X-Ray Spectroscopy	
	2.2.4. Vibrating sample magnetometer	
<b>CHAPTER-3</b>	<b>Optimization of sintering temperature for <i>Mn<sub>0.5</sub>Zn<sub>0.5</sub>Fe<sub>2</sub>O<sub>4</sub></i> nano ferrites</b>	<b>41-54</b>
	3.1 Introduction	
	3.2 Synthesis and characterization of <i>Mn<sub>0.5</sub>Zn<sub>0.5</sub>Fe<sub>2</sub>O<sub>4</sub></i> nano ferrites	
	3.3. Structural and morphological analysis	
	3.4. Conclusion	
<b>CHAPTER-4</b>	<b>Structural and morphological study of La<sup>3+</sup>, Gd<sup>3+</sup> &amp; Nd<sup>3+</sup> doped Mn-Zn nano ferrites</b>	<b>55-80</b>
	4.1. Introduction	
	4.2. Experimental details	
	4.3. Results & discussions	
	4.3.1 X-ray Diffraction	
	4.3.2 FE-SEM and EDS	
	4.3.3 FTIR Spectra	
	4.4. Conclusion	
<b>CHAPTER-5</b>	<b>Cation distribution and magnetic study of La<sup>3+</sup>, Gd<sup>3+</sup> &amp; Nd<sup>3+</sup> doped Mn-Zn nano ferrites</b>	<b>81-110</b>
	5.1. Introduction	

	5.2. Experimental details	
	5.3. Results & Discussion	
	5.3.1 Cation distribution for $\text{La}^{3+}$ , $\text{Gd}^{3+}$ & $\text{Nd}^{3+}$ doped Mn-Zn spinel ferrites	
	5.3.2 Magnetic study of $\text{La}^{3+}$ , $\text{Gd}^{3+}$ & $\text{Nd}^{3+}$ doped Mn-Zn spinel ferrites	
	5.4. Conclusion	
<b>CHAPTER-6</b>	<b>Summary and future scope</b>	<b>111-116</b>
<b>BIBLIOGRAPHY</b>		<b>117-139</b>





## JAYPEE UNIVERSITY OF INFORMATION TECHNOLOGY

(Established by H.P. State Legislative vide Act No. 14 of 2002)  
Dumehar Bani, Kandaghat, Distt. Solan – 173234 (H.P.) INDIA

Website: [www.juit.ac.in](http://www.juit.ac.in)

Phone No. (91) 07192-257999 (30 Lines)

Fax: (91) 01792 245362

### DECLARATION

I hereby declare that the work reported in the Ph.D. thesis entitled **“SUPERPARAMAGNETIC LANTHANIDE ( $La^{3+}$ ,  $Gd^{3+}$ ,  $Nd^{3+}$ ) DOPED MN-ZN FERRITE NANOPARTICLES: EFFECT OF DOPANT CONTENT”** submitted to **Jaypee University of Information Technology, Wagnaghat, India** is original and has been done by me under the supervision of **Dr. Pankaj Sharma**. The work has not been submitted to any other organization for any degree or diploma. I am fully responsible for the contents of my Ph.D. thesis.

**Dated:**

**Prashant Thakur**

Enrollment Number-146952

Department of Physics and Materials Science

Jaypee University of Information Technology

Wagnaghat, Solan, H.P. India-173234





## JAYPEE UNIVERSITY OF INFORMATION TECHNOLOGY

(Established by H.P. State Legislative vide Act No. 14 of 2002)  
Dumehar Bani, Kandaghat, Distt. Solan – 173234 (H.P.) INDIA

Website: [www.juit.ac.in](http://www.juit.ac.in)

Phone No. (91) 07192-257999 (30 Lines)

Fax: (91) 01792 245362

### CERTIFICATE

This is to certify that the work reported in the Ph.D. thesis entitled **“SUPERPARAMAGNETIC LANTHANIDE ( $La^{3+}$ ,  $Gd^{3+}$ ,  $Nd^{3+}$ ) DOPED MN-ZN FERRITE NANOPARTICLES: EFFECT OF DOPANT CONTENT”**, submitted by **Prashant Thakur** at **Jaypee University of Information Technology, Wagnaghat, India** is a bonafide record of his original work carried out under my supervision. This work has not been submitted for the award of any other degree or diploma.

**Dated:**

**Dr. Pankaj Sharma**

**Supervisor**

Associate Professor

Department of Physics and Materials Science

Jaypee University of Information Technology

Wagnaghat, Solan, H.P. (173234) India





**DEDICATED TO  
MY BELOVED  
PARENTS &  
FAMILY**



## ACKNOWLEDGEMENTS

*GOD is my ultimate strength and power who bring best out of me*

*I deem it my privilege and honors to consign my appreciation and thanks to the following without whose supervision, support and apprehension I would not have been able to complete my Ph. D thesis.*

*I feel fortunate to convey my deep sense of reverence and gratitude to my revered mentor, **Dr. Pankaj Sharma**, for his support, immaculate guidance, constructive criticism, constant encouragement and providing requisite facilities to persist my research which otherwise would have remained incomplete. His nurturing and gentle concern has been a stimulus which I will always cherish. I also appreciate his untiring efforts during the entire tenure of my research work and patience during writing of this thesis. I have no words to express my gratitude for everything he has contributed in my Ph.D and without his blessings it was surely impossible for me to finish my work. I thank him from bottom of my heart.*

*I emphatically express my loyal and venerable thanks to **Prof. (Dr.) Vinod Kumar** (Vice Chancellor, JUIT), **Maj Gen (Retd.) Rakesh Bassi** (Registrar and Dean of Student Welfare JUIT), and **Prof. (Dr.) Samir Dev Gupta** (Dean, Academic & Research, JUIT) for giving a opportunity to pursue Doctorate Degree and teaching assistantship.*

*I gratefully acknowledge the help rendered by **Prof. P. B. Barman** (HOD, Department of Physics and Materials Science) for his encouragement, timely help and cooperation throughout my research work. It gives me immense pleasure to express my gratitude to him for his positive disposition coming to my rescue in solving my problems and suggestions which helped me in maintaining my confidence.*

*This document would have remained an infant had it not received its necessary 'diet' in the form of comments, suggestions etc. by **Dr. Vineet Sharma, Prof. (Dr.) Sunil Kumar Khah, Dr. Dheeraj Sharma, Prof. (Dr.) Ashok Kumar Gupta, Dr. Rajesh Kumar, Dr. Ragini Raj Singh, Dr. Surajit Kumar Hazra, Dr. Sanjiv Kumar Tiwari and Dr. Abhishek Chaudhary.***

*I appreciatively acknowledge the help rendered by **Prof. Nagesh Thakur and Prof. Nainjeet Singh Negi** (Department of Physics, Himachal Pradesh University, Summer Hill, Shimla), **Prof. (Dr.) Ravi Kumar and Dr. Vishal Singh** (Department of Material Science and Engineering, NIT Hamirpur), **Dr. Manoj Kumar** (Department of Physics*

and Material Science, Jaypee Institute of Information Technology, Noida), **Dr. Radheshyam Rai** (Department of Physics, Shoolini University, Solan) for their stimulating suggestions and huge help throughout my whole research work.

I am also grateful to all the members of technical and non-technical staff of the department **Er. Kamlesh Mishra, Mr. Ravendra Tiwari, Mr. Deepak Singh and Mr. Ranvijay Singh** for their help and precious assistance.

I am fortunate to have seniors and friends who have always stood beside me. I extend my heartfelt thanks to my best friends **Nikhil Gupta, Parveen Kumar, Anup Jaswal and Rohit Sharma** who have always been listened my insane thoughts and ideas in spite of not understanding a bit of it. I am also grateful to my Seniors **Dr. Hitanshu Kumar, Dr. Rajinder, Dr. Dikshita Gupta, Dr. Sarita Kangoo, Dr. Bandna Bharti, Dr. Rajender Singh, Dr. Abhishek, Dr. Pawan, Dr. Kush Rana, Dr. Ira Vashisht, Dr. Tarun Pal, Ms. Ritika Verma, Ms. Poonam Thakur, Dr. Rohit Randhawa, Mr. Jai Vardhan and Dr. Richa khokhra** for being there so as to make me sail through all the twists and turns of this journey. It is my pleasure to express my gratitude to **Jonny Dhiman, Neha Kondal, Dr. Priyam Dhani, Kavita, Sampan Attri, Dr. Rishi Mahajan, Subhash, Asha, Dipti Rawat, Ekta Sharma, Rajan Sharma, Neha, Priyanka Sharma, Sanjay Kumar Shandil, Kanchan Thakur, Shikha Sinha, Anuradha, Achyut Sharma, Pooja, Swati Sharma, Neha Thakur, Deepak Sharma, Keshav Kondal, Divyansh Thakur** and all the research scholars of the JUIT for keeping me blessed with best wishes. I would like to thank my all students for to provide me positive energy. The time spent with them will be cherished throughout my life. I would like to thank every person who gave me positive and negative experience throughout my life.

The intention of this acknowledgement will be imperfect if I fail to appreciate the moral support and encouragement rendered by the most important person of my life i.e. my **parents, sister and family** who has always been my inspiration and never let me felt abandoned. It was their blessings and love which constantly motivated me and helped in the successful completion of my research work. I would like to express my heartfelt gratitude to all those who have contributed directly or indirectly towards obtaining my doctorate degree and apologize if have missed out anyone.

**DATED:**

**PRASHANT THAKUR**

## ABSTRACT

Superparamagnetic nanoparticles have the ability to tack themselves in a reasonable magnetic field and have got scientific attention for biomedicine applications. In present work, nanoparticles of  $Mn_{0.5}Zn_{0.5}RE_xFe_{2-x}O_4$  ( $x = 0, 0.025, 0.050, 0.075, 0.1$ ) ferrites (where  $RE = La, Gd, Nd$ ) have been prepared using co-precipitation technique. First the sintering temperature has been optimized for  $Mn_{0.5}Zn_{0.5}Fe_2O_4$  ferrite nanoparticles. From the structural analysis using XRD at three sintering temperatures (973 K, 1173 K, 1373 K), a pure spinel phase is observed at 1373 K whereas a secondary phase  $Fe_2O_3$  has been observed at lower sintering temperatures. The absorption bands at  $421\text{ cm}^{-1} - 491\text{ cm}^{-1}$  and  $516\text{ cm}^{-1} - 592\text{ cm}^{-1}$  in FTIR spectra confirm the formation of spinel ferrite. FE-SEM images have shown the formation of homogenous crystalline nanoparticles with increase in sintering temperature. For further investigation of  $RE$  doped  $Mn-Zn$  ferrites, the sintering temperature has been taken as 1373 K. Structural investigations have shown cubic spinel phase for all samples. For the three dopants used in  $Mn-Zn$  ferrites, the crystallite size, lattice constant, interplanar spacing and packing factor have been determined and found to decrease generally. FTIR spectroscopy has confirmed the occurrence of spinel structure in all the investigated samples. FE-SEM micrographs of all investigated samples show sharp crystalline structures. EDS spectroscopy confirms the presence of constituent elements in all the investigated samples. A cation distribution has been proposed for  $RE$  doped manganese-zinc spinel ferrites. Magnetic study has shown paramagnetic and superparamagnetic nature of samples at room temperature.



## ABBREVIATIONS

AC	Alternating current
EDS	Energy dispersive X-Ray spectroscopy
EDTA	Ethylenediaminetetraacetic acid
fcc	Face Centered Cubic
FE-SEM	Field emission scanning electron microscopy
FTIR	Fourier transform infrared spectroscopy
FWHM	Full width at half maximum
IR	Infrared
JCPDS	Joint Committee on Powder Diffraction Standards
MLFCI	Multilayer ferrite chip inductor
MRI	Magnetic resonance imaging
pH	Power of hydrogen
RE	Rare earth (Lanthanide)
SEM	Scanning electron microscope
SPM	Superparamagnetic
SPNs	Superparamagnetic nanoparticles
SQUID	Superconducting quantum interference device
TEM	Transmission electron microscopy
VSM	Vibrating sample magnetometer
W-H	Williamson-Hall
XRD	X-ray diffraction



Figure Number	Caption	Page no.
Figure 1.1	A typical hysteresis Loop	9
Figure 1.2	Hysteresis loop for (a) soft ferrite & (b) hard ferrite	10
Figure 1.3	Unit cell structure of spinel ferrite	14
Figure 2.1	Schematic diagram of co-precipitation technique for the synthesis of lanthanide ( $RE = La, Gd, Nd$ ) doped $Mn-Zn$ ferrites	34
Figure 2.2	Diffraction of X-rays from various planes	35
Figure 2.3	SHIMADZU analytical: XRD 6000 diffractometer	35
Figure 2.4	Perkin Elmer spectrophotometer (model-65)	36
Figure 2.5	FE-SEM Quanta 200 FEG	38
Figure 2.6	Vibrating sample magnetometer (PAR-155)	39
Figure 3.1	Schematic diagram for preparation of $Mn_{0.5}Zn_{0.5}Fe_2O_4$ ferrite powder	46
Figure 3.2	XRD graph of sintered $Mn_{0.5}Zn_{0.5}Fe_2O_4$ nano ferrites	48
Figure 3.3	W-H plots of sintered $Mn_{0.5}Zn_{0.5}Fe_2O_4$ ferrites. The sintering temperature is given in each plot	50
Figure 3.4	FTIR spectra of sintered $Mn_{0.5}Zn_{0.5}Fe_2O_4$ sample	51
Figure 3.5	FESEM images of $Mn_{0.5}Zn_{0.5}Fe_2O_4$ sample sintered at (a) 973 K (b) 1173 K and (c) 1373 K.	52
Figure 4.1.1	XRD graphs of $Mn_{0.5}Zn_{0.5}La_xFe_{2-x}O_4$ ferrites	59
Figure 4.1.2	Zoomed in image of most prominent peak in $Mn_{0.5}Zn_{0.5}La_xFe_{2-x}O_4$ ferrites	59
Figure 4.2.1	XRD graphs of $Mn_{0.5}Zn_{0.5}Gd_xFe_{2-x}O_4$ ferrites	60
Figure 4.2.2	Zoomed in image of most prominent peak in $Mn_{0.5}Zn_{0.5}Gd_xFe_{2-x}O_4$ ferrites	60
Figure 4.3.1	XRD spectra of $Mn_{0.5}Zn_{0.5}Nd_xFe_{2-x}O_4$ ferrites	61
Figure 4.3.2	Zoomed in image of most prominent peak in $Mn_{0.5}Zn_{0.5}Nd_xFe_{2-x}O_4$ ferrites	61
Figure 4.4.1	FE-SEM images for (a) $x = 0$ ; (b) $x = 0.025$ ; (c) $x = 0.050$ of $Mn_{0.5}Zn_{0.5}La_xFe_{2-x}O_4$ spinel ferrites	66
Figure 4.4.2	FE-SEM images for (d) $x = 0.075$ ; (e) $x = 0.1$ of $Mn_{0.5}Zn_{0.5}La_xFe_{2-x}O_4$ spinel ferrites	67

## List of figures

Figure 4.5.1	FE-SEM images for (a) $x = 0$ ; (b) $x = 0.025$ ; (c) $x = 0.050$ of $Mn_{0.5}Zn_{0.5}Gd_xFe_{2-x}O_4$ spinel ferrites	68
Figure 4.5.2	FE-SEM images for (d) $x = 0.075$ ; (e) $x = 0.1$ of $Mn_{0.5}Zn_{0.5}Gd_xFe_{2-x}O_4$ spinel ferrites	69
Figure 4.6.1	FE-SEM images for (a) $x = 0$ ; (b) $x = 0.025$ ; (c) $x = 0.050$ of $Mn_{0.5}Zn_{0.5}Nd_xFe_{2-x}O_4$ spinel ferrites	70
Figure 4.6.2	FE-SEM images for (d) $x = 0.075$ ; (e) $x = 0.1$ of $Mn_{0.5}Zn_{0.5}Nd_xFe_{2-x}O_4$ spinel ferrites	71
Figure 4.7.1	EDS spectra for (a) $x = 0$ ; (b) $x = 0.025$ ; (c) $x = 0.050$ of $Mn_{0.5}Zn_{0.5}La_xFe_{2-x}O_4$ ferrites	72
Figure 4.7.2	EDS spectra for (d) $x = 0.075$ ; (e) $x = 0.1$ of $Mn_{0.5}Zn_{0.5}La_xFe_{2-x}O_4$ ferrites, (f) atomic% of $Mn_{0.5}Zn_{0.5}La_{0.025}Fe_{1.975}O_4$ ferrite as reference	73
Figure 4.8.1	EDS spectra for (a) $x = 0$ ; (b) $x = 0.025$ ; (c) $x = 0.050$ of $Mn_{0.5}Zn_{0.5}Gd_xFe_{2-x}O_4$ ferrites	74
Figure 4.8.2	EDS spectra for (d) $x = 0.075$ ; (e) $x = 0.1$ of $Mn_{0.5}Zn_{0.5}Gd_xFe_{2-x}O_4$ ferrites, (a) atomic% of $Mn_{0.5}Zn_{0.5}Gd_{0.025}Fe_{1.975}O_4$ ferrite as reference	75
Figure 4.9.1	EDS spectra for (a) $x = 0$ ; (b) $x = 0.025$ ; (c) $x = 0.050$ of $Mn_{0.5}Zn_{0.5}Nd_xFe_{2-x}O_4$ ferrites	76
Figure 4.9.2	EDS spectra for (d) $x = 0.075$ ; (e) $x = 0.1$ of $Mn_{0.5}Zn_{0.5}Nd_xFe_{2-x}O_4$ ferrites, (a) atomic% of $Mn_{0.5}Zn_{0.5}Nd_{0.025}Fe_{1.975}O_4$ ferrite as reference	77
Figure 4.10	FTIR spectra of $Mn_{0.5}Zn_{0.5}La_xFe_{2-x}O_4$ nano ferrites. The y-axis scale has been shifted for clarity	79
Figure 4.11	FTIR spectra of $Mn_{0.5}Zn_{0.5}Gd_xFe_{2-x}O_4$ nano ferrites. The y-axis scale has been shifted for clarity	79
Figure 4.12	FTIR spectra of $Mn_{0.5}Zn_{0.5}Nd_xFe_{2-x}O_4$ nano ferrites. The y-axis scale has been shifted for clarity	80
Figure 5.1	Plot of $r_A$ & $r_B$ with La content ( $x$ )	86
Figure 5.2	Plot of $r_A$ & $r_B$ with Gd content ( $x$ )	87
Figure 5.3	Plot of $r_A$ & $r_B$ with Nd content ( $x$ )	87
Figure 5.4	Variation of $a_{th}$ and $U$ with La content ( $x$ ) in	92

	manganese – zinc ferrites	
Figure 5.5	Variation of $a_{th}$ and $U$ with $Gd$ content ( $x$ ) in manganese – zinc ferrites	92
Figure 5.6	Variation of $a_{th}$ and $U$ with $Nd$ content ( $x$ ) in manganese – zinc ferrites	93
Figure 5.7	Graph of $R_A$ and $R_B$ with $La$ content in Mn-Zn ferrites	94
Figure 5.8	Graph of $R_A$ and $R_B$ with $Gd$ content in Mn-Zn ferrites	94
Figure 5.9	Graph of $R_A$ and $R_B$ with $Nd$ content in Mn-Zn ferrites	95
Figure 5.10	Interionic lengths and the angles amongst the ions in spinel ferrites	95
Figure 5.11.1	(a) Magnetic hysteresis curve of $Mn_{0.5}Zn_{0.5}Fe_2O_4$ spinel nanoferrite; (a1) Zoomed Magnetic hysteresis curve of $Mn_{0.5}Zn_{0.5}Fe_2O_4$ spinel nanoferrite; (b) M-H curve of $Mn_{0.5}Zn_{0.5}La_{0.025}Fe_{2-x}O_4$ spinel ferrite; (b1) Zoomed M-H curve of $Mn_{0.5}Zn_{0.5}La_{0.025}Fe_{2-x}O_4$ spinel ferrite	99
Figure 5.11.2	(c) M-H curve of $Mn_{0.5}Zn_{0.5}La_{0.050}Fe_{2-x}O_4$ spinel ferrite; (c1) Zoomed M-H curve of $Mn_{0.5}Zn_{0.5}La_{0.050}Fe_{2-x}O_4$ spinel ferrite; (d) M-H curve of $Mn_{0.5}Zn_{0.5}La_{0.075}Fe_{2-x}O_4$ spinel ferrite; (d1) Zoomed M-H curve of $Mn_{0.5}Zn_{0.5}La_{0.075}Fe_{2-x}O_4$ spinel ferrite; (e) M-H curve of $Mn_{0.5}Zn_{0.5}La_{0.1}Fe_{2-x}O_4$ spinel ferrite; (e1) Zoomed M-H curve of $Mn_{0.5}Zn_{0.5}La_{0.1}Fe_{2-x}O_4$ spinel ferrite	100
Figure 5.12.1	(a) Magnetic hysteresis curve of $Mn_{0.5}Zn_{0.5}Fe_2O_4$ spinel nanoferrite; (a1) Zoomed Magnetic hysteresis curve of $Mn_{0.5}Zn_{0.5}Fe_2O_4$ spinel nanoferrite; (b) M-H curve of $Mn_{0.5}Zn_{0.5}Gd_{0.025}Fe_{2-x}O_4$ spinel ferrite; (b1) Zoomed M-H curve of $Mn_{0.5}Zn_{0.5}Gd_{0.025}Fe_{2-x}O_4$ spinel ferrite; (c) M-H curve of $Mn_{0.5}Zn_{0.5}Gd_{0.050}Fe_{2-x}O_4$ spinel ferrite; (c1) Zoomed M-H curve of $Mn_{0.5}Zn_{0.5}Gd_{0.050}Fe_{2-x}O_4$ spinel ferrite	101
Figure 5.12.2	(d) M-H curve of $Mn_{0.5}Zn_{0.5}Gd_{0.075}Fe_{2-x}O_4$ spinel	102

	ferrite; <b>(d1)</b> Zoomed M-H curve of $Mn_{0.5}Zn_{0.5}Gd_{0.075}Fe_{2-x}O_4$ spinel ferrite; <b>(e)</b> M-H curve of $Mn_{0.5}Zn_{0.5}Gd_{0.1}Fe_{2-x}O_4$ spinel ferrite; <b>(e1)</b> Zoomed M-H curve of $Mn_{0.5}Zn_{0.5}Gd_{0.1}Fe_{2-x}O_4$ spinel ferrite.	
Figure 5.13.1	<b>(a)</b> Magnetic hysteresis curve of $Mn_{0.5}Zn_{0.5}Fe_2O_4$ spinel nanoferrite; <b>(a1)</b> Zoomed Magnetic hysteresis curve of $Mn_{0.5}Zn_{0.5}Fe_2O_4$ spinel nanoferrite; <b>(b1)</b> Zoomed M-H curve of $Mn_{0.5}Zn_{0.5}Nd_{0.025}Fe_{2-x}O_4$ spinel ferrite; <b>(c)</b> M-H curve of $Mn_{0.5}Zn_{0.5}Nd_{0.050}Fe_{2-x}O_4$ spinel ferrite; <b>(c1)</b> Zoomed M-H curve of $Mn_{0.5}Zn_{0.5}Nd_{0.050}Fe_{2-x}O_4$ spinel ferrite	103
Figure 5.13.2	<b>(d)</b> M-H curve of $Mn_{0.5}Zn_{0.5}Nd_{0.075}Fe_{2-x}O_4$ spinel ferrite; <b>(d1)</b> Zoomed M-H curve of $Mn_{0.5}Zn_{0.5}Nd_{0.075}Fe_{2-x}O_4$ spinel ferrite; <b>(e)</b> M-H curve of $Mn_{0.5}Zn_{0.5}Nd_{0.1}Fe_{2-x}O_4$ spinel ferrite; <b>(e1)</b> Zoomed M-H curve of $Mn_{0.5}Zn_{0.5}Nd_{0.1}Fe_{2-x}O_4$ spinel ferrite	104
Figure 5.14	A plot of in magnetic parameters $M_S$ and $n_B$ with $La$ content ( $x$ )	105
Figure 5.15	A plot of magnetic parameters $M_S$ and $n_B$ with $Gd$ content ( $x$ )	106
Figure 5.16	A plot of magnetic parameters $M_S$ and $n_B$ with $Nd$ content ( $x$ )	106

Table Number	Caption	Page no.
Table 3.1	The values of various structural parameters for Mn-Zn nano ferrites with sintering temperature	49
Table 3.2	Tetrahedral and Octahedral force constants ( $K_t$ , $K_o$ ) of $Mn_{0.5}Zn_{0.5}Fe_2O_4$ sintered at 973 K, 1173 K and 1373 K temperatures	53
Table 4.1	Various computed structural parameters for $RE^{3+}$ ( $= La^{3+}$ , $Gd^{3+}$ & $Nd^{3+}$ ) doped $Mn_{0.5}Zn_{0.5}RE_xFe_{2-x}O_4$ ferrites	63
Table 5.1	Proposed cation distribution for lanthanide ( $La^{3+}$ , $Gd^{3+}$ & $Nd^{3+}$ ) ions doped manganese – zinc ferrites	85
Table 5.2	Values of various theoretical parameters calculated from proposed cation distribution for $La^{3+}$ doped manganese-zinc ferrites	89
Table 5.3	Values of various theoretical parameters calculated from proposed cation distribution for $Gd^{3+}$ doped manganese-zinc ferrites	90
Table 5.4	Values of various theoretical parameters calculated from proposed cation distribution for $Nd^{3+}$ doped manganese-zinc ferrites	91
Table 5.5	The interionic distances of cation-anion ( $p$ , $q$ , $r$ & $s$ ) and cation-cation ( $b$ , $c$ , $d$ , $e$ & $f$ ) for $La^{3+}$ doped $Mn_{0.5}Zn_{0.5}La_xFe_{2-x}O_4$ spinel ferrites	97
Table 5.6	The interionic distances of cation-anion ( $p$ , $q$ , $r$ & $s$ ) and cation-cation ( $b$ , $c$ , $d$ , $e$ & $f$ ) for $Gd^{3+}$ doped $Mn_{0.5}Zn_{0.5}Gd_xFe_{2-x}O_4$ spinel ferrites	97
Table 5.7	The interionic distances of cation-anion ( $p$ , $q$ , $r$ & $s$ ) and cation-cation ( $b$ , $c$ , $d$ , $e$ & $f$ ) for $Nd^{3+}$ doped $Mn_{0.5}Zn_{0.5}Nd_xFe_{2-x}O_4$ spinel ferrites	97
Table 5.8	Bond angles ( $\theta_1$ , $\theta_2$ , $\theta_3$ , $\theta_4$ and $\theta_5$ ), saturation magnetization ( $M_s$ ) and magnetic moment ( $n_B$ ) for $La^{3+}$ doped $Mn_{0.5}Zn_{0.5}La_xFe_{2-x}O_4$ spinel ferrites	98
Table 5.9	Bond angles ( $\theta_1$ , $\theta_2$ , $\theta_3$ , $\theta_4$ and $\theta_5$ ), saturation	98

## List of tables

---

	magnetization ( $M_s$ ) and magnetic moment ( $n_B$ ) for $Gd^{3+}$ doped $Mn_{0.5}Zn_{0.5}Gd_xFe_{2-x}O_4$ spinel ferrites	
Table 5.10	Bond angles ( $\theta_1$ , $\theta_2$ , $\theta_3$ , $\theta_4$ and $\theta_5$ ), saturation magnetization ( $M_s$ ) and magnetic moment ( $n_B$ ) for $Nd^{3+}$ doped $Mn_{0.5}Zn_{0.5}Nd_xFe_{2-x}O_4$ spinel ferrites	98

## Journals

1. **Prashant Thakur**, R. Sharma, V. Sharma, Pankaj Sharma. "*Structural and optical properties of  $Mn_{0.5}Zn_{0.5}Fe_2O_4$  nano ferrites: Effect of sintering temperature.*" **Materials Chemistry and Physics** 193 (2017) 285-289 (**SCI, Scopus Indexed, I.F. = 2.210**).
2. **Prashant Thakur**, R. Sharma, V. Sharma, P. B. Barman, M. Kumar, D. Barman, S. C. Katyal, Pankaj Sharma. " *$Gd^{3+}$  doped Mn-Zn soft ferrite nanoparticles: Superparamagnetism and its correlation with other physical properties*" **Journal of Magnetism and Magnetic Materials** 432 (2017) 208-217 (**SCI, Scopus Indexed, I.F. = 3.046**).
3. **Prashant Thakur**, R. Sharma, M. Kumar, S. C. Katyal, N. S. Negi, N. Thakur, V. Sharma, Pankaj Sharma. "*Superparamagnetic La doped Mn–Zn nano ferrites: dependence on dopant content and crystallite size*" **Materials Research Express** 3(7) (2016) 075001 (**SCI, Scopus Indexed, I.F. = 1.151**).
4. **Prashant Thakur**, R. Sharma, M. Kumar, V. Sharma, Pankaj Sharma. "*Structural, morphological, magnetic and optical study of  $Nd^{3+}$  doped Mn-Zn ferrite nanoparticles synthesized via co-precipitation technique*" **Journal of Magnetism and Magnetic Materials** Vol 479 (2019) 317-325 (**SCI, Scopus Indexed, I.F. = 3.046**).

## Conferences

1. **Prashant Thakur**, R. Sharma, V. Sharma, Pankaj Sharma. "*Effect of Gd doping on the optical band gap of Mn-Zn nano ferrites*" National Seminar on Innovations & Challenges in Basic & Applied Sciences (ICBAS-2017) at Maharaja Agrasen University (H.P.) on March 04, 2017.
2. **Prashant Thakur**, R. Sharma, V. Sharma, Pankaj Sharma. "*Structural and optical study of manganese zinc nano ferrite*" National Conference on Recent innovations in Applied Sciences and Humanities (NCASH-2015) at Rawal Institutions, Faridabad on October 10, 2015.
3. **Prashant Thakur**, R. Sharma, V. Sharma, Pankaj Sharma. "*Effect of sintering temperature on structure and morphology of Mn-Zn soft ferrite*" International Conference on Emerging Trends in Basic & Applied Sciences at Maharaja Agrasen University (H.P.) on May 1-2, 2015.



# **CHAPTER-1**

---

## **Introduction**



Mankind and materials have evolved over the passage of time and are continuing to do so. Materials are playing a vital role in the modern age of science and technology. Materials can be broadly classified as dielectric materials, magnetic materials, ceramics, glasses, polymers and semiconducting materials. Among these, magnetic materials have a variety of applications like memory devices, transformers, microwave devices, drug delivery, hyperthermia etc. Further, the rapid developments in the field of nanotechnology have opened large opportunities for understanding and utilization of magnetic materials. The word ‘nano’ was first coined by Feynman in his famous lecture at California Institute of Technology in 1959. He has pronounced “there is plenty of room at the bottom”, but the actual development in nano field has started from 1990. Nano system has not any universal description. A measurement unit of  $1 \text{ nm} = 1 \times 10^{-9} \text{ m} = 10 \text{ \AA}$  formulates the word “nanometer”. Nanoscience is the study of fundamental phenomena of structures of molecules having their dimensions in the range of 10 nm to 100 nm (also termed as nanoscale). Nanoscience is an interdisciplinary field where the expertness of researchers from physics, materials science, chemistry, biology and engineering is required to develop nanomaterials and hence nanodevices. Further, many physical phenomenon become more noticeable as the size of system approaches to nanoscale. In this chapter, the magnetic materials have been described with a focus on ferrites and their classification. Recent literature survey has also been included for the spinel ferrites. Finally, the motivation behind this work has been described.

### **1.1 Magnetic materials**

All materials can be categorized based on their magnetic behaviour into one of five types (diamagnetic, paramagnetic, ferromagnetic, antiferromagnetic and ferrimagnetic) subject to their magnetic susceptibility. The magnetic susceptibility is the proportion of magnetic dipole moment per unit volume to the connected magnetic field. On the basis of magnetic dipole moments magnetic materials are classified into two large groups. The atoms of first group materials carry permanent magnetic dipole moment and second group do not have perpetual magnetic dipole moment. Now, on account of interaction between the individual magnetic dipoles, there are the five types of magnetic materials. The materials are named as diamagnetic materials, paramagnetic materials, ferromagnetic materials, antiferromagnetic materials and ferrimagnetic

materials. At room temperature both diamagnetic and paramagnetic materials have very weak magnetic properties. So both of these materials do not display hysteresis. The materials involving atoms with no net magnetic moment show diamagnetism. By Lenz's law a moment is induced in an atom with the help of magnetic field that resists the applied field. The sum of the orbital and spin contributions is the magnetic moment of an atom. The property of a material which generates a magnetic field in a direction opposite to the applied magnetic field is called diamagnetism. Conditions of Landau levels are helpful to understand the diamagnetism and it is supposed to be due to quantum mechanics [1]. Diamagnetism happens when orbital speed of electrons around their cores is adjusted by the outside field. These progressions the magnetic dipole moment. It is noticed that the relative permeability of diamagnets is under 1. In many materials, diamagnetism is known as a feeble impact.

Paramagnetism is a sort of attraction in which paramagnetic material is just pulled in when there is an externally connected magnetic field. Diamagnetic materials are repelled by magnetic fields due to this behaviour [2]. Paramagnetic materials are attracted by the applied magnetic field and have a relative magnetic permeability  $\geq 1$  (*i.e.*, a positive value). The induced magnetic moment is weak and linear within the applied field strength. It usually requires a responsive systematic balance to sense the paramagnetic effect. A SQUID magnetometer is used for modern measurements on paramagnetic materials. A positive and small value of susceptibility exists for paramagnetic materials in external magnetic fields. At the point when outer magnetic field is connected then these materials are marginally pulled in by a magnetic field. The magnetic properties are not held by the material when the outer magnetic field is evacuated around the material since thermal developments randomizes the dipole ordering. Paramagnetic properties happen because of essence of odd number of electrons and the reordering of the electron tracks induced by outside magnetic field. There is just a little instigated magnetization even within the presence of the field in light of the fact that only a little portion of the dipoles are arranged. The small fraction of dipoles is proportional to the applied field strength and due to this there is linear dependency. This would develop a net magnetization (or magnetic moment per unit volume), equivalent to the product of moment and the density. Saturation magnetization  $M_s$  is the maximum magnetization that can be achieved with this small fraction of the dipoles concentration [3]. A magnetic moment that is possessed by an atom is an integer number of Bohr magnetons. The magnetic moment of an electron,  $\mu_B$ , is one Bohr

magneton and its value in SI units is  $0.9274 \times 10^{-23} \text{ A.m}^2$ . Cases of paramagnetic materials are manganese, magnesium, lithium, molybdenum and tantalum.

The materials which stay magnetized even after the removal of external magnetic field are called permanent magnets. These materials are either ferromagnetic or ferrimagnetic [4]. Ferromagnetic materials experience a non-linear and much stronger attraction in comparison to paramagnetic materials. The strongest type of magnetism is ferromagnetism. This type of magnetism creates strong forces sufficient to be sensed. It is also accountable for the ordinary magnetism phenomenon encountered in our day to day life [5]. The general ferromagnetic materials are nickel, iron, cobalt and mainly their alloys. Some normally happening minerals, for example, lodestone and a few compounds of rare earth metals are ferromagnetic in nature. In modern technologies and industries the ferromagnetic materials are very useful. For many electromechanical (e.g. generators, electric motors), electronics (e.g. hard disks, recorders) and electrical devices (e.g. electromagnets, transformers), the base is ferromagnetism. According to quantum mechanics, the spin and Pauli Exclusion Principle are responsible for the property of ferromagnetism. In magnetically structured materials there is large magnetization and magnetic moment. This is because of the adjusted electron spins of the atoms in the microscopic areas. The magnetization of the domains tends to agree with the field and the domains inclining constructively regarding the outer applied field at the cost of other domains. When ferromagnetic materials are studied with temperature, then a ferromagnetic material is normally a paramagnetic in nature above the Curie temperature.

Materials featuring the magnetic moments of neighboring electrons in opposite direction are termed as anti-ferromagnetic materials and the magnetism associated with them is known as anti-ferromagnetism. In ferromagnetic materials it is vivaciously great for the spins to adjust and prompting an unconstrained magnetization while in antiferromagnetic materials it is vigorously good for the spins to restrict each other and prompting no general magnetization. Normally, at suitably low temperatures the ordering of anti-ferromagnetism may exist but above a certain temperature this ordering disappears. This temperature is called Néel temperature. Louis Néel had first perceived this type of magnetic ordering and so named as Néel temperature [6]. Antiferromagnetic materials are normally paramagnetic above the Néel temperature. To explain the anti-ferromagnetism, two sub lattice model is used. The antiferromagnetic structure represents to a fading complete magnetization when no outer field is connected. With

the total value of one of the sub lattice magnetization differing from the other sub lattice magnetization leading to some net magnetization, a kind of ferromagnetic performance may be observed in the antiferromagnetic phase in the presence of an external magnetic field. Antiferromagnetism exhibits a small positive susceptibility which is comparable to paramagnetism.

Without magnetic field and underneath Néel temperature the spins are antiparallel and thoroughly drop each other. The spin arrangements becomes random above Néel temperature, so with an increase in temperature the magnetic susceptibility decreases and the material becomes classically paramagnetic.

As the temperature is diminished beneath the Néel temperature the magnetic susceptibility,  $\chi_m$ , of an antiferromagnetic material will have a maximal; as opposed to a paramagnet where it always increments with diminishing temperature. Antiferromagnetic materials have a negative pairing between adjacent moments and low disturbance. Antiferromagnetic materials are comparatively rare.

Antiferromagnetism is also recognized as ferrimagnetism (the term coined by Neel to suggest the magnetism of ferrites) showed by materials whose ions or atoms have a tendency to secure an arranged however nonparallel ordering without magnetic field beneath Néel temperature. A substantial net magnetization is there from the antiparallel arrangement of neighboring unequal sub-lattices inside a magnetic area. This naturally visible conduct is like that of ferromagnetism. Ferrimagnetism generally occurs in ionic compounds due to complicated magnetic arrangements in the crystal structure. The magnetic structure of ferrimagnetic materials is including two sub-lattices (called A and B) isolated by  $O_2$  ions. The trade connections between the two sub-lattices are intermediated by the oxygen anions. These associations are named as “indirect or superexchange interactions”. The most ground-breaking superexchange interactions prompt antiparallel arrangement of spins between the two sub-lattices. In ferrimagnetic materials, the magnetic moments of the two sub-lattices are not equivalent and prompt a net magnetic moment. Ferrimagnetism is consequently like ferromagnetism. Ferrimagnetism demonstrates every one of the reserves of ferromagnetism like unconstrained magnetization, Curie temperatures, hysteresis, and retentivity. In any case, ferromagnetic and ferrimagnetic materials have extremely distinguishable magnetic arrangements. Some of the examples for ferrimagnetic materials  $Fe_3O_4$ ,  $NiFe_2O_4$ ,  $SrFe_{12}O_{19}$ ,  $BaFe_{12}O_{19}$ ,  $SrO \cdot 6Fe_2O_3$  and  $PbO \cdot 6Fe_2O_3$  etc. The oldest-known ferrimagnet is magnetite ( $Fe_3O_4$ ) which contains both  $Fe^{2+}$  and  $Fe^{3+}$  ions.

Prior to Néel's revelation of ferrimagnetism and antiferromagnetism in 1948, it was initially attributed a ferromagnet. [6].

Below the Curie temperature ferromagnetic and ferrimagnetic materials hold a spontaneous magnetization whereas above this temperature these materials show no magnetic order and hence become paramagnetic. In specific cases two sub lattices have matching moments beneath the Curie temperature prompting zero magnetic moment, this is known as the magnetization counterbalance or indemnified point. This counterbalance or indemnified point has been discovered effectively in garnets and rare earth - metal compounds. In addition, ferrimagnetic materials may likewise demonstrate an angular momentum counterbalance or indemnified point where the angular momentum of the magnetic sub-lattices is indemnified. This indemnified point is a basic point for attaining rapid magnetisation flip-flop in magnetic memory gadgets. [7]. Anisotropic behaviour and high resistivity are other properties of ferrimagnetic materials. Actually an external applied field induces the anisotropy in ferrimagnetic materials. At the point when an outside magnetic field is connected, the magnetic dipoles get adjusted leading to a total magnetic moment and powers the dipoles to move in a gyrating fashion at a frequency directed by an applied field, called Larmor or precession frequency. As a unique case, a microwave signal circularly polarized in the identical direction as such precession firmly communicates with the magnetic moments; when this microwave signal circularly polarized in the reverse direction the interplay is very weak. In this way, at whatever point the interplay is firm, the microwave signal passes through the material. This directional property has been employed really to develop microwave gadgets e.g. isolators, circulators and gyroscopes. Ferrimagnetic materials have additionally been used to create optical isolators and circulators.

Ferrites having chemical formula  $MFe_2O_4$ , where M represents the divalent metal ions, exhibits ferrimagnetism. In ferrites iron oxide is the main constituent [8]. Ferrites are generally non-conductive ferrimagnetic ceramic compounds. Similar to most other ceramics, ferrites are found to be hard and brittle. Ferrite exhibits ferrimagnetism because super exchange interaction between oxygen ions and metal ions. Ferrite has superior resistivity as compared to ferromagnetic materials because of intrinsic atomic level interactions among metal and oxygen ions. This makes ferrite scientifically highly valuable and tunes the ferrite to discover new applications at higher frequencies.

Ferrites have similar lattice structure as that of magnesium aluminate ( $\text{MgAl}_2\text{O}_4$ ) and the structure is termed as spinel. The magnetic properties of ferrite are dependent on the type of ions (divalent or trivalent) and their relative lattice position. Metal ions are situated at tetrahedral and octahedral positions.  $\text{Zn}^{2+}$  ions substituting  $\text{Ni}^{2+}$  ions in Ni ferrite and  $\text{Zn}^{2+}$  ions substituting  $\text{Mn}^{2+}$  ions in Mn ferrite *i.e.*  $\text{Ni}_{1-x}\text{Zn}_x\text{Fe}_2\text{O}_4$  and  $\text{Mn}_{1-x}\text{Zn}_x\text{Fe}_2\text{O}_4$  respectively are the most significant derivatives of these ferrites. The main difference between these two ferrites lie in their resistivity.  $\text{Fe}^{3+}$ ,  $\text{Zn}^{2+}$  prefer tetrahedral sites and  $\text{Ni}^{2+}$ ,  $\text{Mn}^{2+}$ ,  $\text{Fe}^{2+}$  *etc.* ions favor to occupy the octahedral sites. Mn-Zn ferrites and Ni-Zn ferrite and has reverse spinel structures. The composition and processing parameters, e.g. sintering temperature, are responsible for the variation in magnetic and electrical properties. The synthesis process and composition are the two points in determining the quality of ferrite manufacturing.

At molecular level magnetic moment occurs owing to the electronic interaction among oxygen and metal ions and is termed as super exchange. In bulk ferrites, there are domains called Weiss domains in which each molecular magnet is adjusted in same direction. In the presence of an outer magnetic field, the moments are enforced to adjust in the direction of outer magnetic field. In this process, some energy is consumed and the magnetization lags behind the magnetizing field at all the times and consequences in a magnetization loop. This magnetization loop is named as B-H or M-H loop or hysteresis loop.

Hysteresis loop of a material provide the information about the magnetic behaviour of that material. A clear correlation among induced magnetic flux density (B) along with magnetizing force (H) has been displayed by hysteresis loop (figure 1.1).

Various principle magnetic properties of a material can be dictated by a hysteresis loop;

1. Retentivity - A level of the remaining flux density comparable to the saturation magnetization of a magnetic material. It is the material's capacity to hold a specific measure of remaining magnetic field when the applied magnetic field is disconnected subsequent to accomplishing saturation. In figure 1.1, the estimation of B at point b in the hysteresis loop.

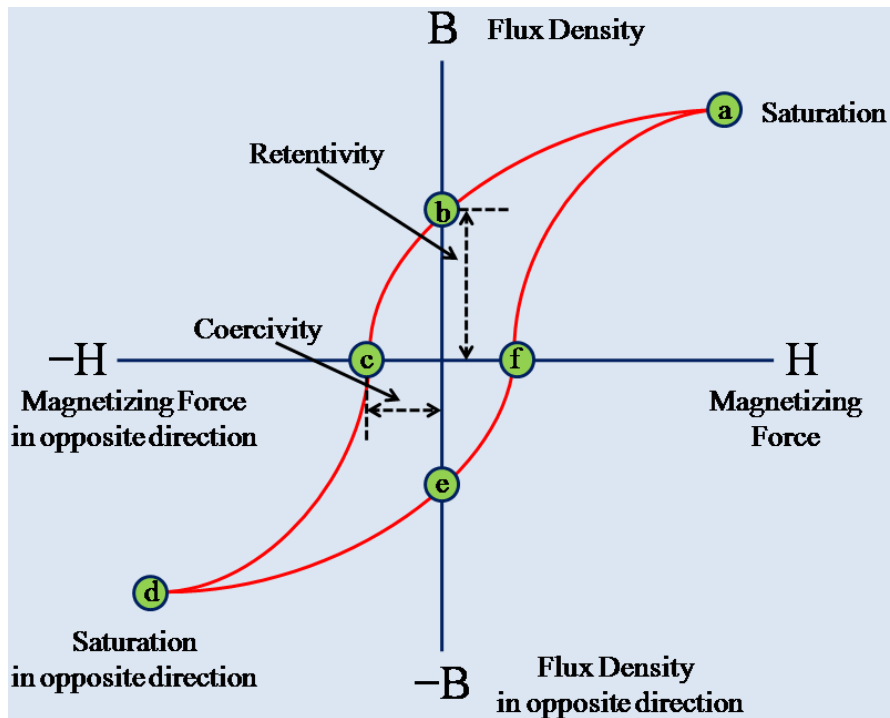


**Figure 1.1:** A typical hysteresis Loop

2. Residual Magnetism or Residual Flux – It is the remaining magnetization in a material at zero value of magnetizing force. Note that on magnetizing the material to saturation point, lasting magnetism and retentivity are the same. However, when the magnetization did not achieve the saturation point, the level of remaining flux might be lesser than the retentivity value.
3. Coercive Force - To influence the magnetic flux to come back to zero, the amount of magnetic field in reverse direction has to be applied. The value of H at point c on the hysteresis curve denotes the coercivity.
4. Permeability - A property of a material that characterizes the effortlessness with which a magnetic flux is set up in the segment.
5. Reluctance – This is the contradiction that a ferromagnetic material shows to the arrangement of a magnetic field. Reluctance is counterpart to the resistance in an electric circuit.

Ferrites have high magnetic permeability and hence can store large magnetic field in comparison to iron.

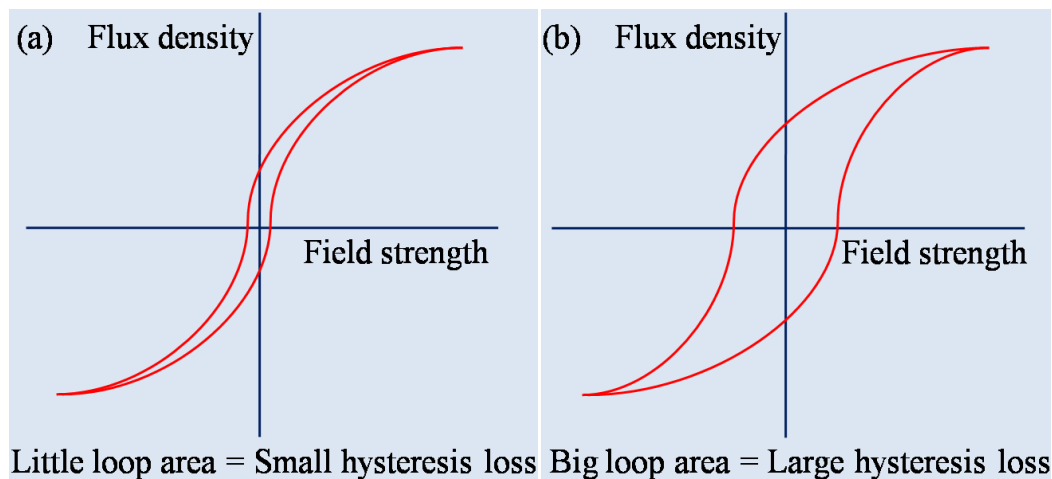


**Figure 1.2:** Hysteresis loop for (a) soft ferrite & (b) hard ferrite

## 1.2 Ferrites: history and development

The term ferrite is ordinarily used to depict a class of magnetic oxide compounds that involve iron oxide as a fundamental constituent. Some representatives of the ferrites are long known, even in Vedic period several centuries B.C. in India, as magnetic minerals [9]. The properties of magnet (loadstone) are well versed by staunch philosopher Sankara [10].

The history of magnetic minerals is quite old. This became possible due to the existence of a natural mineral called ‘magnetite’. Magnetite is an iron oxide ( $\text{Fe}_3\text{O}_4$ ). From the Greek word “Magnesia”, the word ‘Magnet’ is derived. The direction finding application has named magnetite as ‘Lodestone’, meaning ‘Waystone’. Much later, “De Magnete” was the first technical study of magnetism by William Gilbert (1540 - 1603). He recognized that earth is a giant magnet and the compass functions on this rationale.

Michel Faraday (1791 - 1867) has categorized all types of materials into diamagnetic and paramagnetic based on significant experimental studies. In 1819 Hans Christian Oersted observed during a practical that a magnetic compass needle is affected by an electric current in wire. Hertz and many others have then developed the new science of electromagnetism to enhance the experimental knowledge over traditional theoretical perceptions [11].

The discovery of ferrites in the beginning twentieth century and the later the theory of ferrimagnetism put forward by Louis Neel led in an upsurge of research and developments. This has caused potential to develop new materials for several applications.

In the old days the prerequisites of the magnetic hardware for electrical applications have been served by iron and its magnetic compounds. Be that as it may, with the entry of high frequency the great methods of chopping down the eddy current losses by utilizing a layered cover or iron powder cores were not any more powerful or cost productive. This comprehension has actuated a recovered enthusiasm for "magnetic insulators" as first depicted by S. Hilpert in Germany in 1909. This has promptly conceived the idea of consolidating high electric resistivity of oxides with needed magnetic qualities for high frequency applications.

Everywhere throughout the world, several labs have begun research to grow such materials, for example, by V. Kato, T. Takei, and N. Kawai in Japan (1930's) and by J. Snoek in Netherlands amid 1935-45. The basic fundamentals of practical ferrite materials have been established by Snoek. The theoretical understanding of ferrites has been put forward by Neel Theory of ferrimagnetism in 1948. Snoek has prepared the first functional modern ferrite [12, 13]. Snoek and Neel worked together and made a large impact in the research of ferrimagnetism. The unpaired electrons are responsible for the origin of magnetism. In ferrite lattice, cations are separated by oxygen anions ( $O^{2-}$ ). The oxygen anions have zero magnetic moment as they have entirely filled shells. The metal cations *e.g.*  $Ni^{2+}$  (d8),  $Zn^{2+}$  (d10) and  $Fe^{3+}$  (d5) of ferrites have 2, 0, and 5 unpaired electrons in outermost shells respectively and hence divalent nickel and trivalent iron have magnetic moment because of partially filled shells. On the other hand, in divalent  $Zn^{2+}$  ions the outermost shell is totally filled so gives diamagnetic characteristic.

A unique class of compounds consists of lanthanides and fast transition metals, like iron, chromium and manganese is ferrite [8, 14, 15]. Ferrites are hard and brittle, comparable nearly all other ceramics. There are different spinel ferrites with the chemical pattern  $AB_2O_4$ , where A and B constitute to a classification of metal cations, likewise including iron (Fe). A crystal lattice comprising of cubic close-packed (fcc) oxides ( $O^{2-}$ ) with A cations involving  $(1/8)^{th}$  of the tetrahedral locales and B cations possessing  $(1/2)$  of the octahedral sites represents spinel structure for ferrites. Further, if  $(1/8)^{th}$  of the tetrahedral sites are filled by B cation, so afterward  $(1/4)^{th}$  of the octahedral sites are filled by A cation and the other  $(1/4)^{th}$  by B cation and this type of structure is termed as inverse spinel structure. There are also the possibilities for mixed spinel structures in ferrites having formula  $[M^{2+}_{1-\delta}Fe^{3+}_{\delta}][M^{2+}_{\delta}Fe^{3+}_{2-\delta}]O_4$  is mixed ferrite, where  $\delta$  is the degree of inversion. In  $ZnFe_2O_4$  ferrite, octahedral sites are

occupied by  $\text{Fe}^{3+}$  and tetrahedral sites are occupied by  $\text{Zn}^{2+}$ . It is a case of ordinary spinel ferrite structure [16]. There are some hard ferrites, like barium ferrite ( $\text{BaFe}_{12}\text{O}_{19}$ ) and strontium ferrite ( $\text{SrFe}_{12}\text{O}_{19}$ ). The crystal structure of strontium ferrite and barium ferrite is hexagonal [17].

On the application part, with the arrival of high frequencies going up to the gigahertz range, the inductance has got more and more consideration in the design and studies of on-chip interconnect. The decreasing size of electronic devices has led to the growth of new devices having multilayer ferrite chip inductor (MLFCI) components. The conventional wire meandered inductors can only be reduced in size to a particular limit and the lack of magnetic shielding of wire meandered inductors leads to the development of MLFCI. These inductors are one of the significant elements for the modern electronics e.g. cellular phones, video cameras, notebook computers, hard and floppy drives etc. The chip inductor is manufactured by laminating ferrite film and internal metallic conductors (e.g. Ag) alternately and then co-firing to form the monolithic structure.

### **1.3 Types of ferrites**

#### **1.3.1 Soft ferrites**

Soft ferrites have small value of coercivity and they can be easily demagnetized.

Because of low coercivity of the material, magnetization can be authorized effortlessly in opposite direction without disseminating much energy as hysteresis lossess. Because of their low losses at high frequencies, soft ferrites are generally utilized in the centers of little transformers and inductors. Manganese-zinc ferrite, nickel-zinc ferrites are some usual soft ferrites [16]. The estimations of saturation magnetization and permeability of Mn-Zn ferrite is higher than Ni-Zn ferrite. Ni-Zn ferrites are more suited for frequencies over 1 MHz on the grounds that the resistivity of Ni-Zn ferrites is higher than the Mn-Zn ferrite.

#### **1.3.2 Hard ferrites**

Hard ferrites are hard to demagnetize and after magnetization process, hard ferrites have a high estimation of coercivity and remanence. Hard ferrites are utilized to made lasting ferrite magnets. Hard ferrites are likewise used to make magnets for a some of gadgets such as magnets of refrigerators, electric motors and loudspeakers *etc.* Permanent magnets have an essential characteristic of high coercivity. This means the materials have high resistance to become demagnetized. Permeability of permanent

magnet is very high. So these are additionally named as ceramic magnets. These are inexpensive and generally utilized in different household items. Hard ferrite magnets are generally made up of strontium carbonate, barium carbonate and iron oxide [18]. The mainly common hard ferrites are:

- **Strontium ferrites:** These ferrites are very much important and are used as host materials in recording media, micro-wave devices, magneto-optic media and also play a lead role in electronic industry and telecommunication [17].
- **Barium ferrites:** Permanent magnet applications are the regular advantages of these ferrites [19]. Properties like stability against moisture make these ferrites as corrosion-resistant. These ferrites have found applications in subwoofer magnets. These ferrites are also used in magnetic stripe cards and magnetic recording.
- **Cobalt ferrites:** Cobalt ferrites owing to their few special properties (*i.e.* reasonable saturation magnetization nearly 80 emu/g and high coercivity approximately 5400 Oe), are used in some media for magnetic recording [20].

#### 1.4 Classification of ferrites based on crystal structure

Ferrimagnetic materials are ferrites and they can be more categorized into four types according to their crystal structure. These types of ferrites are

(1) Spinel ferrites: A spinel ferrites are given by the formula;  $M^{2+}Fe_2^{3+}O_4$ . Spinel ferrites contains largely iron oxide which is a ferromagnetic material and it is deduced from magnetite [ $Fe^{2+}O \cdot Fe_2^{3+}O_3$ ]. In spinel ferrite formula,  $M$  is a divalent metal cation like manganese ( $Mn^{2+}$ ), Zinc ( $Zn^{2+}$ ), copper ( $Cu^{2+}$ ), cobalt ( $Co^{2+}$ ), magnesium ( $Mg^{2+}$ ), cadmium ( $Cd^{2+}$ ), nickel ( $Ni^{2+}$ ) etc. Trivalent metal cations ( $La^{3+}$ ,  $Al^{3+}$ ,  $Gd^{3+}$ ,  $Cr^{3+}$ ,  $Nd^{3+}$ ,  $In^{3+}$ , etc) may be used to replace trivalent  $Fe^{3+}$  ions. Ionic radii of the replacing ion should be among 0.5 Å to 1.0 Å in all cases of proper substitution. Spinal ferrites generally, exhibits cubic crystal structure.

(2) Orthoferrites: Orthoferrites are given by the formula;  $RFeO_3$ . In orthoferrite formula,  $R$  represents to atleast one rare-earth elements. An orthorhombic crystal structure among a space group Pbnm has been revealed by orthoferrites and generally shows weak ferromagnetic behaviour. Dysprosium orthoferrite ( $DyFeO_3$ ) and lanthanum orthoferrite ( $LaFeO_3$ ) are two common examples of orthoferrites.

(3) Magneto-plumbite ferrites: These types of ferrites have are given by the formula;  $MFe_{12}O_{19}$ . In magneto-plumbite ferrite formula,  $M$  represents divalent cation ( $Sr^{2+}$ ,  $Ba^{2+}$ ,  $Pb^{2+}$ ) having big ionic radius. Hexagonal structure has been revealed by magneto-plumbite ferrites.

(4) Garnet ferrites: These types of ferrites have general formula;  $R_3^{3+}Fe_5^{3+}O_{12}$ . In garnet ferrite formula,  $R$  represents a rare earth cation (gadolinium ( $Gd^{3+}$ ), dysprosium ( $Dy^{3+}$ ), yttrium ( $Y^{3+}$ ) samarium ( $Sm^{3+}$ ), etc). Cubic structure has been revealed by these type of ferrites. Trivalent cations ( $Cr^{3+}$ ,  $In^{3+}$ ,  $Al^{3+}$ , etc) may be used to substitute  $Fe^{3+}$  ions in such ferrites.

### 1.5 Structure of spinel ferrite

The spinel structure has been first found out by Bragg and Nishikawa in 1915 [21]. The ideal structure is formed by a cubic close-packed (fcc) arrangement of oxygen atoms, in which  $(1/8)^{th}$  of the tetrahedral and  $(1/2)$  of the octahedral interstitial positions are filled by cations. The tetrahedral positions and the octahedral sites have been denoted as A sites and B sites respectively. The unit cell of spinel ferrite holds eight formula units (molecules) of  $(A)[B_2]O_4$ . In a unit cell 32 oxygen ions are from cubic close-packed structure and leaving 96 accessible interstitial sites.

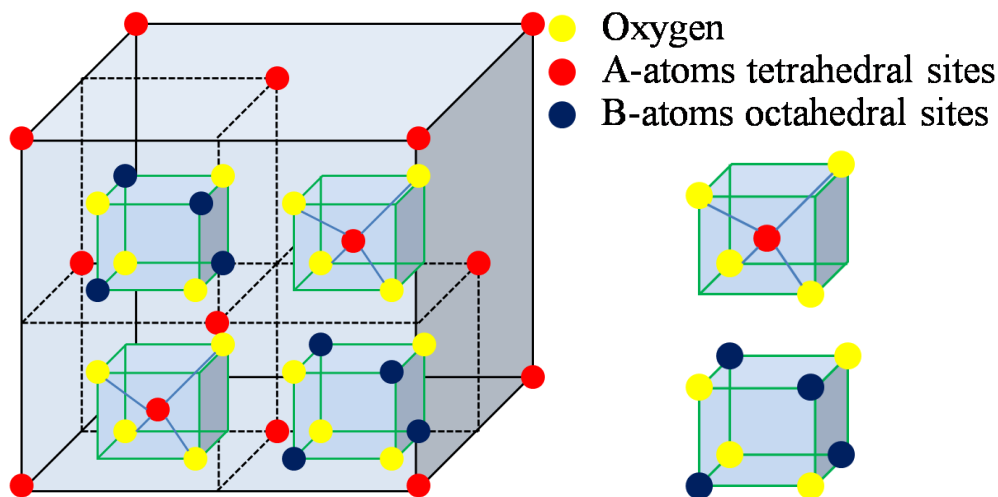


**Figure 1.3:** Unit cell structure of spinel ferrite

From these 96 interstitial sites, 64 are tetrahedral sites (also termed as A-sites) and 32 are octahedral sites [also termed as B-sites]. The A-sites are fenced by four oxygen

ions and B-sites are fenced by six oxygen ions. The organizations of the ions in an ideal ferrite are demonstrated in figure 1.3

## 1.6 Classification of spinel ferrites

Spinel ferrites are categorized into three classes as;

- i) Normal spinel ferrites: In the ordinary spinel ferrites, the tetrahedral destinations are filled by just the divalent metal ( $M^{2+}$ ) ions and octahedral locales are filled through trivalent metal ( $M^{3+}$ ) ions. Case of this ferrite is zinc ferrite ( $ZnFe_2O_4$ ).
- ii) Inverse spinel ferrites: In the inverse spinel ferrites, 8 out of 16 trivalent ions fill the A sites and the B sites are filled by some  $M^{2+}$  ions and left over  $M^{3+}$  ions. Case of this ferrite is nickel ferrite ( $NiFe_2O_4$ ).
- iii) Mixed spinel ferrites: In these ferrites, both A sites and B sites are filled by  $M^{2+}$  ions and  $M^{3+}$  ions. Cases of these ferrites are nickel-zinc ferrites and magnesium-zinc ferrites. The portions which can impact the constitution of the metal ions over the A sites and B sites are; 1) electronic configuration and ionic radii of metal ions, and 2) the electrostatic energy of the spinel lattice. Even though there occur a large number of possible combinations for ferrites. The manganese-zinc, manganese-magnesium and nickel-zinc ferrites are the three main commercial ferrite families. As core materials for inductance coils and transformers up to 1MHz, Mn-Zn ferrites are advantageous. Mn-Mg ferrites are employed for microwave applications. Ni-Zn ferrites are employable at high frequencies as well as low frequencies. Ni-Zn ferrites are found to be the best multipurpose ferrites and have been extensively studied owing to their several applications. Widespread range of applications in the frequency range starting from low to very high (Microwave frequencies) are dealt by these three versatile mixed ferrites.

## 1.7 Literature survey of spinel ferrites

### 1.7.1 Lithium ferrites

Lithium is a monovalent ion and fills the octahedral (B) sites in association with  $Fe^{3+}$  ion in the crystal lattice. The cation arrangement of lithium ferrite having the chemical composition (inverse spinel) has been first showed by Braun [22]. The divalent ion in this ferrite has been expressed as composite ion. The low loss lithium

ferrite has been reported by Collins *et al.* in 1971 [23]. Various researchers have reported the properties of lithium ferrites [24-26].

Hanif *et al.* examined the consequence of sintering temperature on structural as well as dielectric characteristics of lithium nanoferrites doped with rare earth prepared by simplified sol-gel method for sensing applications [24]. The spinel structure has been observed using XRD technique. An increase in the crystallite size (22 nm to 61 nm) up to a sintering temperature 750°C and then crystallite size decreases (44 nm) for a sintering temperature 800°C has been mentioned. The diminishing in lattice constant with increment in sintering temperature has been accounted for. Spherical shape of particles has been found from SEM characterization. A decrease in dielectric constant along with AC electrical conductivity with the raise in sintering temperature has been reported.

Sawant *et al.* examined the aftereffects of cobalt doping on the structural and magnetic characteristics of lithium ferrite arranged via auto-combustion strategy [25]. The spinel structure of prepared samples has been reported after analyzing XRD spectra. There is nearly no change in the crystallite size and an increase in lattice constant with raise in  $\text{Co}^{2+}$  content has been described. From SEM characterization, the morphology of particles has been mentioned to be of cubic and spherical shapes for all prepared samples. Increase in saturation magnetization (140.1 emu/g), coercivity (714.05 Oe) and remnant magnetization (49.4 emu/g) up to 0.3  $\text{Co}^{2+}$  doping and then a decrease in the mentioned magnetic properties has been observed for higher  $\text{Co}^{2+}$  doping.

Gilani *et al.* revealed the impact of praseodymium (Pr) doping on structural and magnetic characteristics of LiCo ferrites prepared by micro-emulsion course for high density storage applications [26]. Establishment of spinel structure has been remarked on XRD characterization. With Pr doping, a trend of increase in particle size (53 nm to 106 nm) has been reported for all the prepared samples. The magnetic properties viz. coercivity, retentivity and saturation magnetization has been reported to generally decrease in comparison to undoped sample.

### **1.7.2 Magnesium ferrites**

Magnesium ferrite ( $\text{MgFe}_2\text{O}_4$ ) is a soft ferrite with spinel structure and n-type semiconducting behaviour having many applications in sensors, heterogeneous catalysis, magnetic technologies and adsorption [27-30]. Various researchers have studied and reported the properties of magnesium ferrites [27-30].

Hussein *et al.* have analyzed the magnetic and structural outcomes of Mg - ferrites synthesized by EDTA supported sol–gel reaction [27]. XRD characterization of prepared samples has affirmed the development of two spinel structures relying on the calcination temperature (400 °C to 600 °C). Increment in crystallite size with enhance in calcination temperature (400 °C to 600 °C) has been accounted for. Pure superparamagnetic behaviour of sample calcined at 400 °C has been observed using VSM results. The change in magnetic properties with the variation in thermal behaviour, cation distribution and phase concentration has been reported.

Choodamani *et al.* examined the impact of Zn doping on the structural, magnetic and electrical characteristics of Mg - ferrite prepared through solution combustion route [28]. Spinel structure has been reported on analyzing XRD spectra for all samples. Up to 0.75 zinc content in magnesium ferrites, there is an increase in crystallite size (53 nm to 80 nm) and then crystallite size decreases for 1.00 zinc content. Morphology obtained from SEM characterization shows homogeneous grains having polyhedral structure for all prepared samples. Usual dielectric conduct (*i.e.* with raise in frequency there is an increase in electrical conductivity) has been reported. Lowest value of AC conductivity, dielectric constant and dielectric loss tangent has been observed for 0.50 zinc content. Using VSM characterization, high saturation magnetization (46.97 emu/g) and low coercivity (2.78 Oe) has been remarked at 0.50 zinc content.

Zaki *et al.* reported the outcome of Cu<sup>2+</sup> doping on structural, magnetic and dielectric characteristics of magnesium zinc ferrite prepared by using co-precipitation technique [29]. Cubic spinel structure has been affirmed from XRD analysis. Spinel structure has additionally been affirmed from IR spectra. A gain in saturation magnetization on raising the Cu<sup>2+</sup> amount up to 0.2 is reported and a decrease has been found for Cu<sup>2+</sup> content above 0.2.

Nasari *et al.* described the consequences of calcination on the structural and magnetic characteristics of magnesium ferrites devised through a thermal-treatment method [30]. Using XRD characterization the crystallite size has been found to increase (7 nm to 12 nm) with raise in calcination temperature (673 K to 973 K). TEM characterization has shown an increase in particle size (5 nm to 8 nm) with raise in calcination temperature (673 K to 973 K). With raise in calcination temperature (673 K to 973 K), the lattice parameter has shown an increasing trend. FTIR characterization has shown two absorption bands close to 400 cm<sup>-1</sup> and 560 cm<sup>-1</sup> affirms the formation of metal ion-oxygen bond at octahedral and tetrahedral sites respectively.

Superparamagnetic behaviour has been reported for all calcined samples (673 K to 973 K) using VSM characterization.

### 1.7.3. Magnesium – Manganese ferrites

Mg–Mn ferrites are soft ferrites with common formula  $MFe_2O_4$  (where divalent metal ion is represented by M) and having spinel structure. The high resistivity and small eddy current losses of Mg–Mn ferrites are worthy for high-frequency applications [31-34]. Several researchers have analyzed and reported the properties of Mg- Mn ferrites [31-34].

Kumar *et al.* observed the influence of gadolinium ( $Gd^{3+}$ ) doping on structural and magnetic characteristics of Mg–Mn nanoferrites processed by self-ignited solution combusting route [31]. Spinel structure has been reported for all the prepared samples using XRD characterization. Superparamagnetic nature has been observed for all prepared samples using VSM characterizations. An expansion in the crystallite size (13.4 nm to 16.1 nm) and lattice parameter (8.35 Å to 8.38 Å) has been specified with an increment in  $Gd^{3+}$  concentration for every studied sample. The saturation magnetization has been accounted for to diminish with increment in  $Gd^{3+}$  concentration for every studied sample.

Modi *et al.* examined the consequences of magnesium doping on the structural and magnetic characteristics of manganese ferrites developed by co-precipitation method [32]. Spinel structure is affirmed from XRD characterization of annealed samples. The crystallite size using XRD characterization has been reported to decrease (38 nm-25 nm) with an increase in magnesium content. The particle size using TEM characterization has been mentioned to decrease (40 nm to 27 nm) with increase in magnesium content. Superparamagnetic behaviour has been observed at room temperature (300 K) for as prepared samples using Mossbauer spectra.

Baba *et al.* have described that Mg-Mn ferrites hold high resistivity ( $>10^8$  ohm.cm) [33]. The discovery of magnetic garnets with resistivity in the range of  $>10^9$  ohm.cm has substituted the role of Mg-Mn ferrites in variety of microwave devices. With temperature Mg-Mn ferrites hold a low Curie temperature and poor stability of magnetic properties. The remanence and squareness ratios in garnets have been reported low in comparison to the values obtained for Mn-Mg ferrites. Garnets are suitable for permanent magnets whereas Mn-Mg ferrites are appropriate materials for circulators, switches, phase shifters and isolators.

Heiba *et al.* checked the consequences of cobalt doping on structural and magnetic characteristics of magnesium–manganese ferrite developed by citrate precursor technique [34]. Using XRD characterization, single phase spinel structure is remarked for all prepared samples. An increment in saturation magnetization and coercivity is reported on an enhancement in cobalt content up to 0.3 using VSM characterization whereas above 0.3 cobalt content saturation magnetization and coercivity decreases.

#### **1.7.4 Nickel-Zinc ferrites**

This class of soft ferrites has been studied owing to its high resistivity in comparison to other soft ferrites like Mg-Zn [28]. Owing to the high resistivity values, Ni-Zn ferrites are materials of selection for devices operating in the range 1 MHz to several hundred megahertz. Various researchers have synthesized a large number of nickel-zinc materials and reported them for different properties [35-38].

Morrison *et al.* studied the structural and magnetic characteristics of Ni-Zn ferrite prepared by using reverse micelle technique at room temperature [35]. Pure spinel crystal structure of prepared sample has been confirmed from XRD characterization. Magnetism has been reported to decrease with the addition of diamagnetic zinc in Ni-Zn ferrite.

Verma *et al.* have analyzed the structural and magnetic properties of Ni-Zn ferrites prepared by the citrate precursor method [36]. Pure spinel structure of prepared samples has been confirmed from XRD characterization. Samples sintered at 1200°C have shown better characteristics like Curie temperature, coercivity and saturation magnetisation.

Ghodake *et al.* have examined the consequences of cobalt doping on the structural and magnetic characteristics of Ni-Zn ferrites processed by citrate-nitrate combustion route [37]. Pure spinel structure of all prepared samples has been observed from XRD characterization. The grains have been reported to be agglomerated from SEM characterization. The magnetic behaviour studied using VSM characterization shows an increase in saturation magnetization, coercivity and retentivity on cobalt doping. The real and imaginary part of initial permeability show a decrease whereas loss factor shows an increase with enhancing the cobalt doping in Ni–Zn ferrites.

Sun *et al.* described the consequences of sintering temperature on Ni-Zn ferrites prepared by solid-state reaction technique [38]. Pure spinel structure for all prepared

samples has been observed from XRD characterization. Using SEM characterization an increase in the growth of grains has been observed with the rise in sintering temperature.

### **1.8 Applications of magnetic materials: ferrites**

The oldest application of natural magnetite (i.e. ferrite) was to identify the direction with the help of compass. For the magnetic applications, natural ferrite is not a good choice due to its poor magnetic properties. The ferrites showing commitment towards commercial applications have been developed by Prof. Takei and Prof. Kato in Japan. Later Snoek and his collaborators in Holland have developed commercial soft ferrites. In USA, Schonberg has developed microwave ferrites and digital memories. For the first time, the large scale commercial application of ferrites are in television (T.V.) tube deflection yokes. With the progress in the synthesis methods of ferrites, the research and development of ferrites have took an unexampled importance. With the advent of new practical applications like communication satellites, radars, computers and memories, an equating increase in an end user market *i.e.* T.V., recorder and internet etc. has emerged. With change in market demands, from analog to digital there is an emergence of high frequency devices. Another potential demand for ferrites has emerged in automobile sector.

Ferrites have also found applications in direct current circuits. The permanent magnets made of ferrite materials are being utilized in microphones, loudspeakers and to a great extent in movable electric motors. In direct current circuits ferrite materials are being employed as high pitch noise filters. The low saturation magnetization and cost has driven the ferrites to be used in direct current power supplies particularly in desktop PC and integrated circuit applications. The electronic devices which employ transistor circuits requires controlled direct current power supplies at reasonably modest voltages (5 V - 15 V). These regulated dc power supplies are of two types *i.e.* linear type and switching type. The linear type dc power supply comprises of a transformer, a rectifier and an output choke to bring down the remainder alternating current wavelet. The ferrites are used in the transformer and inductor region of choke. On the other hand, the switching type power supply produces a high frequency square wave from 50 Hz to 60 Hz alternating current by employing transistors, transformers etc. to obtain needed voltage at high frequency. In this case as the transformer and choke

works at high frequency so ferrite materials which are employed in linear type power supplies are to be replaced with high frequency ferrite materials.

Ferrites are also employed in audio frequency applications. These audio frequency applications (20 Hz to 20 kHz) include devices like speakers, microphones etc. The enhanced frequency of these audio frequency devices above the utility frequencies, *i.e.* 50 Hz to 60 Hz, demands likewise ameliorated ferrites. In the frequency domain  $10^2$  kHz to  $10^2$  MHz the main electronic activities adds the fields of telecommunication *i.e.* radio, telephone and TV. These frequency domains are well covered by ferrites along with high quality and low energy losses.

Ferrite materials are an important part of digital data storage *i.e.* computer memories and have also fulfilled the purpose of audio and video recording. Moreover, the raising miniaturization of various parts of computers and recording devices entails to the development of ferrites in nano dimensions. In magnetic recording ferrites are generally used. The read – write head ferrite material having ability to work at moderately high frequencies for recording applications requires low-coercivity and high permeability. For analog recording, the common option among magnetic materials is soft ferrites. Further the recording environment essentially have sufficiently low coercivity to be written on, sufficiently high retentivity to hold out recording for an indefinite time against local degaussing fields and adequately high magnetization to render a decipherable signal to the read head. The common option for audio recording is  $\gamma$ -Fe<sub>2</sub>O<sub>3</sub> particles in an adaptable matrix.

Ferrites are also finding usage in magnetic shielding. Many electronic gadgets should be protected from undesirable ac and dc attractive fields, and permalloy-type composites are utilized for this reason. For best outcomes, the protecting material must be given a high-temperature annealing subsequent to being framed into its final shape. Ferrites are finding them compatible in this regard.

Magnetic materials particularly ferrites have been used in fluxgate magnetometers. These are instruments for exact estimation of fields practically identical in vastness to the Earth's field. They are utilized for geomagnetic overviews, archeological studying, and as sensors in input frameworks to drop the Earth's field in a test space. Different elaborations of the fluxgate magnetometer configuration have been proposed and constructed, some of which utilize alternate recognition frameworks. All are restricted to the estimation of low fields, commonly 1 or 2 Oe (80 or 160 A/m) utmost.

### 1.9 Mn-Zn spinel ferrites and their applications

Large saturation magnetization, biocompatibility, large electrical resistance and magnetic permeability are some of the gifted properties which makes Mn-Zn ferrite most adaptable among spinel ferrites [39-51]. Moreover, various synthesis techniques such as co-precipitation, auto-combustion, ball milling and hydrothermal *etc.* have the influence on characteristics of Mn-Zn ferrite [52-78]. In the last decade the synthesis and characterization of doped Mn-Zn ferrites with spinel structure has earned an impulse for various applications. To ameliorate the characteristics of doped Mn-Zn ferrites, the dimensions of ferrites are moved from bulk to nano regime. Nanoparticles of Mn-Zn ferrites are broadly utilized in ferrofluid displays, magnetic resonance imaging, drug delivery schemes and medical indicatives *etc.* [78,79]. Further, the synthesis technique, temperature of sintering, elemental composition of sample, ionic radii and distribution of cations over different sites are some of the factors on which structural, electrical and magnetic characteristics of spinel ferrites depend [80-87]. Effect of doping on the structural, magnetic, electrical and some other characteristics of Mn-Zn ferrites are investigated by several authors [47,70,88-91,99,100].

Effect of  $\text{Cr}^{3+}$  doping on structural, magnetic and dielectric characteristics of Mn-Zn ferrites have been reported by Mansour *et al.* [88]. They have reported an increase in crystallite size with  $\text{Cr}^{3+}$  doping up to  $x=0.04$  and thereafter it decreases. Superparamagnetic nature due to the soft ferrimagnetic character has been shown in all the samples. Maximum values of saturation magnetization, a.c. conductivity and dielectric parameters are reported at  $x=0.04$   $\text{Cr}^{3+}$  doping.

Change in structural, magnetic and electrical properties have been analyzed by Angadi *et al.* for ( $\text{Sm}^{3+}$ -  $\text{Gd}^{3+}$ ) doping in Mn-Zn ferrites [89]. They have observed an increment in crystallite size and a decrease in lattice parameter as well as strain with increase in ( $\text{Sm}^{3+}$ -  $\text{Gd}^{3+}$ ) doping content. A decrease in retentivity, coercivity and saturation magnetization are described on an increment in ( $\text{Sm}^{3+}$ -  $\text{Gd}^{3+}$ ) doping concentration.

Jalaiah *et al.* [70] reported structural, electrical and magnetic characteristics of Mn-Zn ferrites with  $\text{Ni}^{2+}$  doping. They have described that the crystallite size increases with  $\text{Ni}^{2+}$  doping up to  $x= 0.06$  and thereafter it decreases. Lattice parameter has been reported to increase up to  $x= 0.09$  and then decreases with further  $\text{Ni}^{2+}$  doping. Coercivity has increased with  $\text{Ni}^{2+}$  doping. Saturation magnetization first shows a decrease up to  $x= 0.09$  and then increases. Maximum magnetic moment has been

reported for the maximum  $Ni^{2+}$  doping ( $x= 0.15$ ) content. The values of dielectric constant and dielectric loss tangent have been described to decrease with  $Ni^{2+}$  doping in *Mn-Zn* ferrites.

Chandrasekaran *et al.* have reported structural and electrical properties of Al doped Mn-Zn ferrites prepared by ceramic double sintering method [90]. XRD study has affirmed the constitution of single phase spinel structure for every studied sample. A decreased in the measures of lattice constant with an increment in Al doping is on account of substitution of bigger  $Fe^{3+}$  ions with small  $Al^{3+}$  ions. In FTIR spectra, peaks from  $400\text{ cm}^{-1}$  to  $650\text{ cm}^{-1}$  have been reported which confirms the origination of metal ions- oxygen bonds at tetrahedral and octahedral sites for Al doped Mn-Zn ferrites.

Anwar *et al.* [91] examined the result of cobalt doping on structural and magnetic characteristics of Mn-Zn nano ferrites processed by utilizing polyethylene glycol-aided co-precipitation and hydrothermal techniques. All peaks in XRD patterns affirm the establishment of pure spinel phase. Hydrothermal technique has shown comparatively spherical, uniform and homogenous nanoparticles as observed from SEM characterization. For samples developed by hydrothermal technique, average crystallite size calculated lie in  $8\text{ nm} - 18\text{ nm} \pm 2\text{ nm}$  range as compared to co-precipitation technique ( $8\text{ nm} - 23\text{ nm} \pm 2\text{ nm}$ ). Average particle size computed from TEM ( $15\text{ nm} - 25\text{ nm} \pm 5\text{ nm}$ ) is in good agreement with the average crystallite size calculated using Scherer formula. Large measures of saturation magnetization  $65\text{emu/g}$  at  $x = 0.25$  cobalt doping has been observed for hydrothermal processed samples.

Szczygieł *et al.* have accounted the structural and magnetic properties of Mn-Zn ferrite prepared by sol-gel autocombustion synthesis technique [92]. Using Scherer formula crystallite size estimated is  $65.9\text{ nm}$  and  $40.8\text{ nm}$  from the (311) peak. In FTIR analysis, they have observed bands at frequencies near to  $540\text{ cm}^{-1}$  indicating the establishment of metal ions oxygen bonds in tetrahedral and octahedral sites. As compare to bulk material the observed saturation magnetization ( $112\text{ emu/g}$  and  $95.7\text{ emu/g}$ ) is lesser at 2 K.

Baykal *et al.* have analyzed structural and magnetic characteristics of triethylene glycol encapsulated Mn-Zn ferrite nanoparticles processed by thermal decomposition [93]. FTIR characterizations reveal that samples show substantial metal cation - oxygen absorption bands around  $550\text{ cm}^{-1}$ . Morphology of nanoparticles shows homogeneous arrangement nanoparticles having spherical configuration along with a small degree of aggregation. This aggregation has been reported due to the existence of

magnetic interactions between the nanoparticles. At room temperature, superparamagnetic nature has been reported for the ferrite nanoparticles. The saturation magnetization has been reported by extrapolation of  $M$  vs  $1/H$  plot to  $1/H = 0$ . For a Zn content of 0.4 in Mn-Zn ferrite nanoparticles a maximum of saturation magnetization has been reported.

Kotsikau *et al.* [94] studied the structural and magnetic characteristics of Mn-Zn ferrites prepared by spray pyrolysis technique. Prepared sample have nanoparticles with an average diameter  $\sim 7$  nm. SEM results show spherically shaped particles for prepared samples. In FTIR analysis, Kotsikau *et al.* [94] have mentioned bands at frequencies (420, 430 and 430)  $\text{cm}^{-1}$ , (551, 571 and 559)  $\text{cm}^{-1}$  showing the establishment of metal ions oxygen bonds at octahedral and tetrahedral sites respectively. Curie temperature has been mentioned to be 375 K - 380 K.

Mohamed *et al.* [95] accounted the structural and magnetic characteristics of Al doped  $\text{Mn}_{0.5}\text{Zn}_{0.5}\text{Fe}_2\text{O}_4$  ferrite synthesized by sol-gel technique. XRD and FTIR results support the pure cubic spinel structure. The crystallite size has been given in range 4.5 nm to 10.1 nm. The very fine particle size of all processed samples has been supported from TEM results. In FTIR study, the absorption bands from 565  $\text{cm}^{-1}$  – 590  $\text{cm}^{-1}$  and 445  $\text{cm}^{-1}$  – 480  $\text{cm}^{-1}$  for all prepared samples supports the establishment of spinel structure of ferrites. Superparamagnetic behaviour has been reported for all prepared samples.

Zhang *et al.* [96] examined the structural and magnetic characteristics of cobalt doped Mn-Zn ferrites devised by co-precipitation route [96]. They have found pure spinel phase of undoped Mn-Zn ferrites at 1150 °C. Using XRD results it is noted that there is a decrement in crystallite size with an increment in cobalt content up to 1.0 % (24.8 nm) and then increases (27.0 nm). Almost spherically shaped along with some agglomeration fine nanoparticles have been observed from TEM results. Superparamagnetic behaviour is revealed for entire cobalt added samples (0 % to 2 %) using VSM characterization.

Gabal *et al.* [97] studied the consequences of aluminium doping on the structural and magnetic characteristics of Mn-Zn ferrites processed by sol-gel auto-combustion technique. The crystallite size figured out using Scherrer formula has been witnessed to decrease with an increase in aluminium doping (*i.e.* 38 nm to 5 nm). In FTIR spectra, two foremost absorption bands at approximately 600  $\text{cm}^{-1}$  and 400  $\text{cm}^{-1}$  supports the spinel ferrite structure of all processed samples. With the increment in aluminium

amount there is a continuing reduction in the saturation magnetization as reported using VSM.

Kumar *et al.* [98] observed the result of indium doping on structural characteristics of Mn-Zn ferrites devised by oxalate co-precipitation route [98]. Increase in crystallite size, lattice constant and X-ray density has been observed with increase in indium ( $\text{In}^{3+}$ ) quantity in Mn-Zn ferrites. From SEM characterization, the morphology of nanoparticles shows uniform and loosely agglomerated spherically shaped particles.

Kumar *et al.* [47] examined the structural and magnetic characteristics of indium ( $\text{In}^{3+}$ ) doped manganese-zinc nano ferrites devised by oxalate co-precipitation technique [47]. Pure spinel structure has been confirmed using XRD characterization. An increase in crystallite size up to  $y = 0.070 \text{ In}^{3+}$  ions doping and thereafter it decreases for  $y = 0.100 \text{ In}^{3+}$  ions doping in Mn-Zn ferrites has been noted. From the VSM data analysis it has been shown that at lower concentration of  $\text{In}^{3+}$  ions there is an increase in saturation magnetization whereas for higher concentration it decreases significantly.

Naik *et al.* [99] have examined the structural as well as magnetic characteristics of Mn-Zn ferrites after  $\text{Nd}^{3+}$  ion doping. Naik *et al.* have mentioned a decrement in crystallite size and an increment in lattice constant with  $\text{Nd}^{3+}$  doping. The saturation magnetization and magnetic moment first found to be decreased with  $\text{Nd}^{3+}$  doping (up to  $x=0.04$ ) in Mn-Zn ferrites and then it increased.

Yadav *et al.* [100] reported the structural as well as magnetic characteristics of  $\text{Sm}^{3+}$  doped Mn-Zn ferrites. There is a decrement in crystallite size and increment in lattice parameter as well as strain with enhance in  $\text{Sm}^{3+}$  doping. With an increment in  $\text{Sm}^{3+}$  content a growth in saturation magnetization has been described. Superparamagnetic (at  $x = 0, 0.1$ ) and ferromagnetic (at  $x = 0.3, 0.5$ ) behaviour has been observed by Yadav *et al.* [100] for investigated samples.

### 1.10 Motivation of thesis work

Extensive research work has been executed on Mn-Zn ferrites [101] motivated especially by their soft magnetism. At high frequencies Mn-Zn ferrites have distinguished properties *e.g.* high starting magnetic permeability, high electrical resistance and low power losses. On the manufacturing scale, Mn-Zn ferrites are created by the exemplary ceramic technique. These Mn-Zn ferrites are usually utilized

in transformer cores, microwave appliances, radio frequency coils, computer memory chips, antenna rods and electromagnetic interference devices. The structural and magnetic attributes of Mn–Zn spinel nanoferrites are governed through dopant, sintering temperature, synthesis technique etc. The possible usages of Mn–Zn nano ferrites are in the disciplines of biomedicine as magnetic carriers or bio-separators, and gas sensors, have been looked into a great extent. The novel spheres of application encourage the search for novel synthesis routes and assumptions.

Large saturation magnetization, biocompatibility, large electrical resistance and magnetic permeability are some of the gifted properties of Mn-Zn ferrite which makes them most adaptable among spinel ferrites [39-51]. When the materials are explored in nano regime their properties has been observed to enhance by many folds. The large surface area and good interaction with different biological entities are the main advantages of magnetic nanoparticles in biomedical research [102-104].

Amongst magnetic nanoparticles, superparamagnetic nanoparticles have shown their competence in biomedical usages [105-107]. At room temperature, superparamagnetic nanoparticles have high saturation magnetization and the absence of both remanence and coercivity makes them appropriate for several biomedical usages like hyperthermia, biosensors bio-imaging, and drug delivery [108-112]. The monodispersity, core nature and size of the magnetic nanoparticles are responsible for the superparamagnetic behaviour [113].

The substitution with different lanthanide ( $RE^{3+} = La^{3+}, Gd^{3+} \& Nd^{3+}$ ) ions on the tetrahedral (A) or octahedral (B) sites of  $Fe^{3+}$  ions may have remarkable outcome on the magnetic properties of spinel ferrites. The magnetism in ferrites is controlled by the spin coupling of the  $d$ - electrons of  $Fe^{3+}-Fe^{3+}$  interaction. The insertion of lanthanides ( $RE^{3+}$ ) in the spinel lattice may contribute to  $RE^{3+}-Fe^{3+}$  interactions which may further modify the magnetic behaviour of lanthanide ion doped *Mn-Zn* spinel ferrites. Since the interactions between  $RE^{3+}-RE^{3+}$  ions are indirect and are weak in nature in comparison to  $d-d$  interactions [114,115]. Moreover, the  $RE^{3+}$  ( $= La^{3+}, Gd^{3+} \& Nd^{3+}$ ) ions have larger radii and also bear a stable valence (3+) state. Further, in literature it has been reported that the doping of lanthanides at higher concentration in soft spinel ferrites leads to the development of secondary phase [116,117]. Synthesis technique and after synthesis treatments (like sintering temperature etc.) have also major impression on the various characteristics of soft spinel ferrites [24,27,30,55,67]. Co-precipitation synthesis technique is one of the best and suitable processing

techniques to prepare magnetic nanoparticles due to its advantages like simple experimental set up, inexpensive, less time consumption and various parameters (pH level, temperature etc.) to control the particle size [118].

Considering the above mentioned points, the lanthanide ( $RE^{3+} = La^{3+}, Gd^{3+} \& Nd^{3+}$ ) doped  $Mn_{0.5}Zn_{0.5}Re_xFe_{2-x}O_4$  ( $x=0, 0.025, 0.050, 0.075, 0.1$ ) spinel ferrites have been synthesized via co-precipitation technique and are investigated for structural, morphological and magnetic characteristics. The X-ray diffraction (XRD), Fourier transform infrared spectroscopy (FTIR), energy dispersive X-ray spectroscopy (EDS), field emission - scanning electron microscopy (FE-SEM) and vibration sample magnetometer have been employed to investigate the structural, morphological and magnetic characteristics of synthesized samples.

### 1.11 Outline of thesis

This thesis has been divided into six chapters. Chapter 1 includes the general introduction of magnetic materials and their classification, ferrites: history and development, soft ferrites and hard ferrites. The literature survey of soft ferrites considering structural, morphological and magnetic properties has also been included in this chapter. A particular stress has been laid on the Mn-Zn spinel ferrites and their applications and finally the motivation behind this thesis work has been described.

In chapter 2, the methods for the synthesis of ferrites along with their characterizations are presented. A short theoretical background has also been given for the various characterization techniques.

Chapter 3 contains the role of sintering temperature to determine the physical properties of the spinel nano ferrites. In this chapter, the synthesis and characterizations (XRD, FTIR and FE-SEM) of  $Mn_{0.5}Zn_{0.5}Fe_2O_4$  nano ferrites have been described for the optimization of sintering temperature.

Chapter 4 includes the importance of dopant in establishing a property-composition relation. In this chapter, the addition of lanthanides ( $La^{3+}, Gd^{3+} \& Nd^{3+}$ ) to Mn-Zn cubic spinel ferrites for the structural and morphological study has been described. XRD, FTIR and FE-SEM characterization techniques have been employed for the structural and morphological study.

Chapter 5 contains the magnetic properties of lanthanides ( $La^{3+}, Gd^{3+} \& Nd^{3+}$ ) doped Mn-Zn spinel ferrites. The chapter also contains the proposed cation distribution

for the investigated spinel ferrites and the viability of distribution is utilized to explain the magnetic properties.

Chapter 6 presents the general discussion and summary of the work done. The future scope of the thesis work has also been included in this chapter.

General chapters, *i.e.* introduction, experimental details and summary are applicable to all the results. The other chapters have their own introduction, experimental details (if different), results, discussion and conclusion. In bibliography, the references are given chapter-wise.

# **CHAPTER-2**

---

## **Experimental details**



In this chapter, the methods for the synthesis of ferrites along with their characterizations have been presented. A short theoretical background has also been given for the various characterization techniques.

## **2.1. Synthesis Techniques**

Particle size as well as grain morphology of ferrite powders strongly depend upon the synthesis technique. The structural, morphological, elemental and magnetic characteristics of Mn-Zn ferrites efficaciously rely on the method of production. Here, a brief description of various techniques *viz.* conventional mixed oxide synthesis, sol gel synthesis, sol gel auto combustion synthesis, hydrothermal synthesis and co-precipitation synthesis used by several researchers for the synthesis of ferrites have been discussed.

### **2.1.1. Conventional Mixed Oxide Synthesis Technique**

Conventional mixed oxide synthesis technique (also known as solid state technique) is an old technique but still is used by various industries in great demand from many years [1,2]. In this synthesis technique purity, particle size and chemical behaviour of the starting materials play an important role. This synthesis technique requires high purity of starting materials in oxide form to get good results for Mn-Zn ferrite powder. The starting materials in oxide form are mixed together and directed to calcination in air at 900 °C – 1300 °C [3,4]. After the calcination process the agglomerated ferrite particles are crushed either using ball milling or mortar & pestle. The crushed powder is then bound into pellet form and sintered at 1100 °C to 1400 °C [3,4].

### **2.1.2. Sol Gel Synthesis Technique**

For the synthesis of nanoparticles sol gel is an extremely aged technique. Historically, Ebelmen in 1846 was the first to employ this technique [5,6]. The major advantage of this technique is that it overcome the problem of unwanted active dirt in nearby atmosphere which is generally produced in mixed oxide synthesis. This technique provides a good way to synthesize high quality nanomaterials with good chemical match. In sol-gel synthesis technique; steady disruption of colloidal particles inside a solvent are meant for sol and ingredient elements make three dimensional porous system are known as gel. During this synthesis technique, some organic acid in the form of a complexing agent is added in the aqueous solution of starting materials

with constant stirring at a temperature of  $80\text{ }^{\circ}\text{C} \pm 5\text{ }^{\circ}\text{C}$  and a gel of extreme thickness has been prepared [7,8]. The prepared gel has been then desiccated all-night in a hot air oven at  $60\text{ }^{\circ}\text{C} \pm 5\text{ }^{\circ}\text{C}$ . The dried gel is then crushed into powder form using mortar & pestle.

### **2.1.3. Sol Gel Auto Combustion Synthesis Technique**

Sol gel auto combustion synthesis technique is a customized form of sol gel method. Combustion synthesis technique or high temperature synthesis by self-circulation could be the proper name for this synthesis technique. This technique is good to obtain nano range particles of ceramic oxides. To attain nanoparticles of transition metals (oxide form), this is an easy, low price and rapid synthesis technique in comparison to earlier mentioned synthesis methods. Mainly, there are three eminent combustion synthesis techniques or may be a combination of the three techniques; (i) condensed phase combustion in which starting materials are in solid state (ii) solution combustion in which starting materials are in liquid state (iii) gas phase combustion in which starting materials are in gaseous state [9]. The third technique is useful to get fine nanoparticles. Generally, to combustion method tartaric acid, glycine, citric acid and urea are mostly used as fuel. During the synthesis an appropriate fuel in organic form is mixed with the aqueous solution of preferred precursors. The pH level is adjusted with the addition of some hard base. The mixture is evaporated at temperature  $65\text{ }^{\circ}\text{C} - 75\text{ }^{\circ}\text{C} \pm 5^{\circ}\text{C}$  to obtain dried out gel. To obtain powder form, this dried out gel is heated at  $250\text{ }^{\circ}\text{C} \pm 50^{\circ}\text{C}$  (say) depending on the fuel used [9].

### **2.1.4. Hydrothermal Synthesis Technique**

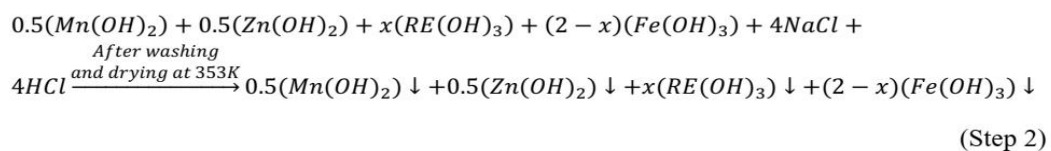
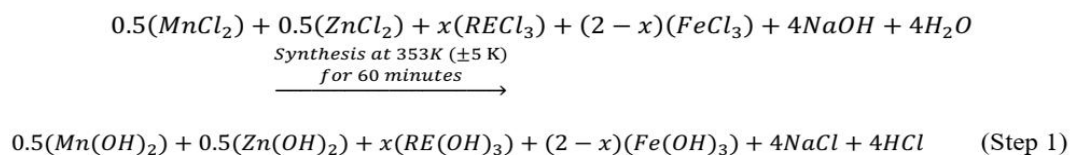
Hydrothermal synthesis technique is a famous process to synthesize nanoparticles at high temperature and high pressure. In this synthesis technique, the solutions of precursors are formed first and an adjustment of pH level is made. After this the solution is put inside an autoclave and tightly closed autoclave is put inside the furnace. As the temperature around the autoclave increases in furnace then pressure inside the autoclave also increase. Mostly at an optimized temperature of  $100\text{ }^{\circ}\text{C} - 150\text{ }^{\circ}\text{C}$  autoclave is kept inside a furnace for few hours. After this sample is taken out of the autoclave, washed a number of times with distilled water and desiccated in a hot air oven. Dried powder of nanoparticles is used for further characterizations. Environment sociable behaviour during preparation of nanoparticles is the main benefit of this

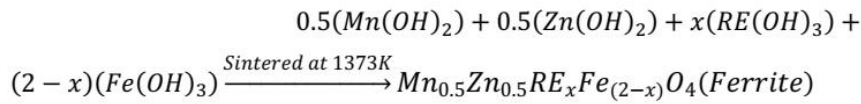
technique. To prepare nanoparticles of soft ferrites various scientists used this technique [10-12].

### 2.1.5 Co-precipitation Synthesis Technique

Extremely simple steps of synthesis, inexpensive, less time consumption and various parameters (pH level, temperature etc.) to control the particle size are some of the major benefits of co-precipitation synthesis technique, which makes it special in comparison to other synthesis methods [13,14]. Co-precipitation synthesis technique is one of the best and suitable synthesis techniques to process magnetic nanoparticles [13,14]. During this process, first solution of precursors (chloride, sulphate, nitrate etc.) is prepared using distilled water and after that there is addition of some solvent (NaOH, KOH, NH<sub>3</sub> etc.) in inorganic form to adjust pH level from 8 to 14 under constant stirring at 70 °C to 80 °C ± 5 °C. The obtained precipitates are washed with distilled water for several times to eliminate the impurities and dried in a hot air oven generally at 60 °C to 80 °C ± 5 °C. Dried out sample of nanoparticles is crushed into powder form and sintered to produce pure crystal structure. Various authors had reported formation of ferrite nanoparticles using this synthesis technique [15-17].

In this thesis work, magnetic nanoparticles of lanthanide ( $RE = La, Gd, Nd$ ) doped  $Mn-Zn$  ferrites are prepared by means of co-precipitation synthesis method. Schematic diagram for the synthesis of lanthanide ( $RE$ ) added  $Mn-Zn$  ferrites is shown in Figure 2.1. To synthesize a composition, the precursors used have been taken in solution form. Solution of chloride as starting materials has been poured into solution of  $NaOH$  under constant stirring at 80 °C ± 5 °C for 60 minutes. The pH of solution has been maintained at 11- 12 during the precipitation of particles. The precipitates are collected, washed a number of times and then dried out all-night at 80 °C in a hot air oven. After this desiccated precipitates are broken down to powder form and sintered at 1373 K for 3 hrs. Planned chemical reaction for the synthesis of  $Mn_{0.5}Zn_{0.5}RE_xFe_{2-x}O_4$  spinel nano ferrites, where  $x=0, 0.025, 0.050, 0.075, 0.1$ , has been given below;





(Step 3)

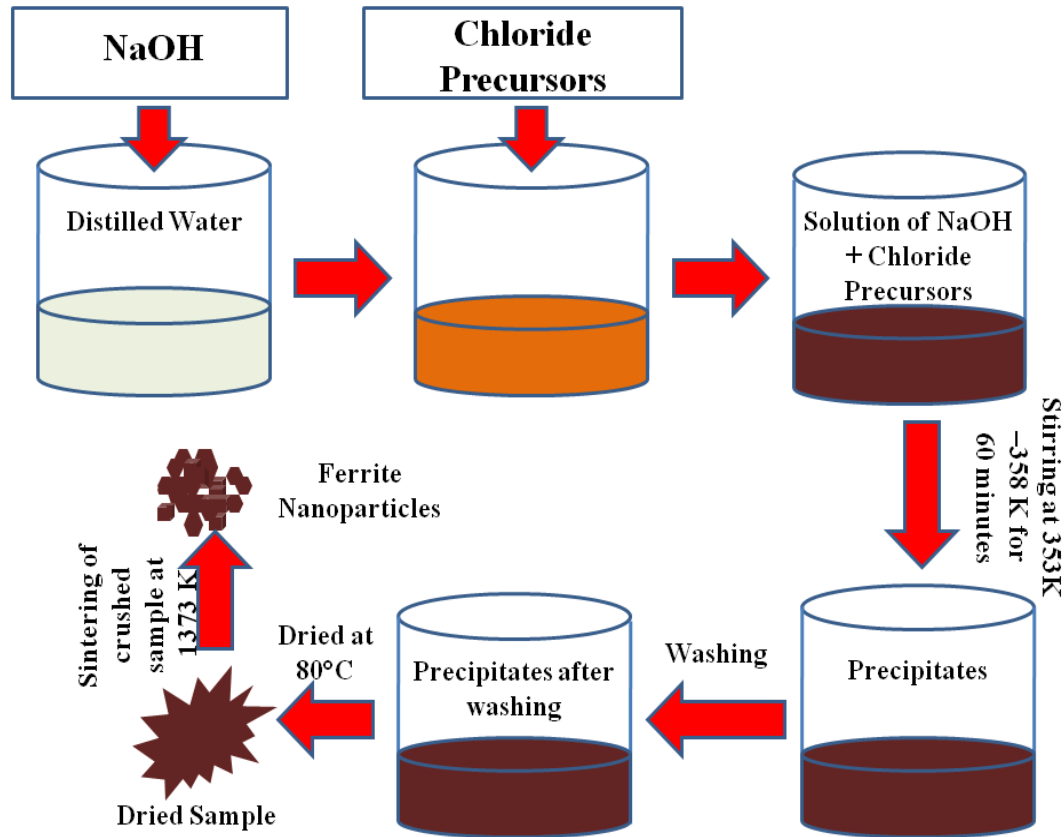


**Figure 2.1:** Schematic diagram of co-precipitation technique for the synthesis of lanthanide ( $RE = La, Gd, Nd$ ) doped  $Mn$ - $Zn$  ferrites.

## 2.2. Characterization Techniques

### 2.2.1. X-Ray Diffraction

To investigate the nanoparticles for their crystal structure and also for the calculation of various structural factors (crystallite size, dislocation density, interplanar spacing, strain, packing factor and lattice constant) X-ray diffraction is generally used as a main characterization technique. X-ray (in collimated form) of wavelength 0.154056 nm incident on a sample and diffraction occurs by the crystalline planes present in that sample during X-ray diffraction.

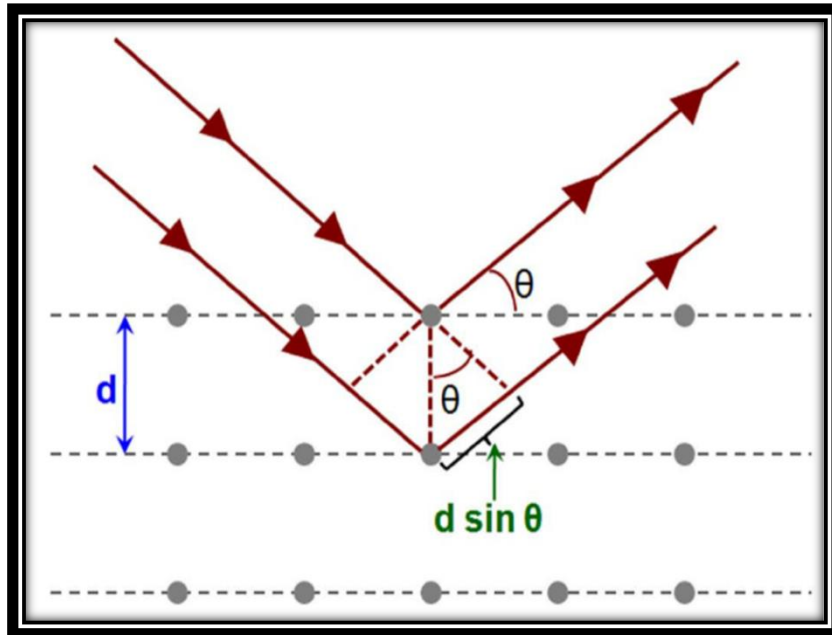


**Figure 2.2:** Diffraction of X-rays from various planes.



**Figure 2.3:** SHIMADZU analytical: XRD 6000 diffractometer.

Bragg's law [18] shows that

$$2d\sin\theta = n\lambda \quad (2.1)$$

where  $\theta$  is angle of diffraction,  $d$  is interplanar spacing,  $n$  denotes an integer and wavelength of X-ray is denoted by  $\lambda$  (figure 2.2). X-ray diffraction graph is plotted using the values of  $2\theta$  (angle of diffraction) in x-axis and intensity of diffracted x-rays in y-axis. Full width at half maximum (FWHM) and  $2\theta$  values of diffraction peaks is used to calculate the crystallite size and also some other structural parameters can be calculated using these values with interplanar spacing ( $d$ ). In present work, X-ray diffraction (XRD) of sintered samples has been carried out using SHIMADZU: XRD 6000 with Cu- $K_{\alpha}$  (1.54056 Å) for the investigation of lanthanide ( $RE = La, Gd, Nd$ ) doped  $Mn-Zn$  ferrites (figure 2.3).

### 2.2.2. Fourier Transform Infrared Spectroscopy

Fourier Transform Infrared Spectroscopy (FTIR) uses the process in which energy ray of infrared region creates vibrational activity in chemical bonds. Sample energy pairs with infrared energy when it is exposed to infrared region. Intensity level of infrared light's ray is evaluated before interaction with the sample as well as after the interaction if a resonance occurs between striking infrared energy and chemical bond's energy with in the sample.



**Figure 2.4:** Perkin Elmer spectrophotometer (model-65).

During experiments of transmission otherwise reflection there is a detection of incident energy in the form of radiation. A plot of intensity in y-axis and frequency in x-axis gives a FTIR spectrum. To obtain the data about the structure of molecules present in a compound, FTIR spectroscopy is a valuable characterization tool. Peaks due to transmittance otherwise absorbance in FTIR spectrum represent vibrational frequencies which occur among the atomic bonds present inside the sample. Various functional groups available in the material can be recognized using these peaks (vibrational frequencies) [19].

In present work, Perkin Elmer (model-65) spectrophotometer (Figure 2.4) is utilized in the spectral region  $400\text{ cm}^{-1}$  to  $1000\text{ cm}^{-1}$  at room temperature to study the origination of spinel ferrite structure of synthesized lanthanide ( $RE = La, Gd, Nd$ ) doped  $Mn-Zn$  ferrites.

### **2.2.3. Field Emission - Scanning Electron Microscopy and Electron Dispersion X-Ray Spectroscopy**

Field emission - scanning electron microscope (FE - SEM) provides us image of sample surface using rich electron beam with raster scanning above the surface of sample. Interaction between the electrons and atoms constituting the sample create signals that specially hold data regarding topography and composition of the sample surface [20]. Little beam of electron gun offers a huge as well as steady current. Thermionic and field emitters are two sources for the emission. In scanning electron microscope (SEM) and field emission - scanning electron microscope (FE-SEM), the type of emitter creates a major difference. Filament is heated up by an electrical current in case of thermionic emitters. Tungsten (W) as well as lanthanum hexaboride ( $LaB_6$ ) are two major materials used in filaments. Electrons become able to escape from the material, as filament material's work function conquers by sufficient heat. In case of thermionic emitters some problems respective to the cathode material's vaporization, thermic drift and poor brightness occur throughout the process. To overcome these problems, single mode to produce electrons is field emission. Filament does not get heating up by cold cathode field emitter (source of field emission). Emission occurs when filament is placed in the presence of giant electrical potential gradient. Tungsten wire shaped into a shrill point ( $\sim 100\text{ nm}$ ) is generally used as field emission source. Focused electric field of great intensity to lower the material's work function and ejection of electrons from cathode is the importance of this sharp tip ( $\sim 100\text{ nm}$ ). This

source of field emission (FE) sensibly merges with the scanning electron microscope (SEM). Source of field emission generates an extremely small electron beam (~1000 times) in comparison to ordinary microscope among thermic electron gun and due to this reason quality of image is enhanced in case of field emission scanning electron microscope (FE-SEM) (Figure 2.5).

Material's elemental composition at low amount (micron level) is recognized using an easy and great technique known as EDX otherwise EDS (energy dispersive X-ray spectroscopy). EDS instrumentation is attached with FE-SEM and SEM to gain data about the elements present in sample during study. In EDS, there is detection of X-rays when an electron beam falls on the sample. Atoms present in the sample get excited and to release the extra energy generate X-rays. This extra energy generated by atoms in the form of X-rays makes peaks in EDS spectrum.



**Figure 2.5:** FE-SEM Quanta 200 FEG

In present work, morphological as well as elemental study of lanthanide ( $RE = La, Gd, Nd$ ) doped  $Mn-Zn$  ferrites samples have been performed using FE-SEM (field emission - scanning electron microscope) and EDS (energy dispersive X-ray spectroscopy) (FE-SEM Quanta 200 FEG and EDS, Oxford Instruments).

### **2.2.4. Vibrating sample magnetometer**

Magnetic moment of sample (in solid form) is obtained using vibrating sample magnetometer (VSM). Faraday's law of induction applies for vibrating sample magnetometer, which shows that an electric field will be created on varying in magnetic

field [21]. Variable magnetic field's data can be calculated after measuring this electric field. A VSM is used to measure the magnetic conduct of magnetic materials. When sample under investigation is subjected to a constant magnetic field, a dipole moment is induced in the sample which is proportional to the product of applied field and susceptibility. An electrical induction will be caused in the fixed electromagnetic coils, when sample experiences a sinusoidal movement. Magnetic moment along with amplitude and frequency of vibration is proportional to this induction.

In present work, magnetic properties of lanthanide ( $RE = La, Gd, Nd$ ) doped  $Mn-Zn$  ferrites samples are studied by employing vibrating sample magnetometer (PAR-155) in a magnetic field range  $-10\text{ kOe}$  to  $+10\text{ kOe}$  at room temperature (Figure 2.6).



**Figure 2.6:** Vibrating sample magnetometer (PAR-155).



# CHAPTER-3\*

---

## Optimization of sintering temperature for $Mn_{0.5}Zn_{0.5}Fe_2O_4$ nano ferrites

\* “Prashant Thakur, Rohit Sharma, Vineet Sharma, Pankaj Sharma, *Structural, Morphological and Optical Properties of  $Mn_{0.5}Zn_{0.5}Fe_2O_4$  Nano Ferrites: Effect of Sintering Temperature*, **Materials Chemistry and Physics** Vol 193 (2017) 285-289”.



Sintering temperature assumes an essential part in deciding the physical properties of the spinel nano ferrites. In this chapter, the synthesis and characterizations (XRD, FTIR and FE-SEM) of  $Mn_{0.5}Zn_{0.5}Fe_2O_4$  nano ferrites have been described for the optimization of sintering temperature.

### 3.1 Introduction

In soft magnetic materials,  $Mn-Zn$  ferrites are highly significant due to their large electrical resistivity, large early magnetic permeability and large saturation magnetization along with small power losses [1-3]. For high frequency applications, soft ferrites are being majorly used among the magnetic materials due to their low price [4-6]. The presence of five odd electrons in the outer shell of  $Fe^{3+}$  ions mainly governs the magnetic properties and are responsible for the large magnetic moment of  $Mn-Zn$  ferrite in contrast to the presence of other ions in  $Mn-Zn$  ferrite [7]. As discussed in chapter 2 the synthesis technique of nanomaterials play a vital role in determining their properties. Several authors have reported the synthesis of  $Mn-Zn$  ferrite employing different methods and found that the properties are improved to a great extent [1, 8-10]. When studying the properties at nanoscale the synthesis method's role has an intense effect on the properties of ferrites [11-13]. Post synthesis treatments of ferrites (like sintering temperature etc.) has also shown their effect on the structural, morphological and other properties [1].

The sintering process can be understood via two methods *i.e.* sintering in liquid state and sintering in solid state. For solid state sintering the densification can be achieved in the absence of any melting of phase. To make the sintered packs impenetrable, the diffusion between the grains spielt a crucial role. On the other hand for liquid state sintering the melting is a compulsorily required state. In liquid state sintering, the high densification of the pack can be achieved on the application of capillary forces. In other processes of sintering, there is viscous flow sintering where densification can be achieved for grains without any modification in their shape. One more process of sintering is transient liquid state sintering where the combination of sintering in liquid state and sintering in solid state may also be explored for the sintering of samples.

#### 3.1.1 Contemporary sintering processes

Sintering is generally performed in a muffle furnace where one can control the temperature. This process is well known and also named as conventional sintering.

There are various issues associated with this conventional sintering, *e.g.* inhomogeneous heating, ungoverned grain development and disappearing of nano-crystallinity on account of sustained sintering time *etc.* To overcome the problems faced in conventional heating some other sintering processes have been developed. The sintering methods which have been regarded with great favour and approval to obtain high quality microstructures in innovative ceramics are discussed below.

### **3.1.2 Plasma sintering process**

This process involves the formation of pellets of ferrite powder (say) with the help of a graphite die by employing a uniaxial pressure along with the application of direct current in flip-flop way. The plasma discharge in ferrite powder, which is the phenomenon of Joule heating, will make high density pellets of ferrites.

### **3.1.3 Hot press sintering process**

This process is utilized to obtain high density ceramic oxides. In this process the ceramic oxide powder is hot pressed on the application of high pressure. The high pressure is maintained during the whole sintering process. This high mechanical pressure ameliorates the reactivity of ceramic oxide powder constituents. The development of grains can be controlled on varying the compressing duration.

### **3.1.4 Microwave sintering process**

The formal sintering process involves the flow of heat from the surface of sample to region that is inside of the sample leading to generate a temperature gradient. On the other hand, in microwave assisted sintering process the whole sample heats up at a faster rate and thereby deprived of creating a temperature gradient between surface and inner region of sample. The microwave assisted sintering process is a very rapid process. The compactness in the sample is achieved through the microwave frequency (GHz) which produce sufficient amount of heat. In this process one can optimize the heating rate and sintering temperature.

### **3.1.5 Two-step sintering process**

The simple and improved sintering process which sinters the ceramics without compromising their nano crystallinity is termed as two-step sintering process. The first step in this process is to heat the sample to suitable higher temperature and then in second step this high temperature is brought quickly down to 50 °C – 100 °C. The second step temperature is retained for a sufficiently long time to sinter the sample. This method is suitable to form high density ceramics having fine grained microstructures.

The various sintering processes discussed above provides different scientific ways, but these processes are not up to the mark *i.e.* are not totally consistent. To consider these sintering processes on commercial scale similar to conventional sintering process, a lot of research is required further. In our work, conventional sintering process has been employed to optimize the sintering temperature of prepared manganese – zinc ferrite samples. Result of sintering temperature upon the structural and additionally magnetic characteristics of *Mn-Zn* ferrites are described by several authors [1, 8-10]. Structural along with magnetic characteristics of *Mn-Zn* ferrite with sintering from 500 °C to 900 °C has been examined by Mathur *et al.* [8]. Increase in crystallite size from 19.3 nm to 36.4 nm and also a rise in saturation magnetization with an increment in the sintering temperature have been reported. Structural along with magnetic characteristics of annealed *Mn-Zn* nano-ferrites from 160 °C (untreated) to 900 °C have been reported by Kumar *et al.* [9]. It is described that with the rise in annealing temperature hematite phase goes on diminishing. Further, an enhancement in crystallite size as well as saturation magnetization is accounted with the rise in annealing temperature. Role of sintering temperature upon the magnetic characteristics of manganese-zinc nano ferrite (from 700 °C to 950 °C) has also been examined by Azadmanjiri [10]. The initial permeability has been found to rise with sintering temperature. Impression of sintering (400 °C to 1200 °C for 1 hr) upon microstructure as well as magnetic characteristics of manganese-zinc ferrite samples processed by auto-combustion method has been analyzed by Ping Hu *et al.* [1]. An enhancement in the crystallite size on increasing the sintering temperature up to 1100 °C is reported and above 1100 °C temperature crystallite size reduce. An increase in saturation magnetization has also been reported by Ping Hu *et al.* on an increment of sintering temperature.

In this chapter, the Mn-Zn ferrites synthesized by co-precipitation method have been sintered at 973 K, 1173 K and 1373 K and investigated the impact of sintering temperature using XRD, FE-SEM and FTIR analysis.

### **3.2 Synthesis and characterization of $Mn_{0.5}Zn_{0.5}Fe_2O_4$ nano ferrites**

Co-precipitation synthesis technique has been employed aiming to the formation of  $Mn_{0.5}Zn_{0.5}Fe_2O_4$  ferrite powder. The starting materials, manganese chloride, zinc chloride, iron (III) chloride and NaOH have been procured from Merck

India (98% purity) and are used as received. The general details of co-precipitation technique are already discussed in section 2.1.5. For the synthesis of  $Mn_{0.5}Zn_{0.5}Fe_2O_4$  nano ferrites, a schematic diagram has been depicted in figure 3.1.

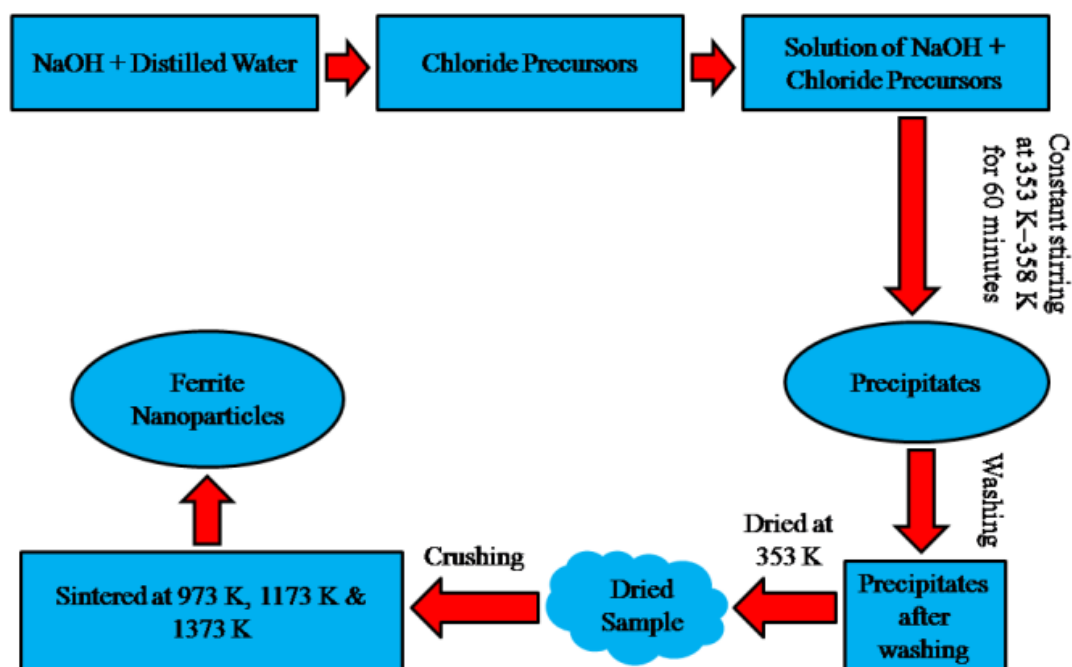


**Figure 3.1:** Schematic diagram for preparation of  $Mn_{0.5}Zn_{0.5}Fe_2O_4$  ferrite powder.

In 60 ml of distilled water, 3M solution (0.5M manganese chloride + 0.5M zinc chloride + 2M iron (III) chloride) of starting materials has been prepared (say stock 1). In 100 ml of distilled water, 4M NaOH solution has been prepared (say stock 2). The stock 1 has been decanted into the bubbling solution of NaOH under mixing. The value of pH has been held at 11 to 12 throughout the co-precipitation. The reaction has been put to force at 353 K–358 K temperature for an hour under energetic stirring. The obtained precipitates have been left to settle at room temperature. The obtained precipitates are washed a number of times with double distilled water followed by overnight drying in an oven at 353 K. The desiccated sample has been broken down to powder with the help of mortar and pestle. Some of the dried powdered sample has been divided into three parts and subjected to different sintering temperatures *i.e.* 973 K, 1173 K and 1373 K. After sintering, the samples have been examined by employing X-ray diffraction, field emission scanning electron microscopy and Fourier transform infrared spectroscopy. The instrumental details have been given in chapter 2.

### 3.3. Structural and morphological analysis

Figure 3.2 shows XRD plots of manganese-zinc ferrites sintered at 973 K, 1173 K and 1373 K temperatures. Origin of perfect spinel phase for sample sintered at 1373 K has been confirmed from the presence of (111), (220), (311), (222), (400), (422), (511), (440) and (533) planes which are in accordance with JCPDS 74-2401. The obtained results show that the co-precipitation method when combined with sintering (at 1373 K) can be utilized to synthesize a pure phase of *Mn-Zn* ferrite. Table 3.1 shows the calculated average crystallite size at different sintering temperatures (973 K, 1173 K and 1373 K) using Scherer's formula. A few secondary XRD reflections of  $Fe_2O_3$  phases (JCPDS 33-0664) have been observed for *Mn-Zn* nano ferrites sample sintered at 973 K & 1173 K [14].  $Fe_2O_3$  start to fade out over 1173 K. Furthermore, a good-crystallized clear *Mn-Zn* ferrite phase appears at 1373 K. An increment in crystallite size on enhancing the sintering temperature to 1373 K has been observed. Coalescence process is responsible for the enhancement in crystallite size with raise in sintering temperature [15]. On an increment in the sintering temperature there is a reduction in dislocation density whereas the values of lattice constant increases. A reduction in the lattice stress is created because of inward shrinking of atoms lying on the crystallite surface with increasing the sintering temperature. This leads to an increase in lattice constant with an increment in crystallite size in the prepared samples. An increase in cell volume leads to a decrease in density and this is the cause for the increase in crystallite size on raising the sintering temperature [15]. A pure crystallized single *Mn-Zn* nano ferrite phase has occurred because of this higher sintering temperature (1373 K).

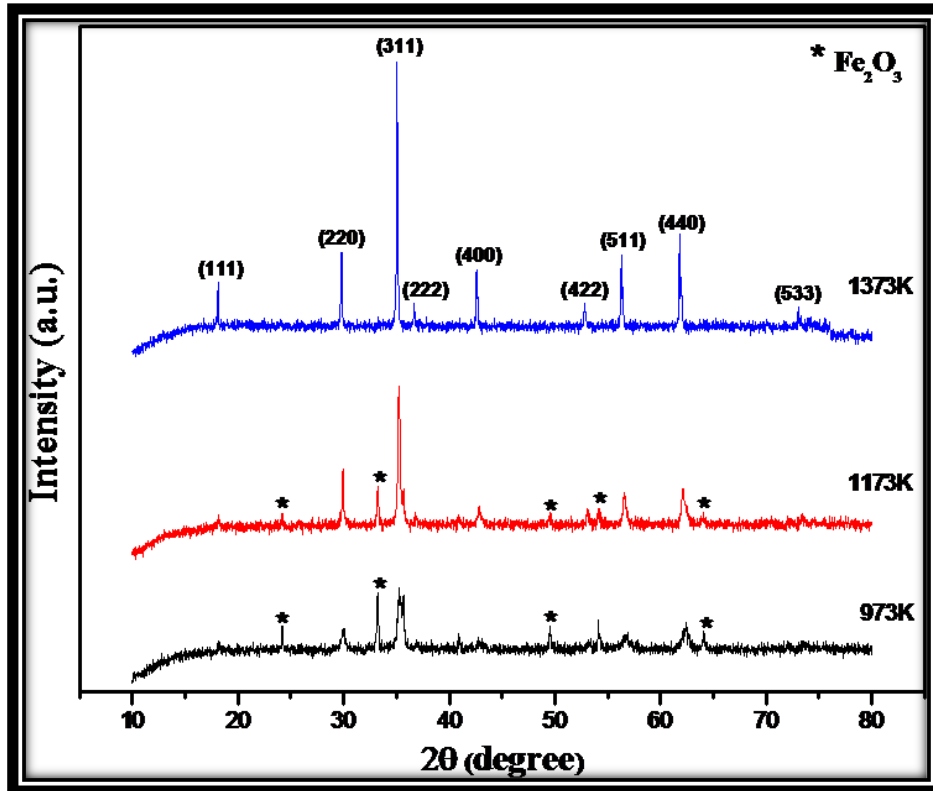


Figure 3.2: XRD graph of sintered  $Mn_{0.5}Zn_{0.5}Fe_2O_4$  nano ferrites

Scherrer's formula;  $D = 0.9\lambda / \beta \cos\theta$  has been used to determine the average crystallite size ( $D$ ), where  $\theta$  is Bragg's angle,  $\lambda = 0.154056$  nm makes up the wavelength of X-ray and  $\beta$  makes up the FWHM value. The relation;  $P = D/d$  has been used to calculate the packing factor ( $P$ ), where  $d$  makes up the interplanar spacing and  $D$  represents the average crystallite size. The relation;  $a = d(h^2 + k^2 + l^2)^{1/2}$  is employed to determine the lattice constant ( $a$ ), where  $d$  is the interplanar spacing. Williamson–Hall relation;  $\beta \cos\theta = (k\lambda/D) + 4\varepsilon \sin\theta$  is utilized to determine the strain ( $\varepsilon$ ), where  $k (=0.9)$  is a constant. The relation;  $\delta = 15\varepsilon / aD$  has been used to determine the dislocation density ( $\delta$ ). The Bragg's relation;  $2d \sin\theta = n\lambda$  has been used to determine the interplanar spacing ( $d$ ), where  $\theta$  is Bragg's angle and  $\lambda = 1.54056$  Å (X-ray wavelength). The values of average crystallite size ( $D$ ), dislocation density ( $\delta$ ), strain ( $\varepsilon$ ), packing factor ( $P$ ), lattice constant ( $a$ ) and interplanar spacing ( $d$ ) estimated from XRD data have been presented in table 3.1. Figure 3.3 shows Williamson-Hall (W-H) plot for the determination of strain.

**Table 3.1:** The values of various structural parameters for Mn-Zn nano ferrites with sintering temperature.

T (K)	D (nm)	a (Å)	P	$\varepsilon$	$\delta$ (Å <sup>-2</sup> )	d (Å)
973	11.38	8.409	44.92	$47.4 \times 10^{-4}$	$15.6 \times 10^{-5}$	2.535
1173	39.02	8.444	153.25	$1.69 \times 10^{-4}$	$1.33 \times 10^{-5}$	2.546
1373	67.42	8.483	263.62	$-1.10 \times 10^{-4}$	$0.44 \times 10^{-5}$	2.557

The positive slope for the sintered samples sintered at 973 K, 1173 K shows tensile strain. Kumar *et al.* have also showed similar results which are comparable to these results [16]. For the sample sintered at 1373 K, the W-H plot shows a negative slope allowing to conclude a compressive strain. Thankachan *et al.* have also described similar results [17]. A decrease in the values of  $\varepsilon$  and  $\delta$  has been observed with sintering temperature (Table 3.1). On increment in sintering temperature an enhancement in average crystallite size, lattice constant, packing factor and interplanar spacing has been observed (Table 3.1).

Figure 3.4 shows the Fourier transform infrared (FTIR) spectra of sintered  $Mn_{0.5}Zn_{0.5}Fe_2O_4$  nano ferrites. The spinel ferrite structure of the synthesized  $Mn_{0.5}Zn_{0.5}Fe_2O_4$  nano ferrites is confirmed by the presence of two absorption bands i.e.  $\nu_1$  at  $421 \text{ cm}^{-1}$  -  $491 \text{ cm}^{-1}$  and  $\nu_2$  at  $516 \text{ cm}^{-1}$ - $592 \text{ cm}^{-1}$ . The absorption band  $\nu_2$  (at  $516 \text{ cm}^{-1}$ - $592 \text{ cm}^{-1}$ ) supports the origination of metal - oxygen ions linkage at tetrahedral position whereas the absorption band  $\nu_1$  (at  $421 \text{ cm}^{-1}$  -  $491 \text{ cm}^{-1}$ ) affirms the appearance of cation - oxygen bonds at the octahedral position [18]. The effect of increasing the sintering temperature is visible from the shift of absorption bands.

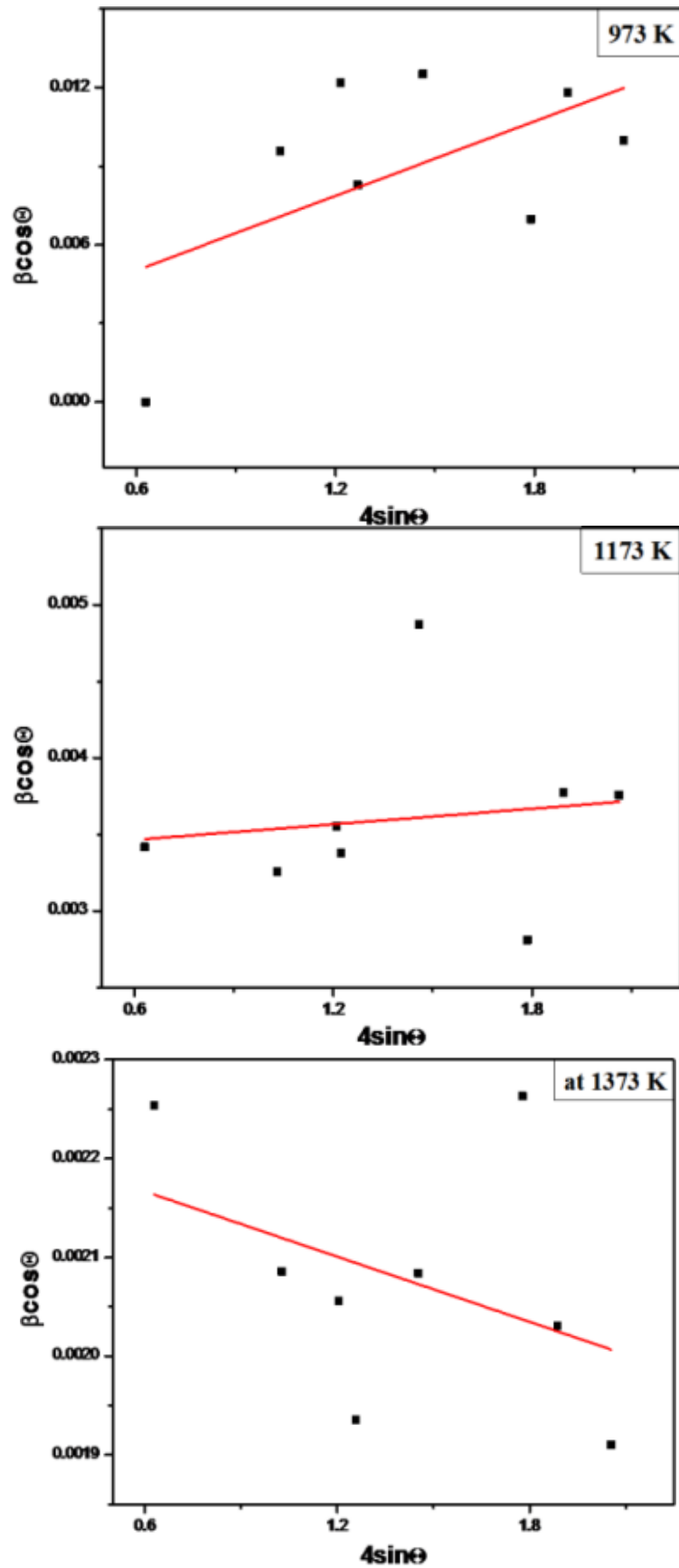


**Figure 3.3:** W-H plots of sintered  $Mn_{0.5}Zn_{0.5}Fe_2O_4$  ferrites. The sintering temperature is given in each plot

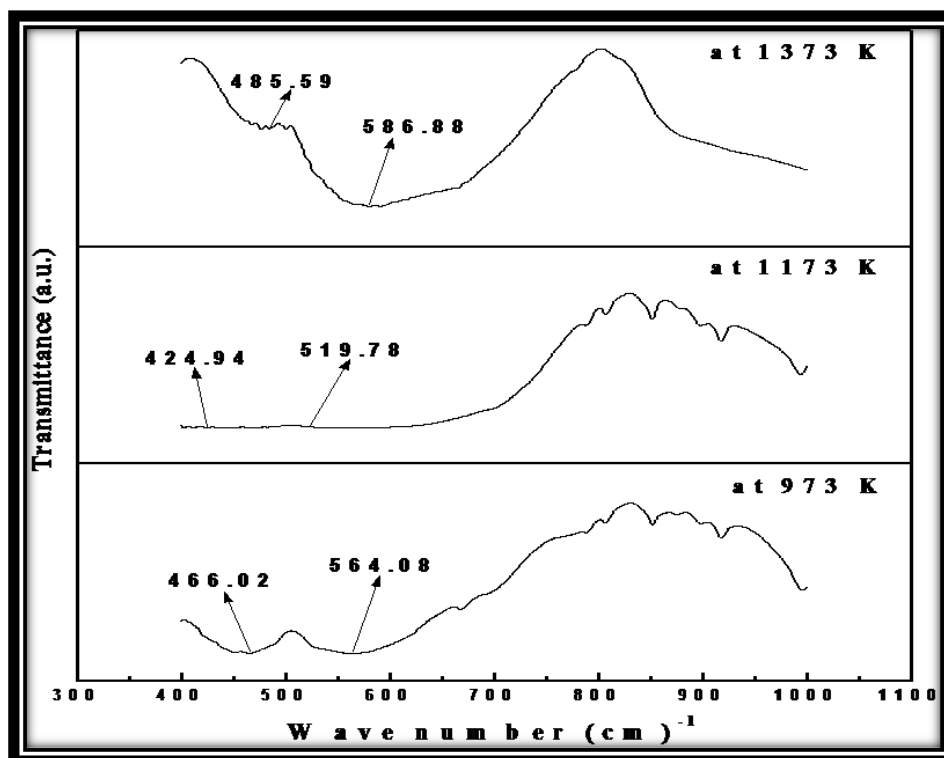


**Figure 3.4:** FTIR spectra of sintered  $Mn_{0.5}Zn_{0.5}Fe_2O_4$  sample.

For octahedral and tetrahedral sites, the force constants of ions have been estimated using the absorption band frequencies ( $\nu_1$  &  $\nu_2$ ) [19];  $K = 4\pi^2 c^2 \nu^2 \mu$ , where  $K$  makes up the force constant ( $K_o$  for octahedral position and  $K_t$  for tetrahedral position),  $c$  represents the speed of light (used in cgs),  $\mu$  represents the reduced mass of  $Fe^{3+}$  and  $O^{2-}$  ions ( $= 2.601 \times 10^{-23}$  g) and  $\nu$  makes up the vibrational frequency ions at tetrahedral and octahedral locations. The measures of  $K_o$  and  $K_t$  calculated using above relation are presented in table 3.2. With an increment in sintering temperature of 973 K to 1373 K there is variance in the estimations of force constants  $K_o$  and  $K_t$ . This exhibits a variation in the distance of cation - oxygen ions at the tetrahedral and octahedral positions [19].

The sintered manganese-zinc nano powder has been looked into by the field emission scanning electron microscopy (FE-SEM) for the morphological analysis.

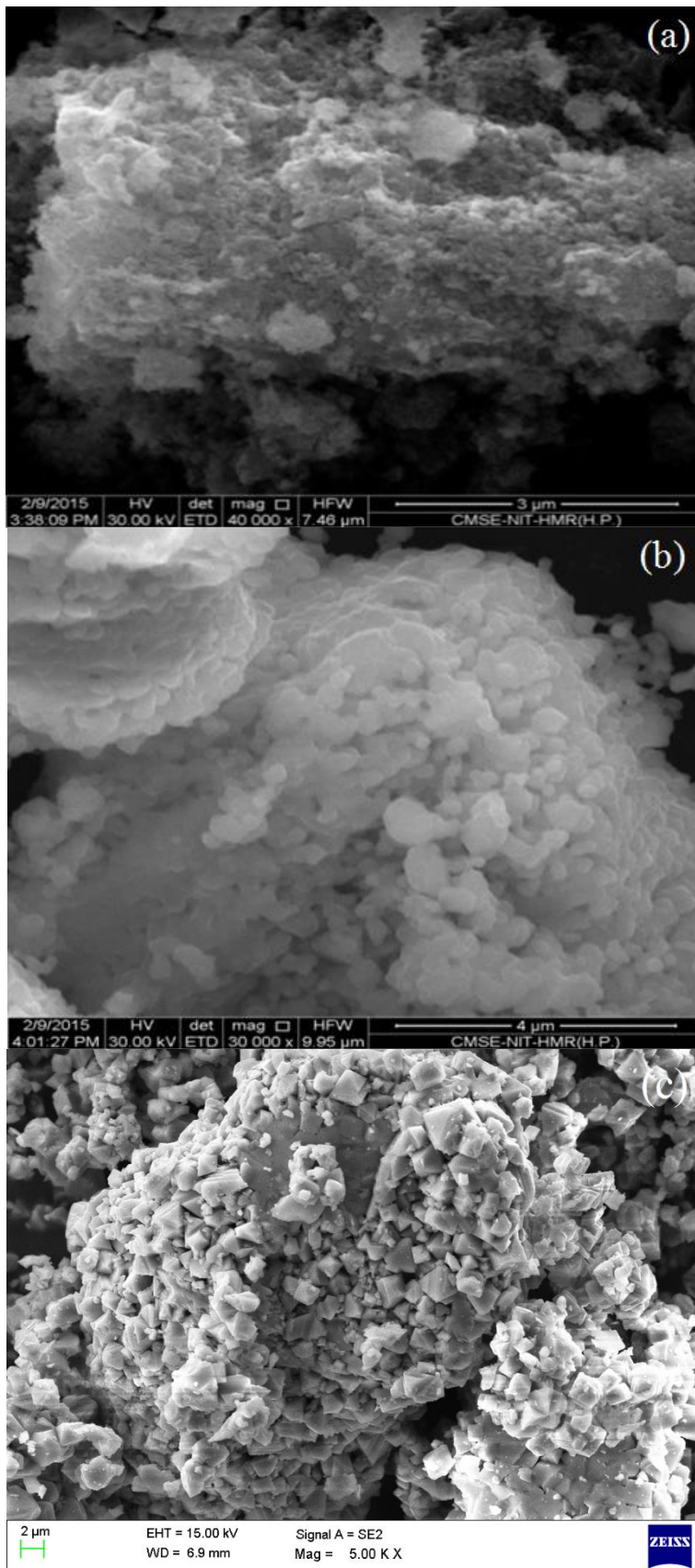


**Figure 3.5:** FESEM images of  $Mn_{0.5}Zn_{0.5}Fe_2O_4$  sample sintered at (a) 973 K (b) 1173 K and (c) 1373 K.

**Table 3.2:** Tetrahedral and octahedral force constants ( $K_t$ ,  $K_o$ ) of  $Mn_{0.5}Zn_{0.5}Fe_2O_4$  sintered at 973 K, 1173 K and 1373 K temperatures

T (K)	$\nu_1$ (cm <sup>-1</sup> )	$\nu_2$ (cm <sup>-1</sup> )	$K_o \times 10^5$ (dynes/cm)	$K_t \times 10^5$ (dynes/cm)
973	466.02	564.08	1.995	2.923
1173	424.94	519.78	1.658	2.482
1373	485.59	586.88	2.166	3.164

The manganese-zinc ferrite nanoparticles sintered at 973 K temperature has less particle size in comparison to the nanoparticles sintered at higher temperature (i.e. 1373 K). From the FE-SEM images (figure 3.5(a), 3.5(b) and 3.5 (c)) it is clear that the particle size enhances as the sintering temperature is raised from 973 K to 1373 K. The high sintering temperature leads to the development of homogeneous crystalline structure.

### 3.4. Conclusion

The co-precipitation synthesis technique has been used for the preparation of  $Mn_{0.5}Zn_{0.5}Fe_2O_4$  ferrite. The synthesized ferrite sample has been subjected to sintering at 973 K, 1173 K and 1373 K temperatures. Structural analysis (using XRD) at three sintering temperatures detects a single phase cubical spinel at 1373 K whereas a secondary phase  $Fe_2O_3$  has been observed at lower sintering temperatures. The average crystallite size is detected to increase (11.38 nm to 67.42 nm) with the increasing sintering temperature (973 K to 1373 K). The presence two absorption bands (421 cm<sup>-1</sup> - 491 cm<sup>-1</sup> and 516 cm<sup>-1</sup> - 592 cm<sup>-1</sup>) in FTIR spectra have supported the formation of spinel ferrite. FE-SEM images have shown the constitution of homogeneous crystalline nanoparticles with raise in sintering temperature. Considering these results, we have taken the sintering temperature as 1373 K for further investigation of doped Mn-Zn ferrites.



# CHAPTER-4\*

---

## Structural and morphological study of $\text{La}^{3+}$ , $\text{Gd}^{3+}$ & $\text{Nd}^{3+}$ doped Mn-Zn nano ferrites

- \* 1. “**Prashant Thakur**, R. Sharma, M. Kumar, S.C. Katyal, N.S Negi, N. Thakur, V. Sharma, Pankaj Sharma, *Superparamagnetic La Doped Mn-Zn Nano Ferrites: Dependence on Dopant Content and Crystallite Size*, Materials Research Express Vol 3 (2016) 075001”
2. “**Prashant Thakur**, R. Sharma, V. Sharma, P.B. Barman, M. Kumar, D. Barman, S.C. Katyal, Pankaj Sharma,  *$\text{Gd}^{3+}$  doped Mn-Zn soft ferrite nanoparticles: Superparamagnetism and its correlation with other physical properties*, Journal of Magnetism and Magnetic Materials Vol 432 (2017) 208–217”.
3. “**Prashant Thakur**, R. Sharma, M. Kumar, S.C. Katyal, P.B. Barman, V. Sharma, Pankaj Sharma, *Structural, morphological, magnetic and optical study of  $\text{Nd}^{3+}$  doped Mn-Zn ferrite nanoparticles synthesized via co-precipitation technique*, Journal of Magnetism and Magnetic Materials Vol 479 (2019) 317-325”.



Addition of dopant is an important parameter in establishing a property-composition relation. In this chapter, the addition of lanthanides ( $RE^{3+} = La^{3+}, Gd^{3+}$  &  $Nd^{3+}$ ) to Mn-Zn cubic spinel ferrites for the structural and morphological study has been described. XRD, FTIR and FE-SEM characterization techniques have been employed for the structural and morphological study. The chapter has been divided into four sections comprising; introduction, experimental details, results & discussion and conclusion.

#### 4.1. Introduction

Over the last few years spinel ferrites have shown the competence in various technological applications like high-frequency devices, catalysis, microwave devices etc. [1-5]. These materials have also shown their usefulness in biomedical applications particularly for hyperthermia and drug delivery [6, 7]. Spinel ferrites exist in  $AB_2O_4$  form with  $A$  as divalent metal ion (*e.g.*  $Mn^{2+}, Co^{2+}, Zn^{2+}, Mg^{2+}, Ni^{2+}$  etc.) and  $B$  as trivalent metal ions {*e.g.* rare earth metals ( $La^{3+}, Gd^{3+}$  etc.),  $In^{3+}, Al^{3+}$  etc.}. The places occupied by  $A$  ions are known as tetrahedral sites and the places occupied by  $B$  ions are known as octahedral or B-sites. For the different characteristics of spinel ferrites the arrangement of ions in these sites is responsible [1]. The structural, electrical and magnetic characteristics of spinel ferrites are being systematized by way of their chemical configuration, synthesis technique, type of dopant and particle size [2].

Among various soft ferrites, manganese-zinc spinel ferrites have shown their importance due to their application in high frequency devices and property of high initial magnetic permeability [8,9]. The magnetic properties of manganese-zinc spinel ferrites have shown their dependence on sintering temperature, sintering time, particle size, microstructure, etc. [8]. Manganese-zinc spinel ferrites are widely used in computer memory chips, antenna rods, electromagnetic interference devices, transformer cores, microwave devices, radio frequency coils and some other devices of microelectronics due to some unique properties [8]. Different synthesis techniques *viz.* sol-gel, sol-gel autocombustion, hydrothermal, co-precipitation etc. have been employed by various researchers to prepare manganese-zinc spinel ferrites [6,10-21]. Evolution of microstructure and homogeneous compositions on mixing the precursors at molecular stage are the primary advantages of these synthesis techniques [10-20].

Addition of rare earth elements to manganese-zinc spinel ferrites has shown large magnetization, magnetocrystalline anisotropy and elastic distortion on the action of magnetizing force at low temperatures [22]. The confined electrons of 4*f* shell and firm spin-orbit coupling of the angular momentum of RE<sup>3+</sup> ions are mainly causative for the appearance of these prominent properties in manganese-zinc spinel ferrites [22]. Further, a shielding is provided to 4*f* electrons by 5*s*<sup>2</sup> and 5*p*<sup>6</sup> shells and this leads to make a little effect of potential field of adjacent ions on the 4*f* electrons. There is migration of some divalent metal ions from B site to the A site with the transposition of the RE<sup>3+</sup> ions in spinel ferrite. Relocation of metal ions from octahedral (B) location to the tetrahedral (A) location also depends upon the size of ionic radii in spinel ferrite [22]. It is difficult to put in RE<sup>3+</sup> ions into the spinel structure of ferrite owing to their large ionic radii via classical ceramic method [1]. Therefore, co-precipitation technique has been employed for the synthesis of RE<sup>3+</sup> doped manganese-zinc spinel nanoferrites [1].

In this chapter, the effect of RE<sup>3+</sup> (La<sup>3+</sup>, Gd<sup>3+</sup>, Nd<sup>3+</sup>) doping on manganese-zinc ferrites synthesized via co-precipitation method has been studied for the structural and morphological properties. The general composition under investigation is of  $Mn_{0.5}Zn_{0.5}Re_xFe_{2-x}O_4$ , where the values of *x* varies from 0 to 0.1 at an interval of 0.025.

## 4.2. Experimental details

RE<sup>3+</sup> (= La<sup>3+</sup>, Gd<sup>3+</sup>, Nd<sup>3+</sup>) doped manganese zinc ferrites have been processed utilizing co-precipitation approach. Preparation of samples has been described in paragraph 2.1.5. The sintered samples have been explored by X-ray diffraction, field emission scanning electron microscope, Fourier transform infrared spectra and energy dispersive spectroscopy (EDS) spectroscopy. The details of instrument type are given in chapter 2, section 2.2.

## 4.3. Results & discussions

### 4.3.1 X-ray Diffraction

Figure 4.1.1, 4.2.1 & 4.3.1 shows the XRD spectra of  $Mn_{0.5}Zn_{0.5}RE_xFe_{2-x}O_4$  ferrites sintered at 1373 K for RE<sup>3+</sup> = La<sup>3+</sup>, Gd<sup>3+</sup> & Nd<sup>3+</sup> respectively.

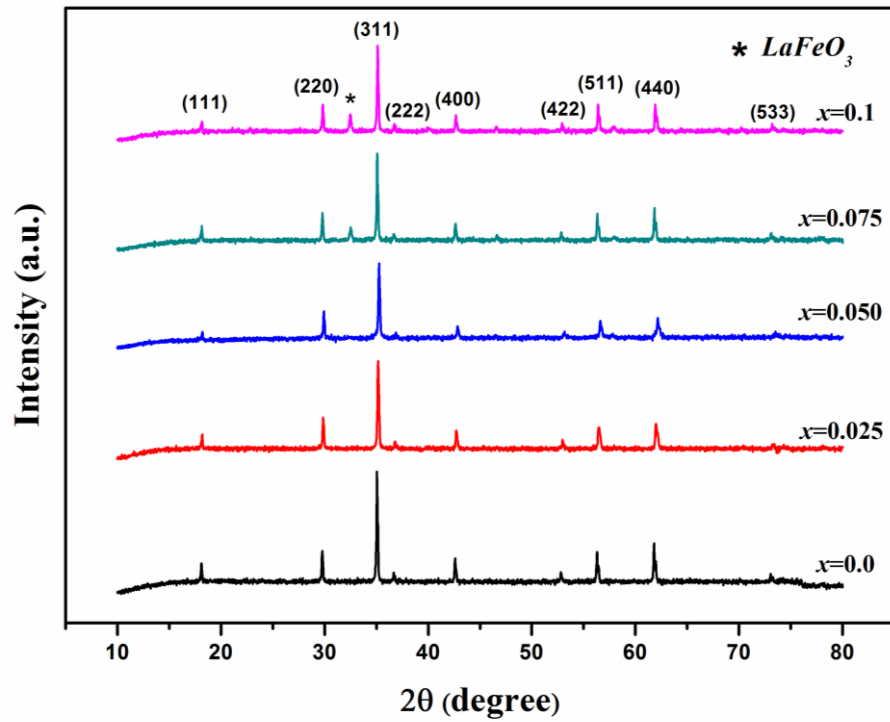


Figure 4.1.1: XRD graphs of  $Mn_{0.5}Zn_{0.5}La_xFe_{2-x}O_4$  ferrites.

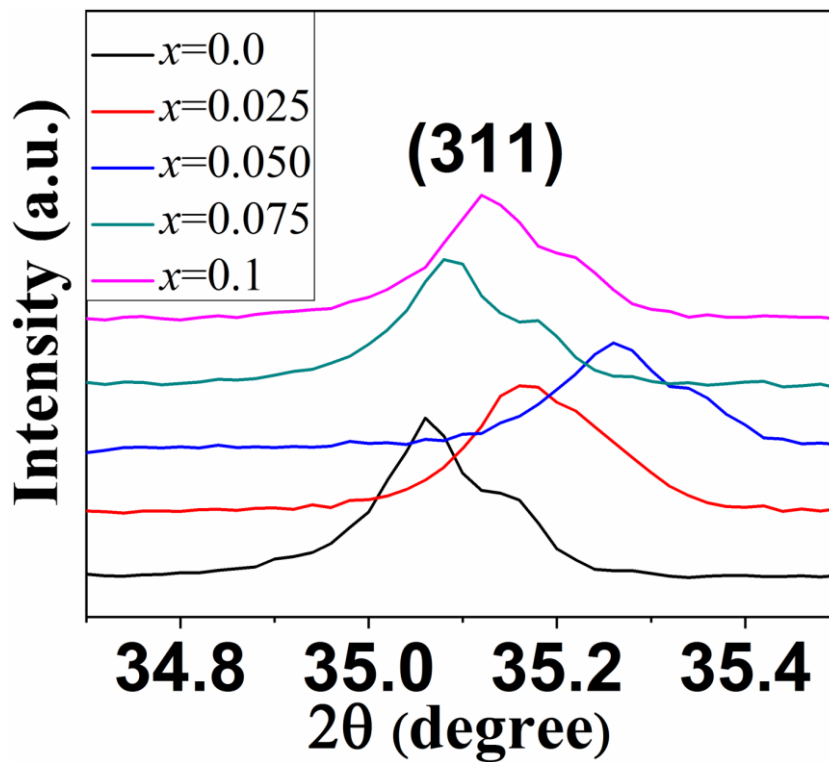


Figure 4.1.2: Zoomed in image of most prominent peak in  $Mn_{0.5}Zn_{0.5}La_xFe_{2-x}O_4$  ferrites.

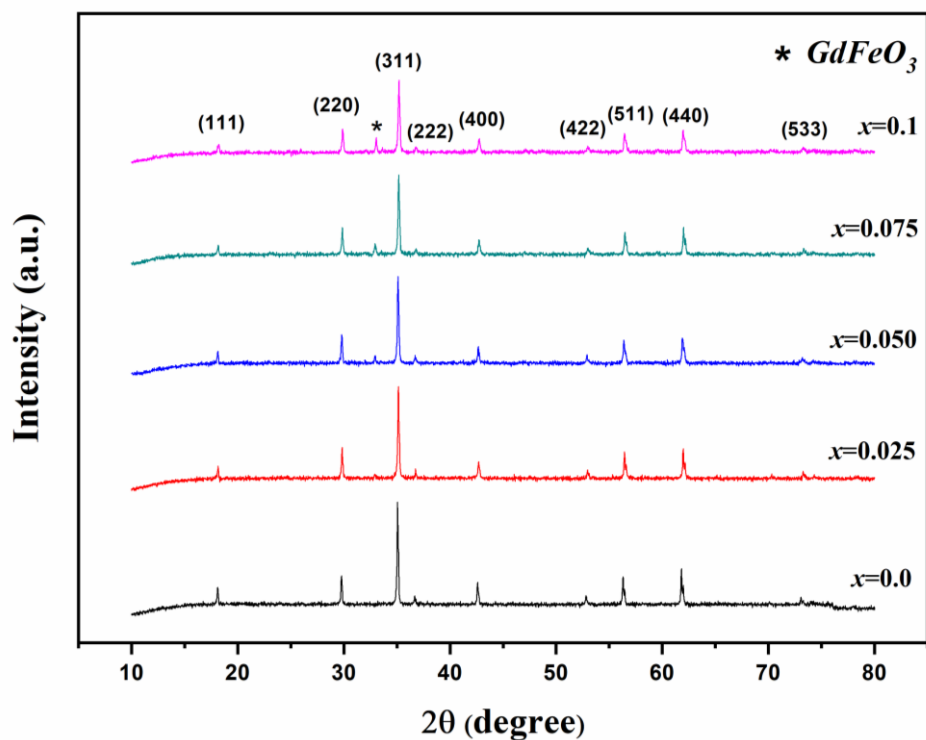


Figure 4.2.1: XRD graphs of  $\text{Mn}_{0.5}\text{Zn}_{0.5}\text{Gd}_x\text{Fe}_{2-x}\text{O}_4$  ferrites.

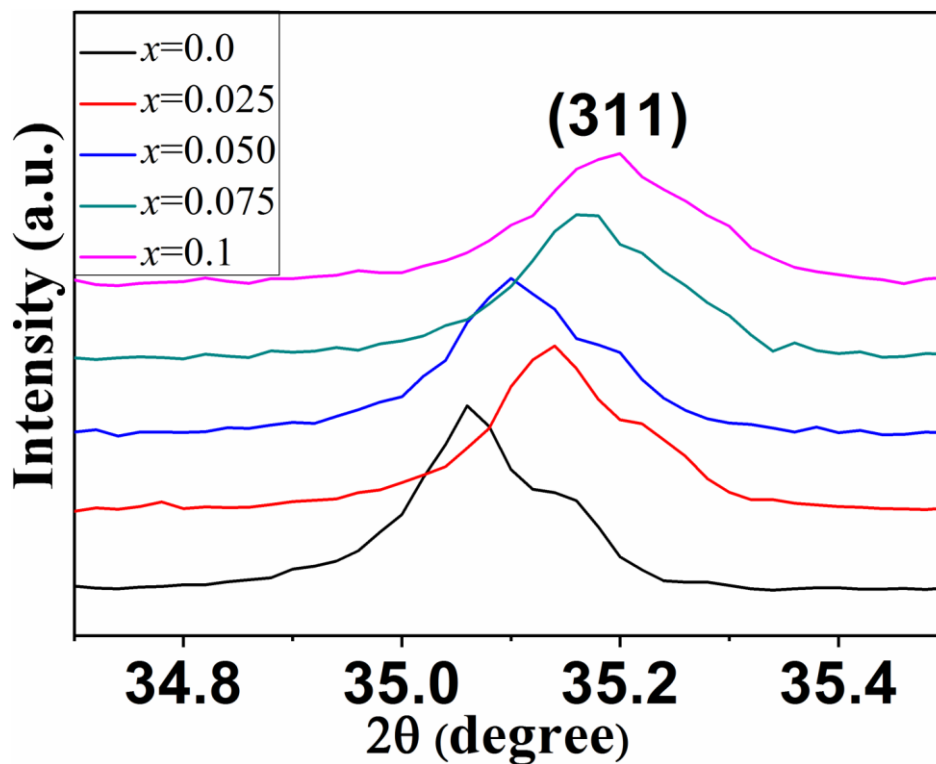


Figure 4.2.2: Zoomed in image of most prominent peak in  $\text{Mn}_{0.5}\text{Zn}_{0.5}\text{Gd}_x\text{Fe}_{2-x}\text{O}_4$  ferrites.

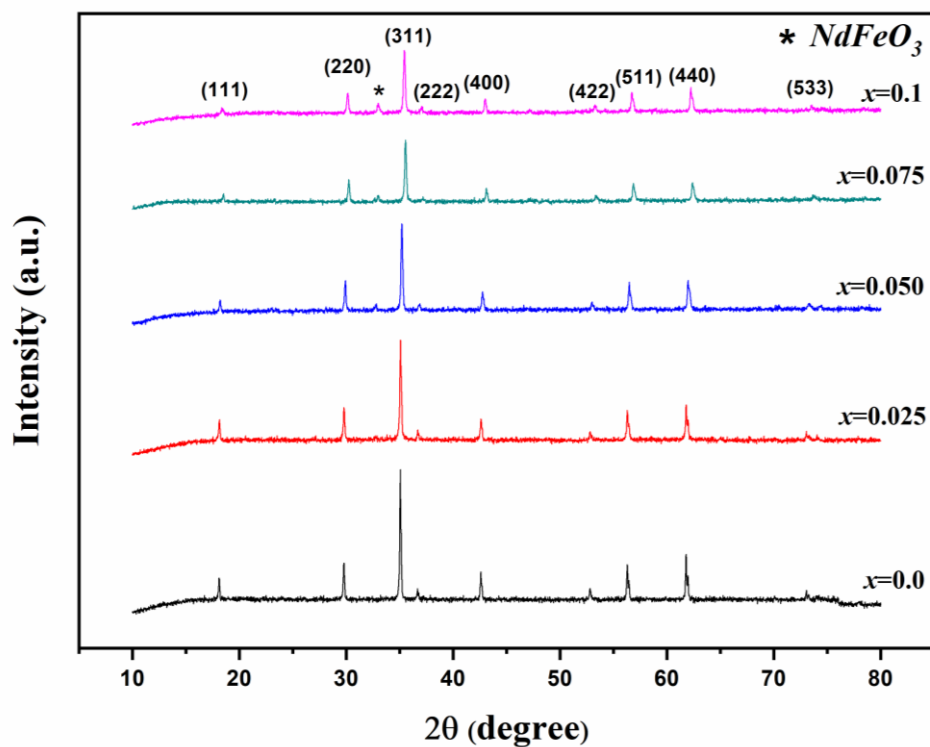


Figure 4.3.1: XRD spectra of  $Mn_{0.5}Zn_{0.5}Nd_xFe_{2-x}O_4$  ferrites.

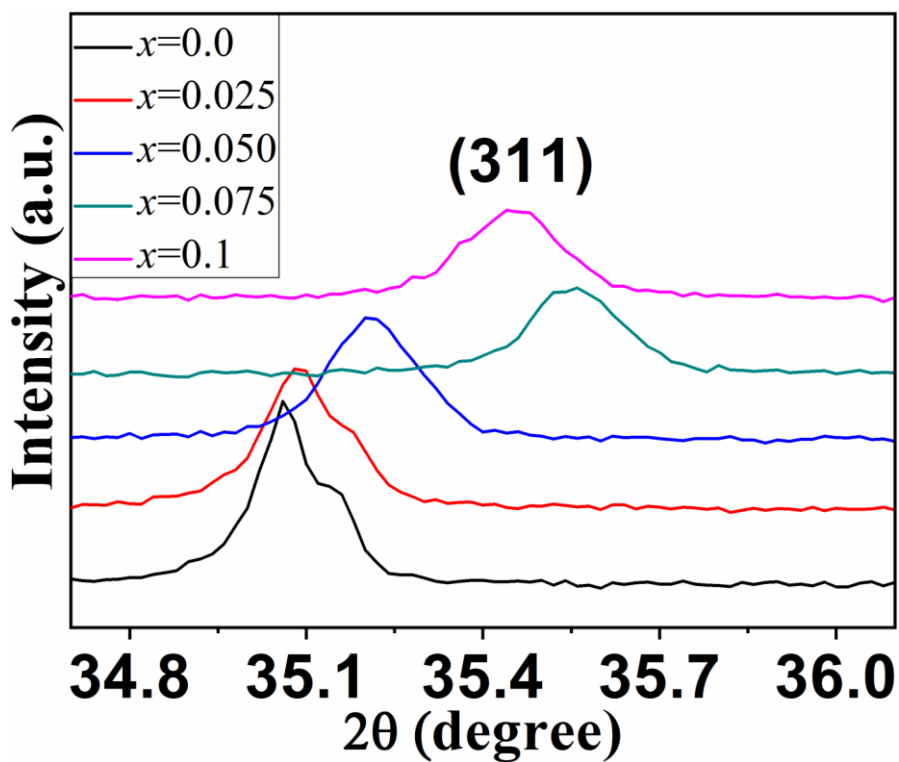


Figure 4.3.2: Zoomed in image of most prominent peak in  $Mn_{0.5}Zn_{0.5}Nd_xFe_{2-x}O_4$  ferrites.

The values of  $x$  in the studied composition corresponding to different RE<sup>3+</sup> ions are 0, 0.025, 0.050, 0.075 and 0.1. After analyzing figure 4.1.1, it has been observed that for  $x \leq 0.050$ , there is creation of pure spinel structure (as confirmed by JCPDS 74-2401). Spinel structure of La<sup>3+</sup> doped manganese-zinc ferrites has been affirmed by the presence of planes at (111), (220), (311), (222), (400), (422), (511), (440) and (533). There is creation of LaFeO<sub>3</sub> compound (JCPDS 75-0541) for higher content of La ( $x > 0.050$ ). This may be due to the effect of sintering above 1000 K for samples as reported by Nakayama [23]. Lesser solubility of La<sup>3+</sup> ions in different ferrites has also been indicated by various other authors showing similar results [24-26].

Figures 4.2.1 and 4.3.1 for the Gd<sup>3+</sup> and Nd<sup>3+</sup> doped Mn-Zn ferrites have also revealed the presence of spinel structure (as confirmed by JCPDS 74-2401) for all the investigated compositions. The establishment of spinel structure for the Gd<sup>3+</sup> and Nd<sup>3+</sup> doped ferrites have been supported from the presence of planes (111), (220), (311), (222), (400), (422), (511), (440) and (533). There is also a creation of GdFeO<sub>3</sub> compound (JCPDS 47-0067) and NdFeO<sub>3</sub> compound (JCPDS 74-1473) for higher content of Gd & Nd ( $x > 0.050$ ) (Figure 4.2.1 & 4.3.1). Crystallite size, packing factor, interplanar spacing and lattice constant are estimated using the most prominent peak at (311) for all the investigated compositions. Crystallite size of the La<sup>3+</sup>, Gd<sup>3+</sup> and Nd<sup>3+</sup> doped manganese-zinc ferrites has been estimated employing Scherrer's formula;  $D = 0.9\lambda / \beta \cos\theta$ , where  $D$  represents the crystallite size,  $\lambda = 0.154056$  nm is X-ray wavelength,  $\beta$  represents the full width at half maximum value and  $\theta$  represents Bragg's angle. Other structural parameters like lattice constant ( $a$ ), interplanar spacing ( $d$ ) and packing factor ( $P$ ) are computed by employing relations [27];  $a = d(h^2 + k^2 + l^2)^{1/2}$ ,  $2d \sin \theta = n\lambda$  and  $P = D/d$  respectively.

From the computed structural parameters given in table 4.1, it has been found that up to a minor content of La (*i.e.*  $x$  less than and equal to 0.050) the crystallite size and the packing factor decreases on the other hand above this amount (*i.e.*  $x$  greater than 0.050) the crystallite size and the packing factor increases. At  $x = 0.050$ , the values of  $a$  as well as  $d$  are minimum. Transposition of ferric ions with lanthanum ions on the lattice sites is the main reason for the change in various parameters values. The substantial ionic radii of La<sup>3+</sup> ions (1.06 Å) play a major role in the variation of structural parameters values. The large La<sup>3+</sup> ions (1.06 Å) find it difficult to substitute Fe<sup>3+</sup> ions (0.67 Å).

**Table 4.1:** Various computed structural parameters for  $RE^{3+}$  ( $= La^{3+}$ ,  $Gd^{3+}$  &  $Nd^{3+}$ ) doped  $Mn_{0.5}Zn_{0.5}RE_xFe_{2-x}O_4$  ferrites.

$x$	For $La^{3+}$ doping				For $Gd^{3+}$ doping				For $Nd^{3+}$ doping			
	$D$ (nm)	$d$ (Å)	$a$ (Å)	$P$	$D$ (nm)	$d$ (Å)	$a$ (Å)	$P$	$D$ (nm)	$d$ (Å)	$a$ (Å)	$P$
0	67.42	2.557	8.483	263.624	67.42	2.557	8.483	263.624	67.42	2.557	8.483	263.624
0.025	55.49	2.550	8.459	217.585	56.79	2.546	8.445	223.036	56.00	2.556	8.478	219.073
0.050	54.17	2.544	8.438	212.921	53.93	2.559	8.488	210.708	47.73	2.548	8.451	187.340
0.075	59.35	2.556	8.478	232.200	51.45	2.546	8.445	202.096	52.11	2.524	8.372	206.449
0.1	65.53	2.553	8.468	256.637	45.72	2.546	8.445	179.580	44.05	2.531	8.397	174.021

Therefore, a small number of  $\text{La}^{3+}$  ions may occupy themselves on the grain boundaries. The smaller solubility with increment in  $\text{La}^{3+}$  content ( $x > 0.050$ ) contributes to an increment in  $\text{LaFeO}_3$  phase intensity (figure 4.1.1). Further, similar ionic radii and identical valency are the two main factors required for the substitution of two ions. Since the bond energy of  $\text{La}^{3+}-\text{O}^{2-}$  bond is larger than the bond energy of  $\text{Fe}^{3+}-\text{O}^{2-}$  bond, so a large amount of energy is necessitated to replace  $\text{La}^{3+}$  ions for  $\text{Fe}^{3+}$  ions. It may be the reason for the presence of  $\text{LaFeO}_3$  compound for  $x > 0.050$ . A few  $\text{La}^{3+}$  ions might be occupying the grain boundaries during the transposition of  $\text{La}^{3+}$  ions in place of  $\text{Fe}^{3+}$  ions. The smaller crystallite size may be due to the pressure created by bulkier  $\text{La}^{3+}$  ions (big ionic radii) upon the grain boundaries [28, 29].

The effect of  $\text{Gd}^{3+}$  and  $\text{Nd}^{3+}$  ions doping on Mn-Zn ferrites for various structural parameters has also been analyzed using the XRD spectra. The calculated values of various structural parameters have been given in table 4.1 for  $\text{Gd}^{3+}$  and  $\text{Nd}^{3+}$  ions doping respectively. It is witnessed that generally there is a decrease in the structural parameters ( $D$ ,  $a$ ,  $d$  and  $P$ ) with increase in  $\text{Gd}^{3+}$  and  $\text{Nd}^{3+}$  doping in manganese-zinc ferrites. The reason for the reduction in the measure of  $D$ ,  $a$ ,  $d$  and  $P$  is on account of the variation in the ionic radii of different  $\text{RE}^{3+}$  ions and ferric ions. As, it happens hard to substitute ferric ion (ionic radius = 0.67 Å) with bulkier  $\text{Gd}^{3+}$  ion (ionic radius = 0.94 Å) in  $\text{Mn}_{0.5}\text{Zn}_{0.5}\text{Gd}_x\text{Fe}_{2-x}\text{O}_4$  ferrites. This leads to a smaller solubility with increment in  $\text{Gd}^{3+}$  concentration ( $x > 0.050$ ) and creates  $\text{GdFeO}_3$  phase whose intensity also show an increase with increment in  $\text{Gd}^{3+}$  concentration ( $x > 0.050$ ) (figure 4.2.1). Similarly, it is also hard to substitute  $\text{Fe}^{3+}$  ion (ionic radius = 0.67 Å) with bigger  $\text{Nd}^{3+}$  ion (ionic radius = 0.983 Å) in  $\text{Mn}_{0.5}\text{Zn}_{0.5}\text{Nd}_x\text{Fe}_{2-x}\text{O}_4$  ferrites. This leads to a smaller solubility with increment in  $\text{Nd}^{3+}$  concentration ( $x > 0.050$ ) and creates  $\text{NdFeO}_3$  phase whose intensity also show an increase with increment in  $\text{Nd}^{3+}$  concentration ( $x > 0.050$ ) (figure 4.3.1). Hence, on substitution of  $\text{Gd}^{3+}$  ions in  $\text{Mn}_{0.5}\text{Zn}_{0.5}\text{Gd}_x\text{Fe}_{2-x}\text{O}_4$  ferrites and  $\text{Nd}^{3+}$  ions in  $\text{Mn}_{0.5}\text{Zn}_{0.5}\text{Nd}_x\text{Fe}_{2-x}\text{O}_4$  ferrites for ferric ions on the respective lattice sites, a portion of the  $\text{Gd}^{3+}$  and  $\text{Nd}^{3+}$  may possess the grain boundaries (in the form of  $\text{GdFeO}_3$  and  $\text{NdFeO}_3$ ) and thereby producing more compression on the grain boundaries leading to a decrease in crystallite size of  $\text{Gd}^{3+}$  and  $\text{Nd}^{3+}$  ions doped manganese - zinc spinel ferrites in comparison to manganese-zinc ferrites [30].

Figures 4.1.2, 4.2.2 & 4.3.2 show the zoomed in images of most prominent peak (311) for  $\text{RE}^{3+} = \text{La}^{3+}$ ,  $\text{Gd}^{3+}$  &  $\text{Nd}^{3+}$  doped Mn-Zn ferrites respectively. All investigated  $\text{RE}^{3+}$  doped samples have shown some shift either towards higher or towards lower

value of Bragg's angle ( $\theta$ ) as compared to undoped ( $x=0$ ) sample. According to Bragg's equation ( $2d \sin\theta = n\lambda$ ), Bragg's angle ( $\theta$ ) is reciprocally proportional to interplanar spacing ( $d$ ) and further is correlated to the lattice constant ( $a$ ). So the change in prominent peak position is fully responsible for variation in the values of interplanar spacing and lattice constant.

#### 4.3.2 FE-SEM and EDS

The morphology of  $Mn_{0.5}Zn_{0.5}RE_xFe_{2-x}O_4$  (where,  $RE = La, Gd, Nd$ ) nano ferrites have been investigated by using FE-SEM microscopy. Figure 4.4.1 & 4.4.2, figure 4.5.1 & 4.5.2 and figure 4.6.1 & 4.6.2 show the FE-SEM micrographs of  $La^{3+}$  ions,  $Gd^{3+}$  ions and  $Nd^{3+}$  ions doped manganese-zinc nano ferrites respectively. A non-uniform grain size as seen in FE-SEM micrographs is witnessed for all prepared samples. Nearness of agglomeration is seen on  $La^{3+}$ ,  $Gd^{3+}$  and  $Nd^{3+}$  ions doping to  $Mn$ - $Zn$  ferrite samples. Distinct crystalline structures have also been witnessed for all samples.

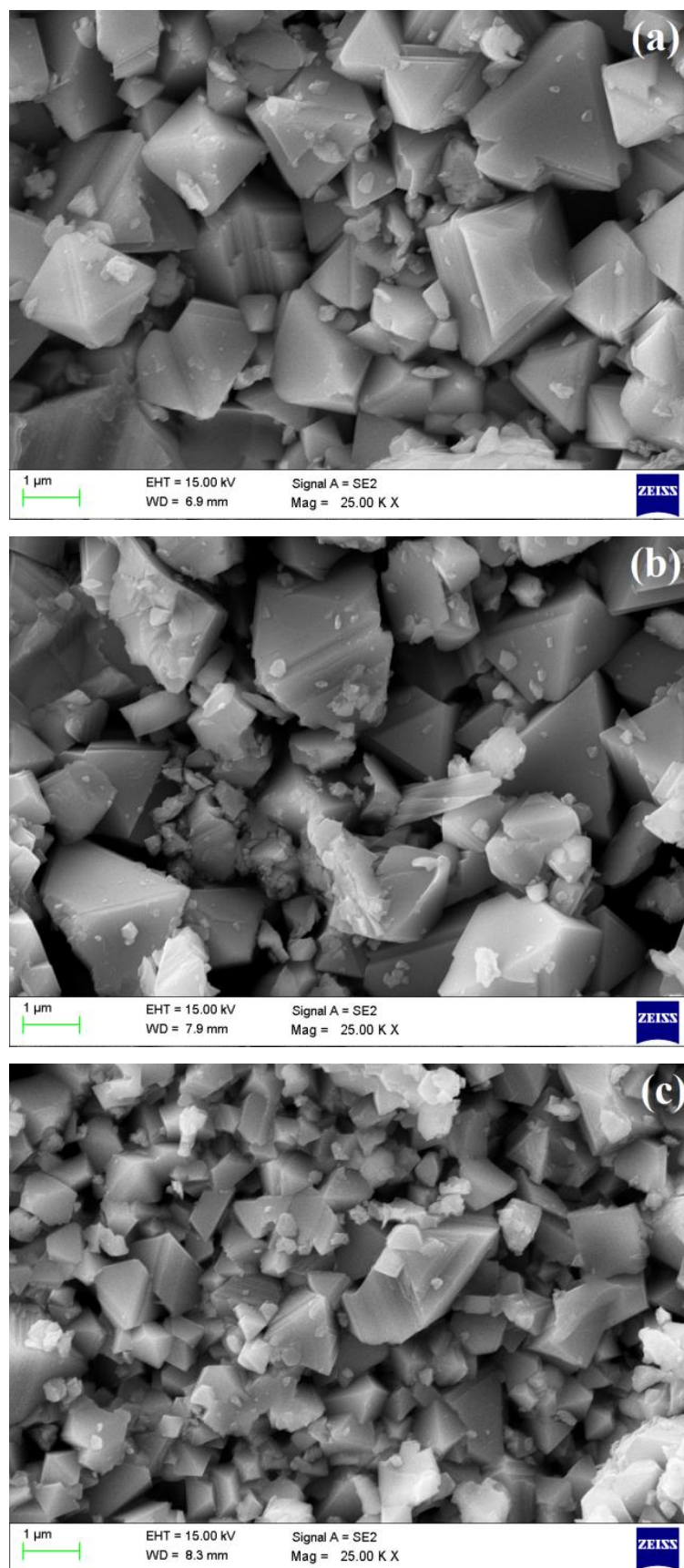


**Figure 4.4.1:** FE-SEM images for (a)  $x = 0$ ; (b)  $x = 0.025$ ; (c)  $x = 0.050$ ; of  $\text{Mn}_{0.5}\text{Zn}_{0.5}\text{La}_x\text{Fe}_{2-x}\text{O}_4$  spinel ferrites.

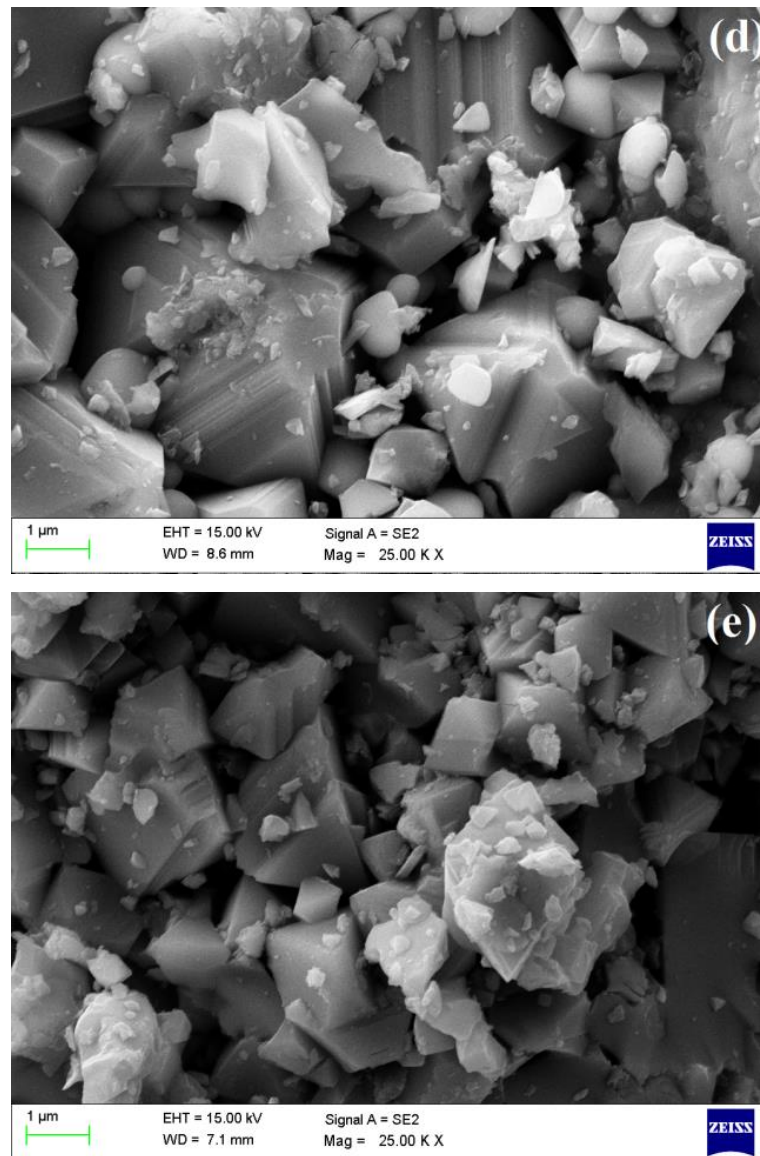


**Figure 4.4.2:** FE-SEM images for (d)  $x = 0.075$ ; (e)  $x = 0.1$  of  $Mn_{0.5}Zn_{0.5}La_xFe_{2-x}O_4$  spinel ferrites.

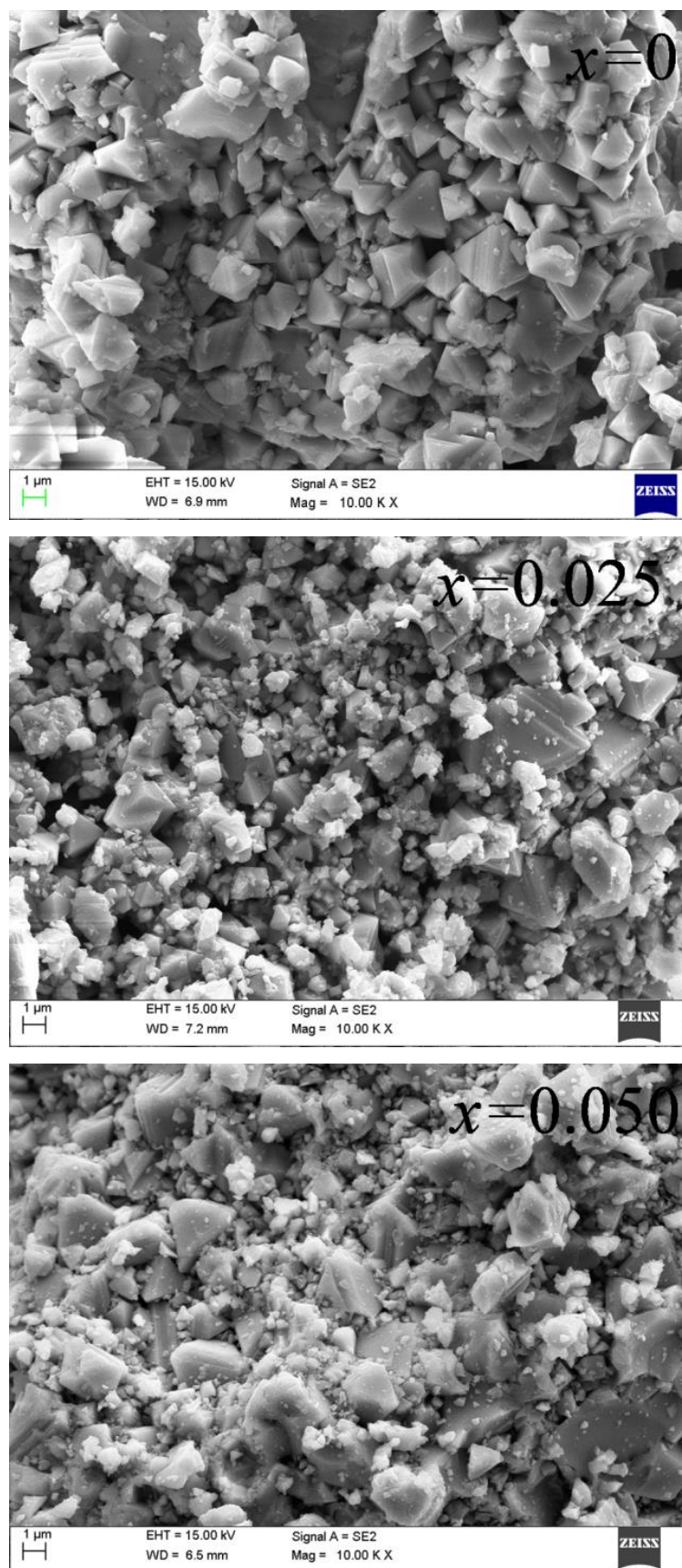


**Figure 4.5.1:** FE-SEM images for (a)  $x = 0$ ; (b)  $x = 0.025$ ; (c)  $x = 0.050$ ; of  $\text{Mn}_{0.5}\text{Zn}_{0.5}\text{Gd}_x\text{Fe}_{2-x}\text{O}_4$  spinel ferrites.

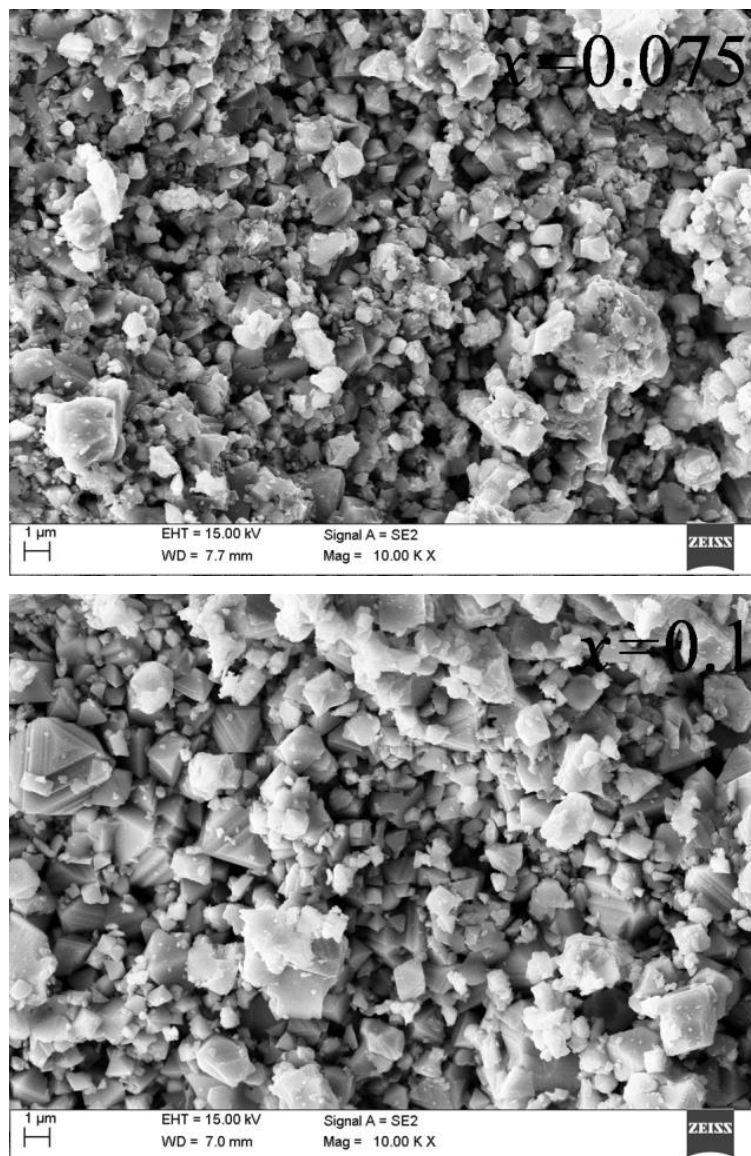


**Figure 4.5.2:** FE-SEM images for (d)  $x = 0.075$ ; (e)  $x = 0.1$  of  $Mn_{0.5}Zn_{0.5}Gd_xFe_{2-x}O_4$  spinel ferrites.

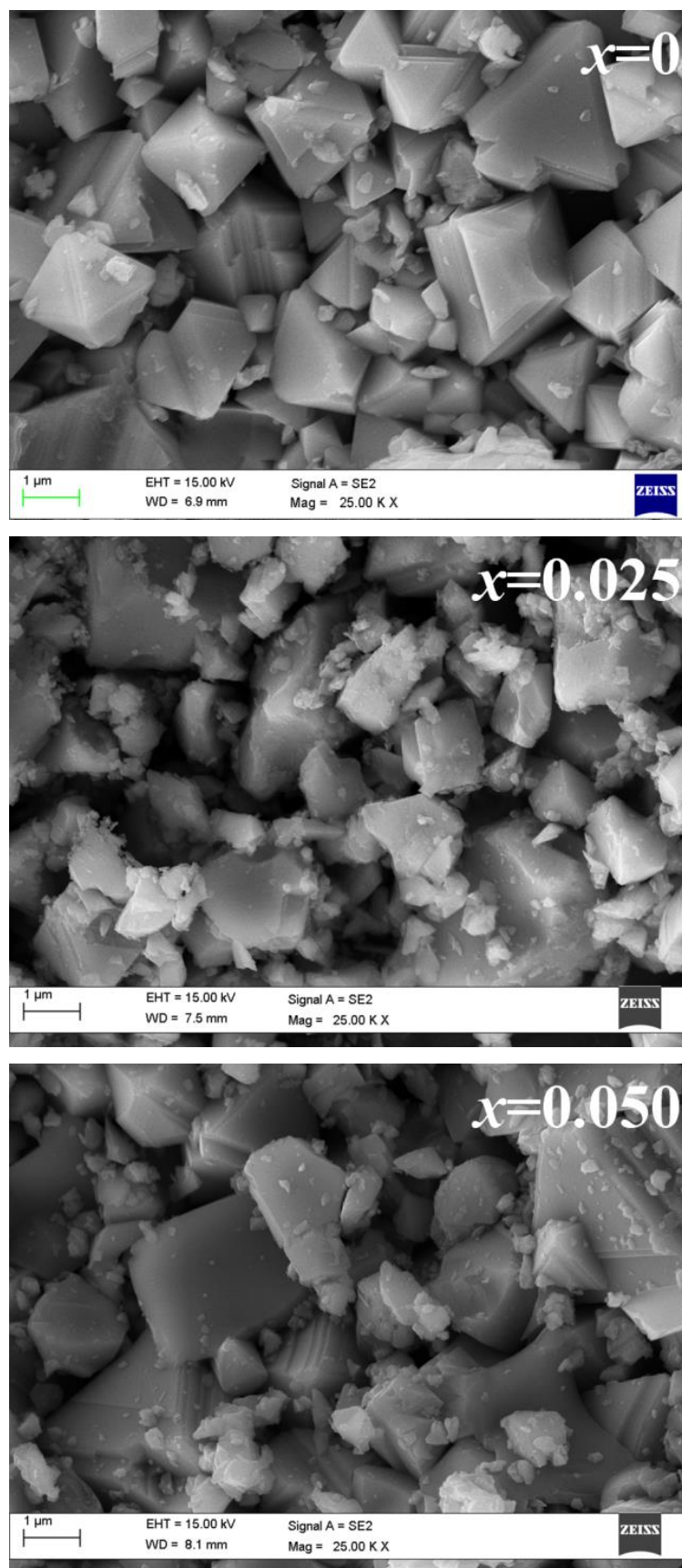


**Figure 4.6.1:** FE-SEM images for (a)  $x = 0$ ; (b)  $x = 0.025$ ; (c)  $x = 0.050$ ; of  $\text{Mn}_{0.5}\text{Zn}_{0.5}\text{Nd}_x\text{Fe}_{2-x}\text{O}_4$  spinel ferrites.

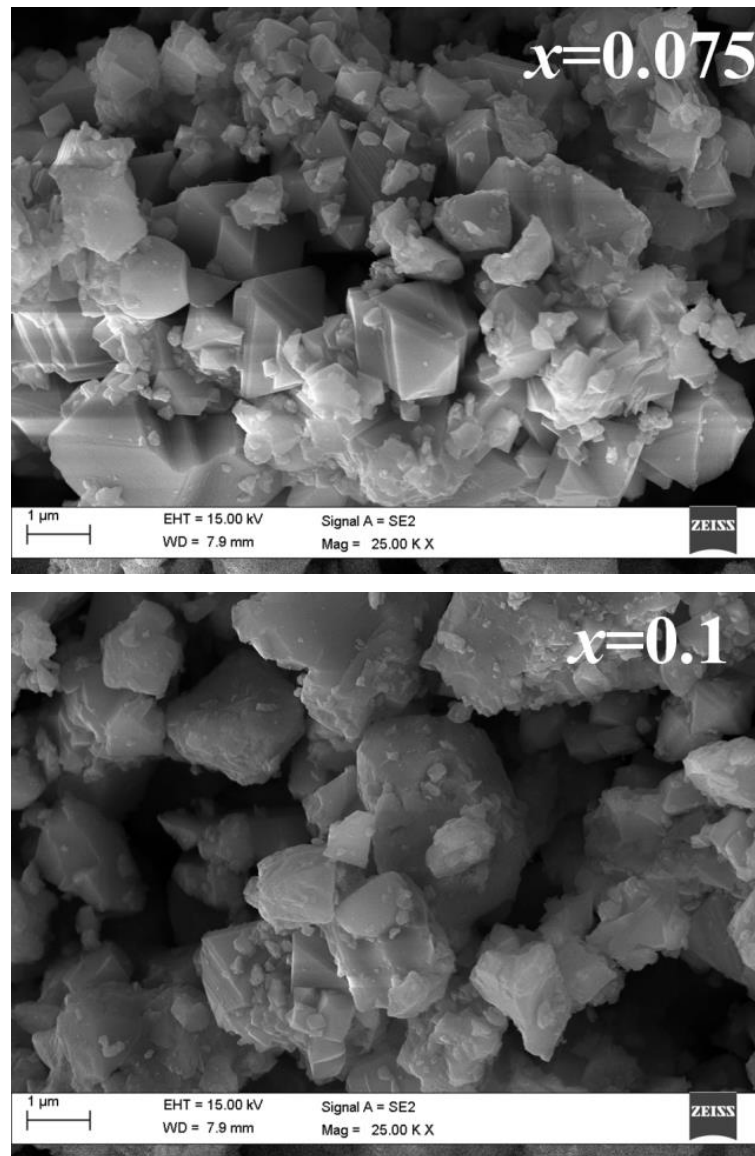


**Figure 4.6.2:** FE-SEM images for (d)  $x = 0.075$ ; (e)  $x = 0.1$  of  $Mn_{0.5}Zn_{0.5}Nd_xFe_{2-x}O_4$  spinel ferrites.

To analyze the synthesized  $Mn_{0.5}Zn_{0.5}RE_xFe_{2-x}O_4$  ferrite samples for the stoichiometry in composition, EDS has been used. Figure 4.7.1 & 4.7.2, figure 4.8.1 & 4.8.2 and figure 4.9.1 & 4.9.2 show the EDS spectra of  $La^{3+}$ ,  $Gd^{3+}$  and  $Nd^{3+}$  ions doped manganese-zinc nano ferrites respectively.

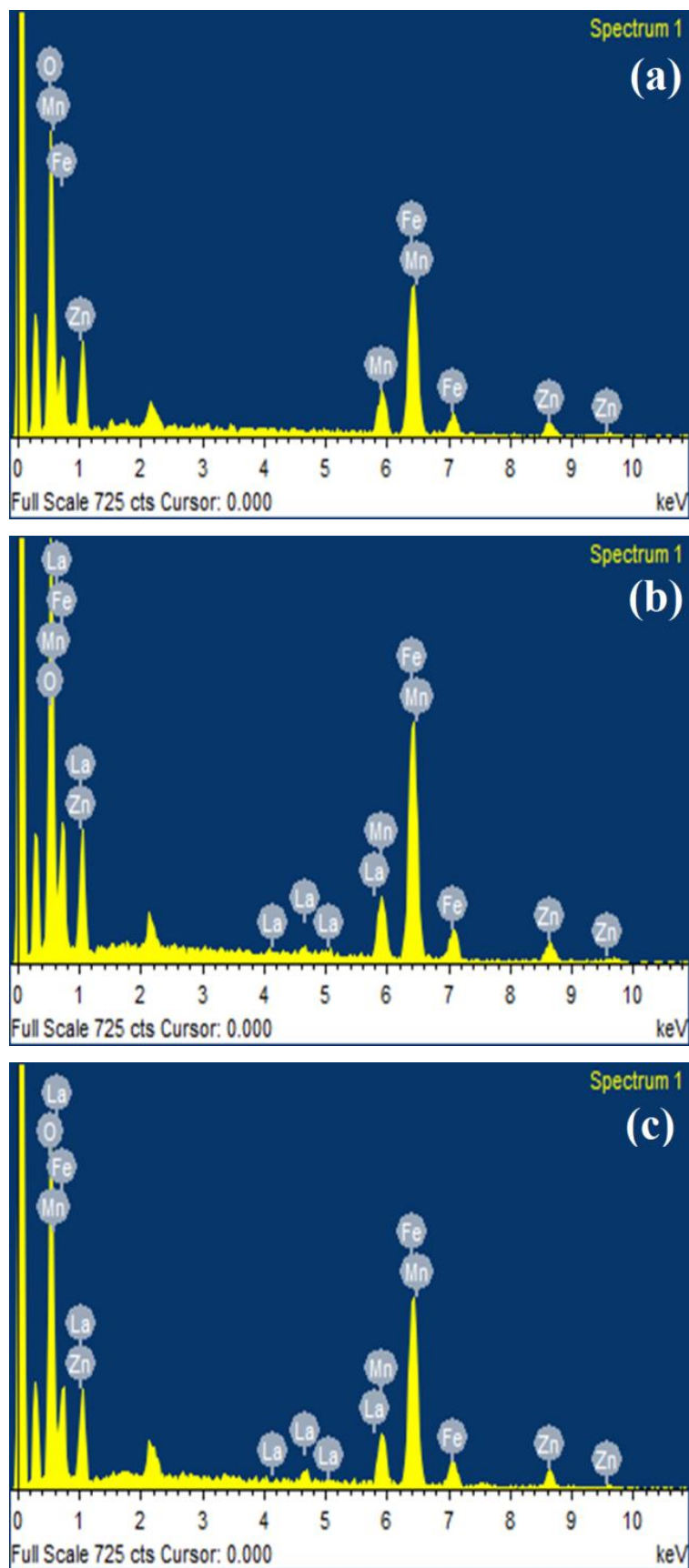
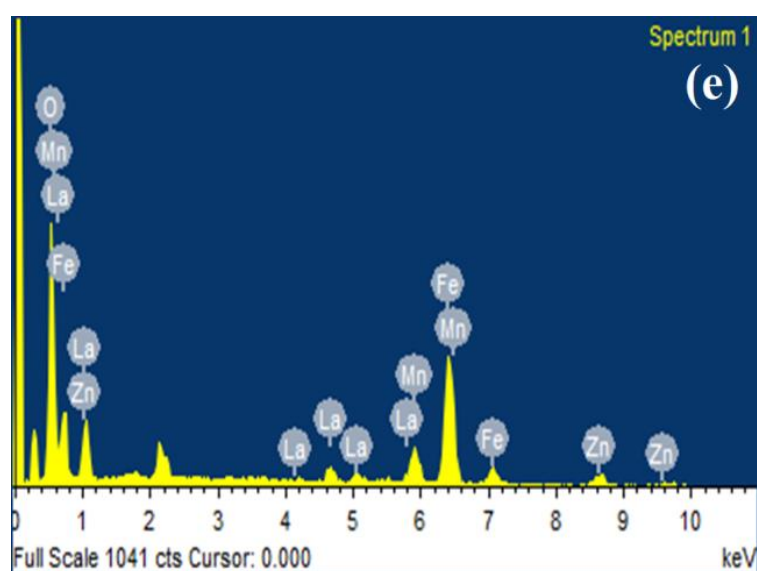
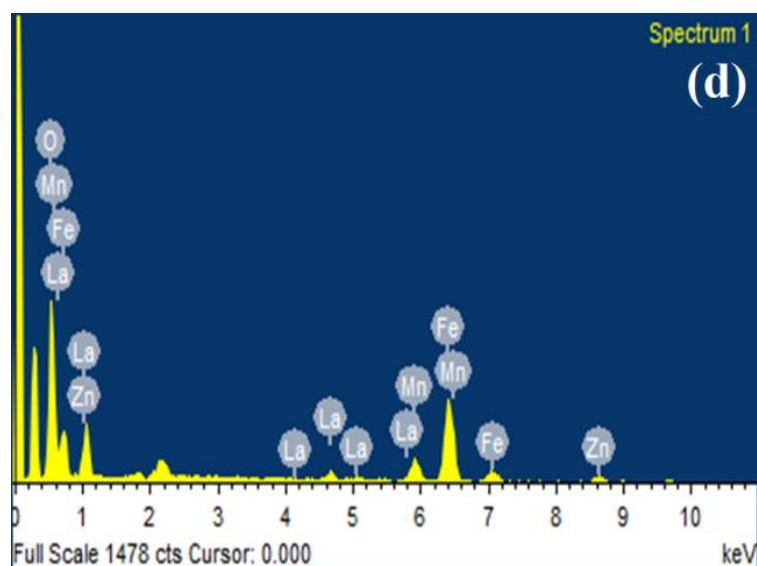


**Figure 4.7.1:** EDS spectra for (a)  $x = 0$ ; (b)  $x = 0.025$ ; (c)  $x = 0.050$  of  $\text{Mn}_{0.5}\text{Zn}_{0.5}\text{La}_x\text{Fe}_{2-x}\text{O}_4$  ferrites.



### Element Atomic% (f)

<b>O</b>	<b>50.93</b>
<b>Mn</b>	<b>6.93</b>
<b>Fe</b>	<b>33.49</b>
<b>Zn</b>	<b>8.28</b>
<b>La</b>	<b>0.38</b>

**Figure 4.7.2:** EDS spectra for (d)  $x = 0.075$ ; (e)  $x = 0.1$  of  $Mn_{0.5}Zn_{0.5}La_xFe_{2-x}O_4$  ferrites, (f) atomic% of  $Mn_{0.5}Zn_{0.5}La_{0.025}Fe_{1.975}O_4$  ferrite as reference.

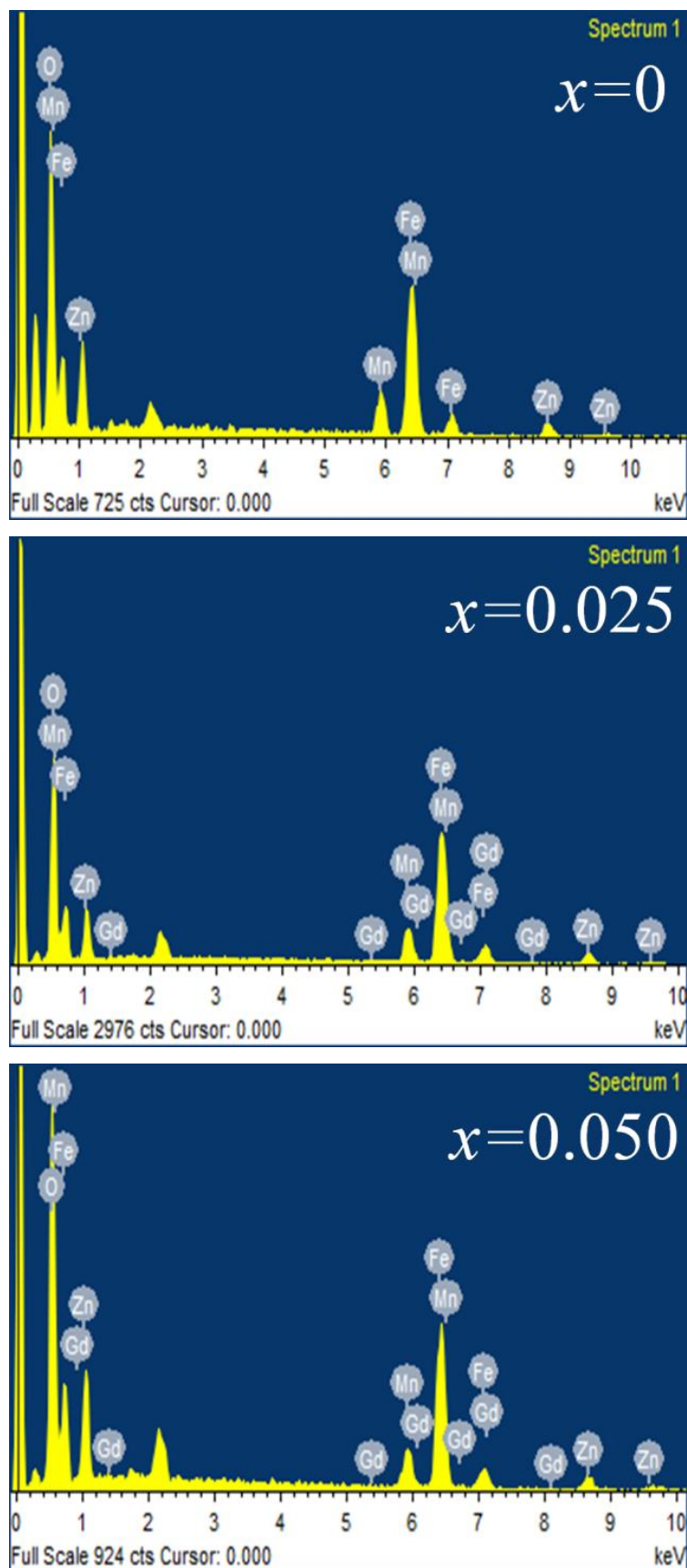
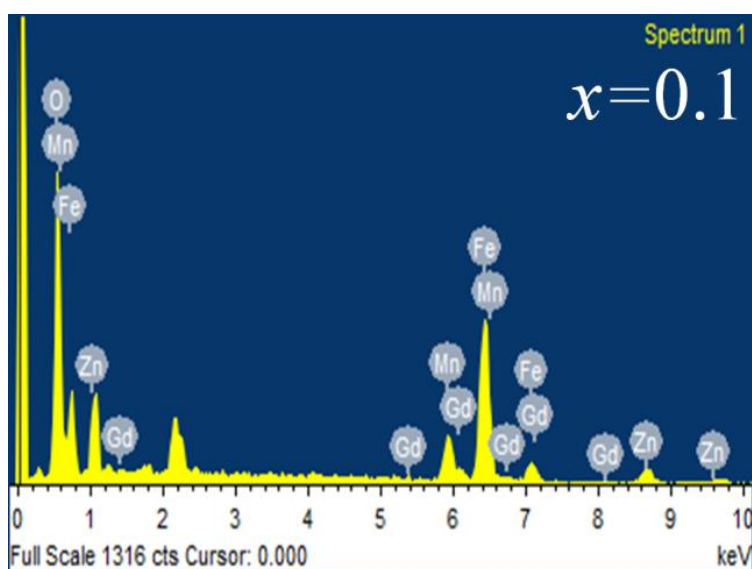
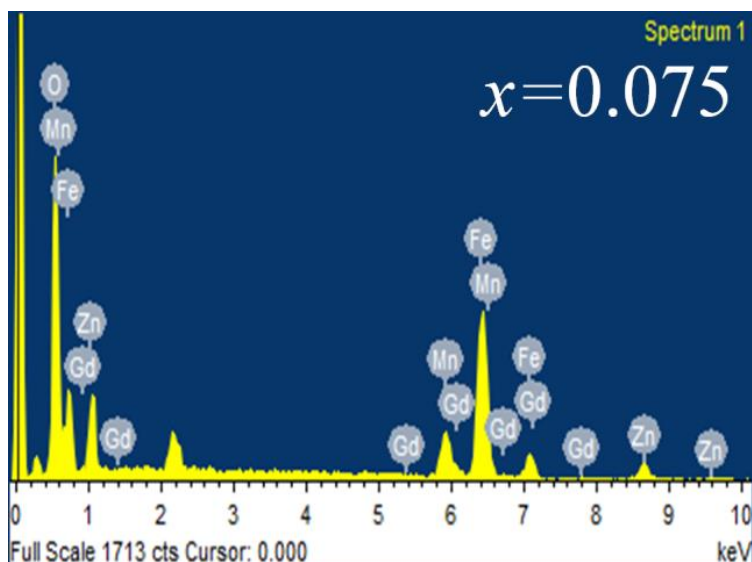


**Figure 4.8.1:** EDS spectra for (a)  $x = 0$ ; (b)  $x = 0.025$ ; (c)  $x = 0.050$ ; of  $\text{Mn}_{0.5}\text{Zn}_{0.5}\text{Gd}_x\text{Fe}_{2-x}\text{O}_4$  ferrites



### Element Atomic% (a)

<b>O</b>	<b>45.50</b>
<b>Mn</b>	<b>8.53</b>
<b>Fe</b>	<b>38.31</b>
<b>Zn</b>	<b>7.26</b>
<b>Gd</b>	<b>0.40</b>

Figure 4.8.2: EDS spectra for (d)  $x = 0.075$ ; (e)  $x = 0.1$  of  $Mn_{0.5}Zn_{0.5}Gd_xFe_{2-x}O_4$  ferrites, (a) atomic% of  $Mn_{0.5}Zn_{0.5}Gd_{0.025}Fe_{1.975}O_4$  ferrite as reference.

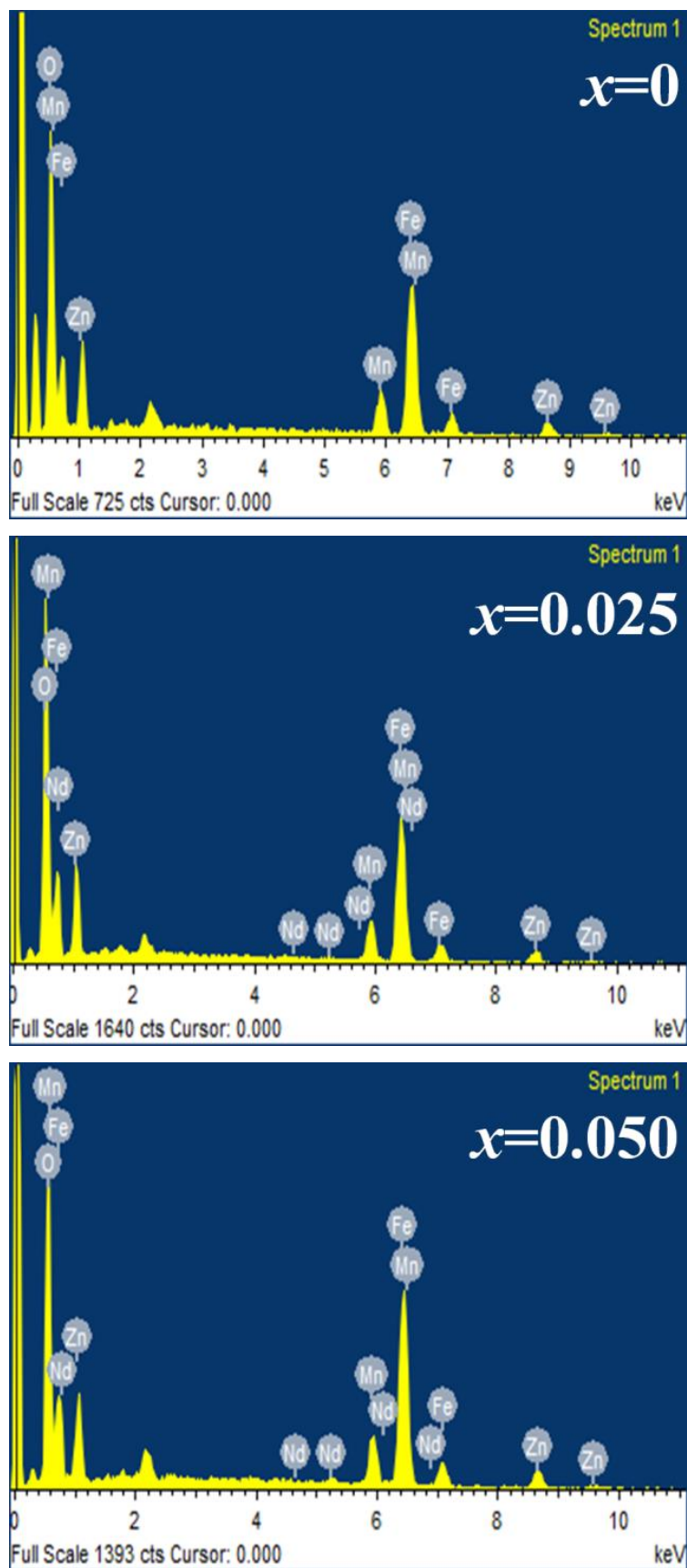
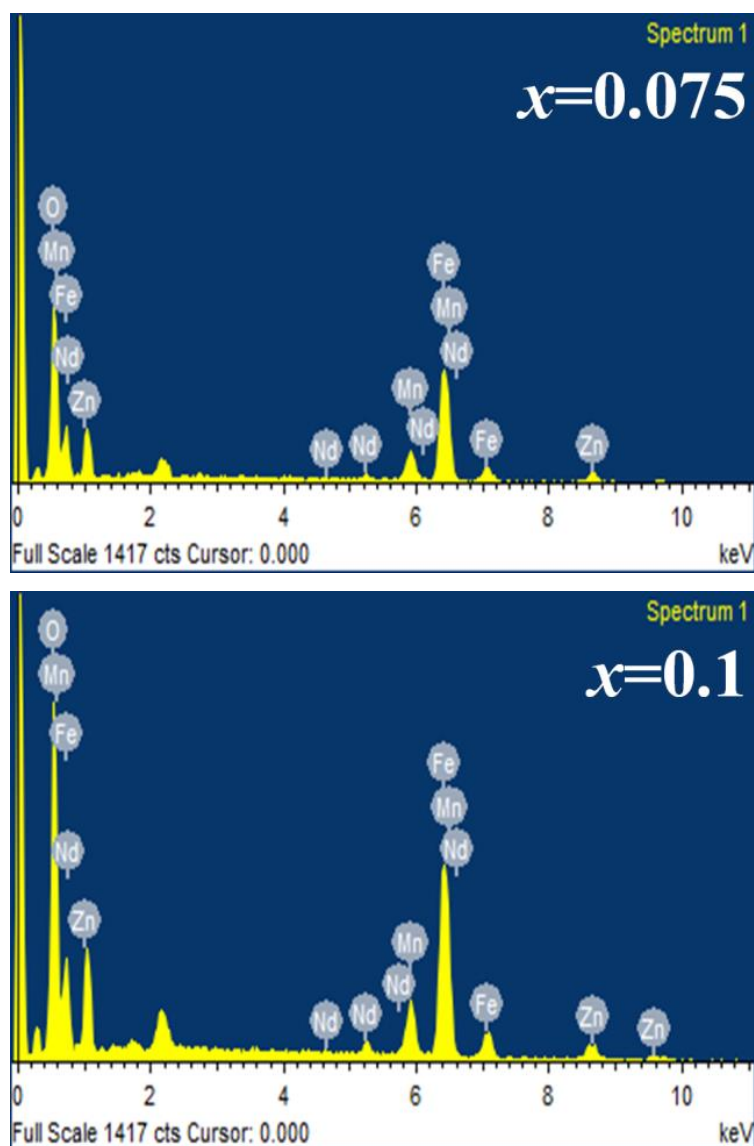


**Figure 4.9.1:** EDS spectra for (a)  $x = 0$ ; (b)  $x = 0.025$ ; (c)  $x = 0.050$ ; of  $\text{Mn}_{0.5}\text{Zn}_{0.5}\text{Nd}_x\text{Fe}_{2-x}\text{O}_4$  ferrites.



Element	Atomic%	(a)
<b>O</b>	55.42	
<b>Mn</b>	6.47	
<b>Fe</b>	29.43	
<b>Zn</b>	8.51	
<b>Nd</b>	0.17	

**Figure 4.9.2:** EDS spectra for (d)  $x = 0.075$ ; (e)  $x = 0.1$  of  $Mn_{0.5}Zn_{0.5}Nd_xFe_{2-x}O_4$  ferrites, (a) atomic% of  $Mn_{0.5}Zn_{0.5}Nd_{0.025}Fe_{1.975}O_4$  ferrite as reference.

The results show that all the constituent elements are present in the synthesized compositions. Atomic% of  $Mn_{0.5}Zn_{0.5}RE_{0.025}Fe_{1.975}O_4$  ferrite samples (where  $RE = La, Gd$  and  $Nd$ ) has been shown in figures 4.7.2, 4.8.2 & 4.9.2 as reference.

### 4.3.3 FTIR Spectra

The development of spinel ferrite structure has also been verified by using the Fourier transform infrared spectroscopy (FTIR). Figure 4.10, figure 4.11 and figure 4.12 shows FTIR spectra of La<sup>3+</sup>, Gd<sup>3+</sup> and Nd<sup>3+</sup> ions doped manganese-zinc nano ferrites respectively. In figure 4.10, two absorption bands,  $\nu_1$  from 430  $cm^{-1}$  to 490  $cm^{-1}$  and  $\nu_2$  from 530  $cm^{-1}$  to 590  $cm^{-1}$  have been observed for La<sup>3+</sup> ions doped manganese-zinc nano ferrites. In figure 4.11, two absorption bands,  $\nu_1$  from 460  $cm^{-1}$  to 495  $cm^{-1}$  and  $\nu_2$  from 565  $cm^{-1}$  to 590  $cm^{-1}$  have been observed for Gd<sup>3+</sup> ions doped manganese-zinc nano ferrites. In figure 4.12, two absorption bands,  $\nu_1$  from 465  $cm^{-1}$  to 495  $cm^{-1}$  and  $\nu_2$  from 570  $cm^{-1}$  to 590  $cm^{-1}$  have been observed for Nd<sup>3+</sup> ions doped manganese-zinc nano ferrites. The substitution of RE<sup>3+</sup> ions for Fe<sup>3+</sup> ions can be clearly seen with a change in the place of absorption bands ( $\nu_1, \nu_2$ ) on La<sup>3+</sup>, Gd<sup>3+</sup> and Nd<sup>3+</sup> ions doping. Further, the absorption band  $\nu_1$  depicts the presence of cation - oxygen bonds in the octahedral (*i.e.* B site) site. Moreover,  $\nu_2$  records the presence of metal ion – oxygen ion bonds in the tetrahedral (*i.e.* A site) site.

Practically equivalent to these results have prior been accounted for spinel ferrites [31-35]. Szczygieł *et al.* have reported the FTIR spectra of Mn-Zn ferrites prepared by sol-gel auto-combustion synthesis technique [32]. They have observed the absorption bands at frequencies near to 540  $cm^{-1}$  indicating the origination of metal ions - oxygen ions bonds in tetrahedral and octahedral location. Baykal *et al.* have analyzed the FTIR spectra of Mn-Zn ferrites prepared by thermal decomposition [33]. They have found some cation-oxygen absorption bands approximately at 550  $cm^{-1}$ . Kotsikau *et al.* have studied the FTIR spectra of Mn-Zn ferrites prepared by spray pyrolysis technique [34]. They have reported absorption bands at frequencies (420, 430 & 430)  $cm^{-1}$  and (551, 571 & 559)  $cm^{-1}$  showing the appearance of metal ions - oxygen bonds at octahedral and tetrahedral locations respectively. Kumar *et al.* [35] published the FTIR spectra of Gd<sup>3+</sup> doped Mn-Zn ferrite prepared by co-precipitation technique [35].

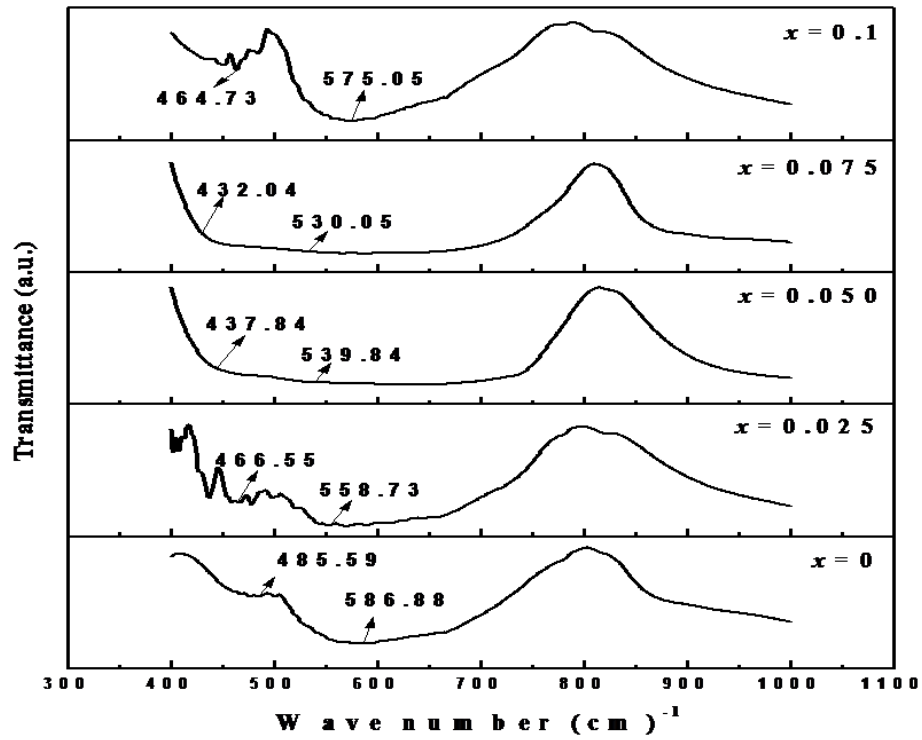


**Figure 4.10:** FTIR spectra of  $Mn_{0.5}Zn_{0.5}La_xFe_{2-x}O_4$  nano ferrites. The y-axis scale has been shifted for clarity.

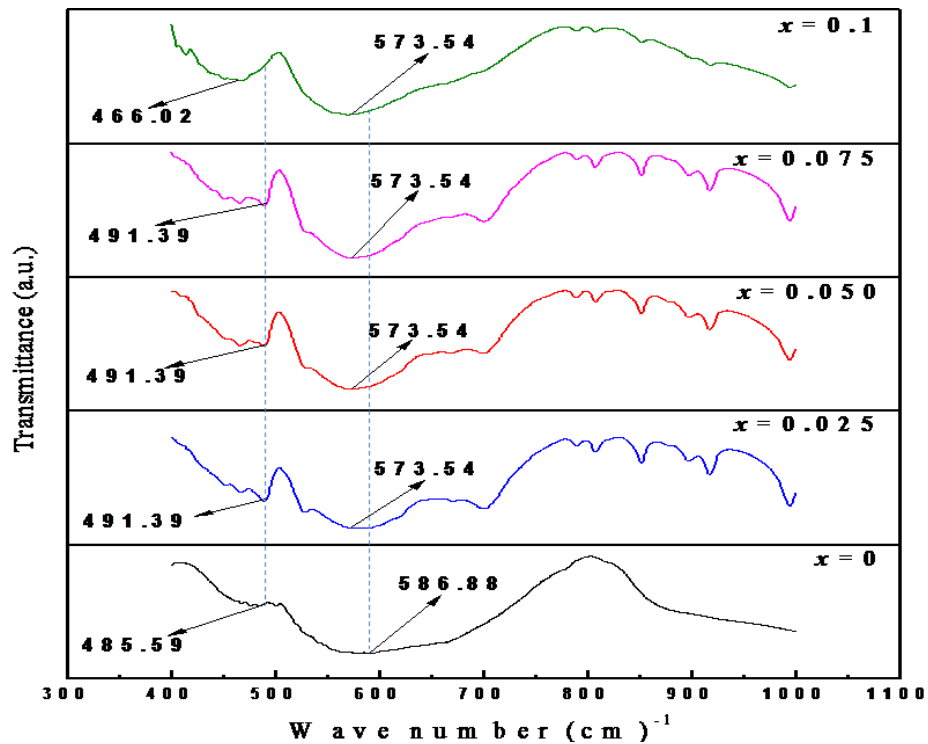


**Figure 4.11:** FTIR spectra of  $Mn_{0.5}Zn_{0.5}Gd_xFe_{2-x}O_4$  nano ferrites. The y-axis scale has been shifted for clarity.

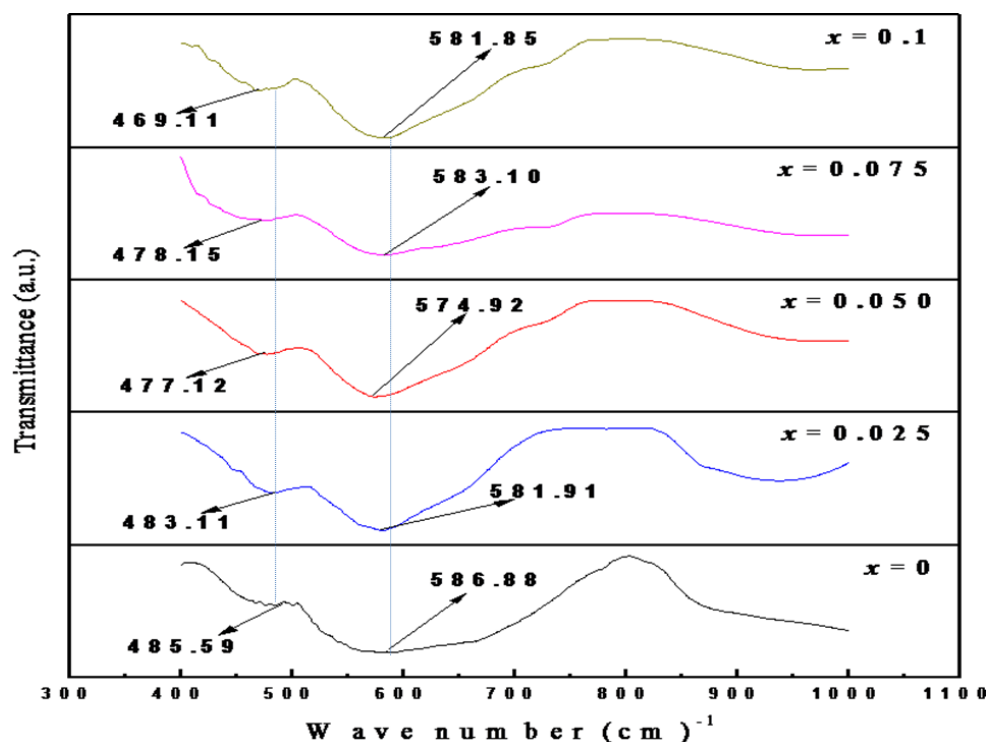


**Figure 4.12:** FTIR spectra of  $Mn_{0.5}Zn_{0.5}Nd_xFe_{2-x}O_4$  nano ferrites. The y-axis scale has been shifted for clarity.

They have noticed that for all the samples, absorption bands at frequencies  $570\text{ cm}^{-1}$  and  $416\text{ cm}^{-1}$  shows the appearance of iron - oxygen bonds at tetrahedral sites and gadolinium - oxygen bonds at octahedral sites. Hence in the present work, the origination of spinel ferrite arrangement is confirmed with the presence of two absorption  $\nu_1$  and  $\nu_2$  bands.

#### 4.4. Conclusion

Cubic spinel phase has been observed for  $Mn_{0.5}Zn_{0.5}RE_xFe_{2-x}O_4$  (where  $x = 0, 0.025, 0.050, 0.075$  &  $0.1$ ) nanoferrites synthesized through co-precipitation synthesis technique. For the three dopants used in *Mn-Zn* ferrites, the values of structural parameters ( $D$ ,  $a$ ,  $d$  and  $P$ ) have been observed to decrease generally. Occurrence of spinel structure in all the investigated samples has been confirmed from FTIR spectroscopy. A clear change in the place of absorption bands with  $RE$  ( $= La, Gd$  &  $Nd$ ) doping has also been observed. FESEM micrographs of  $Mn_{0.5}Zn_{0.5}RE_xFe_{2-x}O_4$  (where  $RE=La, Gd, Nd$ ) ferrites show sharp crystalline structures. EDS spectroscopy confirms the presence of constituents *i.e.*  $Mn, Zn, RE$  ( $= La, Gd$  &  $Nd$ ),  $Fe, O$  in all the investigated samples.

# CHAPTER-5\*

---

## Cation distribution and magnetic study of $\text{La}^{3+}$ , $\text{Gd}^{3+}$ & $\text{Nd}^{3+}$ doped Mn-Zn nano ferrites

- \* 1. “**Prashant Thakur**, R. Sharma, M. Kumar, S.C. Katyal, N.S Negi, N. Thakur, V. Sharma, Pankaj Sharma, “*Superparamagnetic La Doped Mn-Zn Nano Ferrites: Dependence on Dopant Content and Crystallite Size*” Materials Research Express Vol 3 (2016) 075001”
2. “**Prashant Thakur**, R. Sharma, V. Sharma, P.B. Barman, M. Kumar, D. Barman, S.C. Katyal, Pankaj Sharma, *Gd<sup>3+</sup> doped Mn-Zn soft ferrite nanoparticles: Superparamagnetism and its correlation with other physical properties*, Journal of Magnetism and Magnetic Materials Vol 432 (2017) 208–217”.
3. “**Prashant Thakur**, R. Sharma, M. Kumar, S.C. Katyal, P.B. Barman, V. Sharma, Pankaj Sharma, *Structural, morphological, magnetic and optical study of Nd<sup>3+</sup> doped Mn-Zn ferrite nanoparticles synthesized via co-precipitation technique*, Journal of Magnetism and Magnetic Materials Vol 479 (2019) 317-325”.



Spinel ferrites have immense potential in the field of memory storage, magnetic recording, biomedical applications *etc.* Magnetic characteristics are vital to find out the application domain of these spinel ferrites. In this chapter, magnetic characteristics of lanthanides ( $RE^{3+} = La^{3+}, Gd^{3+} \& Nd^{3+}$ ) doped Mn-Zn spinel ferrites have been described. Cation distribution for the above mentioned spinel ferrites has also been proposed and is utilized to explain the magnetic characteristics.

## 5.1. Introduction

The distribution of cations at A-site and B-site in spinel ferrites is responsible for several physical properties especially magnetic properties [1]. There is a migration of some divalent metal ions from octahedral (B) location to the tetrahedral (A) location with the substitution of the lanthanide ions in spinel ferrite. This movement of metal ions from octahedral (B) site to the tetrahedral (A) site in spinel ferrites also depend on the size of the cationic radii [2]. Superparamagnetic (SPM) nanoparticles have superparamagnetic characteristic and ability to tack themselves in a reasonable magnetic field owing to their unique characteristics such as a large magnetic susceptibility in a small dimension. This is the main reason to get scientific attention for various important biomedicine applications like drug delivery, cell manipulation and tissue repair *etc.*[3, 4].

Several researchers have described the result of lanthanides transposition on the magnetic characteristics of spinel ferrites [1,2,5-8]. Samoila *et al.* [1] have reported *Gd* doped *Ni–Mn–Cr* ferrites synthesized via auto-combustion approach for structural and magnetic characteristics. The average crystallite size (27.4 nm to 5.4 nm), coercivity, magnetization (22.3 emu/g to 8.3 emu/g) and Curie temperature (432 °C to 406 °C) was reported to decrease on enhancing the *Gd* concentration in *Ni–Mn–Cr* ferrites. Yadav *et al.* [2] have investigated *Gd* doped cobalt ferrite for their structural and magnetic properties. They have observed *GdFeO<sub>3</sub>* phase for higher *Gd* content. The crystallite size (4.11 nm to 6.57 nm), coercivity (51.75 Oe to 92.86 Oe) and saturation magnetization (14.59 emu/g to 16.11 emu/g) have been described to enhance with the increment in *Gd* concentration. The structural as well as magnetic characteristics of *La<sup>3+</sup>* ions doped magnesium ferrites have been researched by Gaba *et al.* [5]. The crystallite size has been first reported to decrease (14 nm to 12 nm) with La doping for lower concentration and then increase (12 nm to 14 nm) for higher concentration.

## **Cation distribution and magnetic study of La<sup>3+</sup>, Gd<sup>3+</sup> & Nd<sup>3+</sup> doped Mn-Zn nano ferrites**

---

Indication of superparamagnetic behaviour with La doping has been given by magnetic study. The magnetic and structural characteristics of neodymium doped Mn-Zn ferrite have been studied [6]. A decrement in particle size with Nd<sup>3+</sup> doping has been detected. At lower concentration of Nd<sup>3+</sup> ions, value of saturation magnetization as well as magnetic moment found to be decrease and after that increase for higher concentration. The magnetic nature of all the samples has been reported to be superparamagnetic. The magnetic and structural characteristics of gadolinium doped cobalt ferrite have been reported [7]. The coercivity (575 Oe to 50 Oe), magnetization (87.56 emu/g to 52.03 emu/g) and average crystallite size (13.9 nm to 8.5 nm) have been reported to decrease with the increment of gadolinium proportion in cobalt ferrite. The role of cerium and gadolinium doping on the magnetic and structural characteristics of Ni ferrite have been recorded by Dixit *et al.* [8]. The average crystallite size, coercivity and magnetization are described to decrease with doping of cerium and gadolinium in Ni ferrite.

In this work, a cation distribution is presented for lanthanide (La<sup>3+</sup>, Gd<sup>3+</sup> & Nd<sup>3+</sup>) doped manganese-zinc spinel ferrites. The magnetic study has also been performed using vibrating sample magnetometer.

### **5.2. Experimental details**

RE<sup>3+</sup> (La<sup>3+</sup>, Gd<sup>3+</sup>, Nd<sup>3+</sup>) doped manganese zinc ferrites are synthesized employing co-precipitation route. Preparation of samples has been described in section 2.1.5. The sintered samples are investigated with VSM (PAR-155) in -10 kOe to +10 kOe magnetic field at room temperature. Some important theoretical parameters have also been calculated for all prepared samples of Mn<sub>0.5</sub>Zn<sub>0.5</sub>RE<sub>x</sub>Fe<sub>2-x</sub>O<sub>4</sub>, where x = 0, 0.025, 0.050, 0.075 and 0.1) nano ferrites using cation distribution.

### **5.3. Results & Discussion**

#### **5.3.1 Cation distribution for La<sup>3+</sup>, Gd<sup>3+</sup> & Nd<sup>3+</sup> doped Mn-Zn spinel ferrites**

A cation distribution is presented for Mn<sub>0.5</sub>Zn<sub>0.5</sub>RE<sub>x</sub>Fe<sub>2-x</sub>O<sub>4</sub> spinel ferrites, where RE = La, Gd & Nd. Spinel ferrites comprises of two sites; one is tetrahedral (A site) having 8 sites and second is octahedral (B site) having 16 sites. The A and B sites are engaged by the bivalent and trivalent cations [9].

**Table 5.1:** Proposed cation distribution for lanthanide ( $La^{3+}$ ,  $Gd^{3+}$  &  $Nd^{3+}$ ) ions doped manganese – zinc ferrites.

$x$	For $La^{3+}$ doping		For $Gd^{3+}$ doping		For $Nd^{3+}$ doping	
	A site	B site	A site	B site	A site	B site
0.0	$Zn_{0.5}^{2+}Fe_{0.5}^{3+}$	$Mn_{0.5}^{2+}Fe_{1.5}^{3+}$	$Zn_{0.5}^{2+}Fe_{0.5}^{3+}$	$Mn_{0.5}^{2+}Fe_{1.5}^{3+}$	$Zn_{0.5}^{2+}Fe_{0.5}^{3+}$	$Mn_{0.5}^{2+}Fe_{1.5}^{3+}$
0.025	$Zn_{0.5}^{2+}Fe_{0.5}^{3+}$	$Mn_{0.5}^{2+}Fe_{1.475}^{3+}La_{0.025}^{3+}$	$Zn_{0.5}^{2+}Fe_{0.5}^{3+}$	$Mn_{0.5}^{2+}Fe_{1.475}^{3+}Gd_{0.025}^{3+}$	$Zn_{0.5}^{2+}Fe_{0.5}^{3+}$	$Mn_{0.5}^{2+}Fe_{1.475}^{3+}Nd_{0.025}^{3+}$
0.050	$Zn_{0.5}^{2+}Fe_{0.5}^{3+}$	$Mn_{0.5}^{2+}Fe_{1.450}^{3+}La_{0.050}^{3+}$	$Zn_{0.5}^{2+}Fe_{0.5}^{3+}$	$Mn_{0.5}^{2+}Fe_{1.450}^{3+}Gd_{0.050}^{3+}$	$Zn_{0.5}^{2+}Fe_{0.5}^{3+}$	$Mn_{0.5}^{2+}Fe_{1.450}^{3+}Nd_{0.050}^{3+}$
0.075	$Zn_{0.5}^{2+}Fe_{0.5}^{3+}$	$Mn_{0.5}^{2+}Fe_{1.425}^{3+}La_{0.075}^{3+}$	$Zn_{0.5}^{2+}Fe_{0.5}^{3+}$	$Mn_{0.5}^{2+}Fe_{1.425}^{3+}Gd_{0.075}^{3+}$	$Zn_{0.5}^{2+}Fe_{0.5}^{3+}$	$Mn_{0.5}^{2+}Fe_{1.425}^{3+}Nd_{0.075}^{3+}$
0.1	$Zn_{0.5}^{2+}Fe_{0.5}^{3+}$	$Mn_{0.5}^{2+}Fe_{1.4}^{3+}La_{0.1}^{3+}$	$Zn_{0.5}^{2+}Fe_{0.5}^{3+}$	$Mn_{0.5}^{2+}Fe_{1.4}^{3+}Gd_{0.1}^{3+}$	$Zn_{0.5}^{2+}Fe_{0.5}^{3+}$	$Mn_{0.5}^{2+}Fe_{1.4}^{3+}Nd_{0.1}^{3+}$

## Cation distribution and magnetic study of $La^{3+}$ , $Gd^{3+}$ & $Nd^{3+}$ doped Mn-Zn nano ferrites

A-locations are engaged by zinc ions and B-locations are engaged by  $Mn^{2+}$  ions. The  $Fe^{3+}$  ions goes to both A and B-sites. The lanthanide ( $RE^{3+} = La^{3+}, Gd^{3+}, Nd^{3+}$ ) ions have large ionic radii, hence they occupy the octahedral sites. Table 5.1 shows the proposed cation distribution for the lanthanide ( $La^{3+}, Gd^{3+}, Nd^{3+}$ ) doped Mn-Zn ferrites.

For A-sites and B-sites, the average cation radius  $r_A$  and  $r_B$  have been computed using the following equations [10];

$$r_A = (C_{Mn^{2+}}^A)(r_{Mn^{2+}}) + (C_{Zn^{2+}}^A)(r_{Zn^{2+}}) + (C_{Fe^{3+}}^A)(r_{Fe^{3+}}) + (C_{RE^{3+}}^A)(r_{RE^{3+}}) \quad (1)$$

$$r_B = \frac{1}{2} [(C_{Mn^{2+}}^B)(r_{Mn^{2+}}) + (C_{Zn^{2+}}^B)(r_{Zn^{2+}}) + (C_{Fe^{3+}}^B)(r_{Fe^{3+}}) + (C_{RE^{3+}}^B)(r_{RE^{3+}})] \quad (2)$$

where,  $C_{Mn^{2+}}^A, C_{Zn^{2+}}^A, C_{Fe^{3+}}^A, C_{RE^{3+}}^A$  are the ionic proportion of  $Mn^{2+}$  ions,  $Zn^{2+}$  ions,  $Fe^{3+}$  ions &  $RE^{3+}$  ( $= La^{3+}, Gd^{3+}, Nd^{3+}$ ) ions respectively at A-sites and  $C_{Mn^{2+}}^B, C_{Zn^{2+}}^B, C_{Fe^{3+}}^B, C_{RE^{3+}}^B$  are the ionic proportion of  $Mn^{2+}$  ions,  $Zn^{2+}$  ions,  $Fe^{3+}$  ions &  $RE^{3+}$  ( $= La^{3+}, Gd^{3+}, Nd^{3+}$ ) ions respectively at B-sites, the ionic radii of  $Mn^{2+}$  ions,  $Zn^{2+}$  ions,  $Fe^{3+}$  ions &  $RE^{3+}$  ( $= La^{3+}, Gd^{3+}, Nd^{3+}$ ) ions have been termed as  $r_{Mn^{2+}}, r_{Zn^{2+}}, r_{Fe^{3+}}$  and  $r_{RE^{3+}}$  respectively. The computed values  $r_A$  and  $r_B$  are given in tables 5.2, 5.3 & 5.4. Enlargement of octahedral positions on doping with large ionic radii  $RE^{3+}$  ions has been observed with the increased value of  $r_B$  for all the three dopants (figure 5.1, figure 5.2 & figure 5.3).

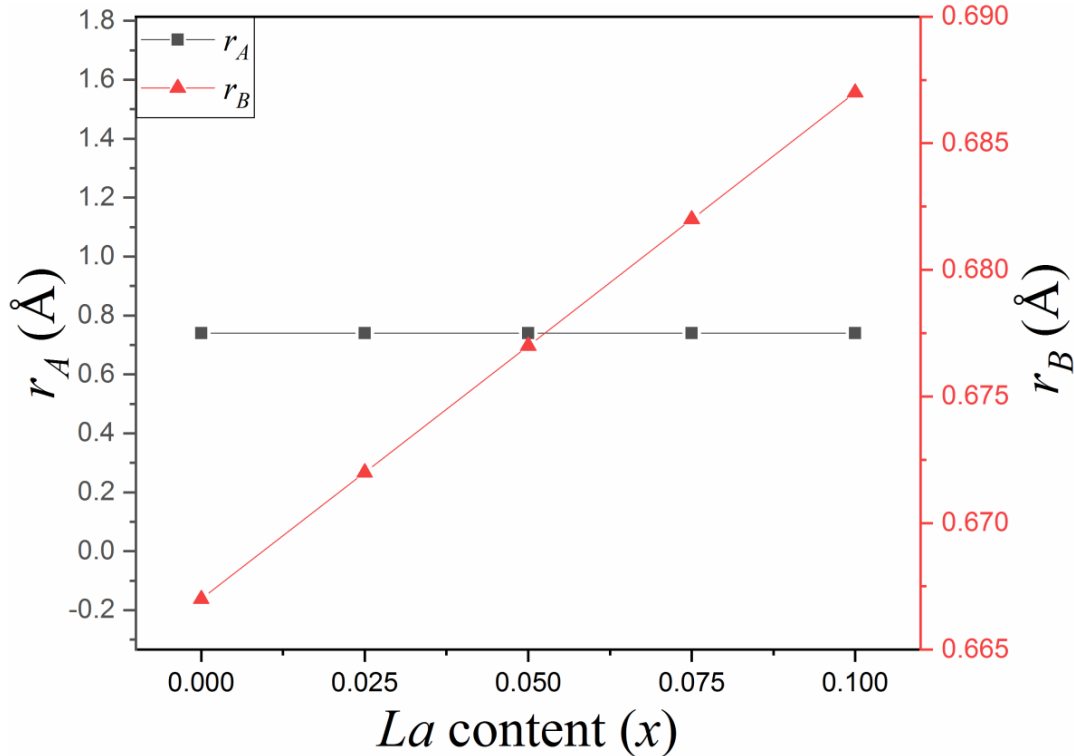


Figure 5.1: Plot of  $r_A$  &  $r_B$  with  $La$  content ( $x$ ).

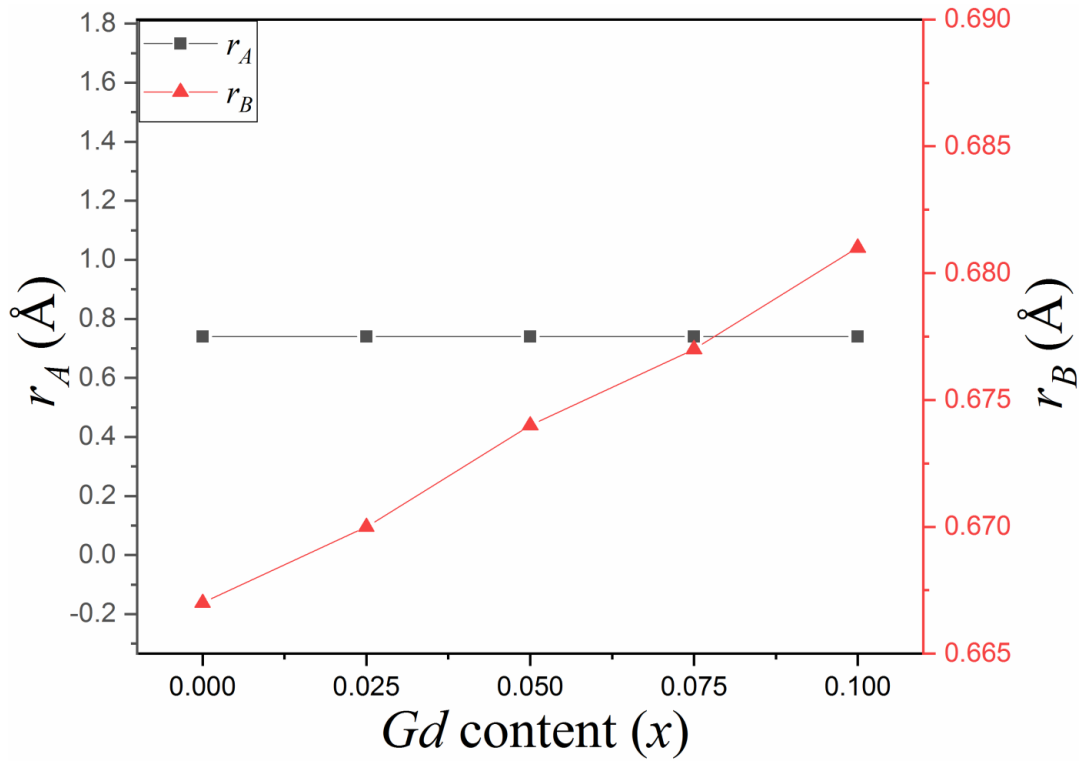


Figure 5.2: Plot of  $r_A$  &  $r_B$  with Gd content ( $x$ ).

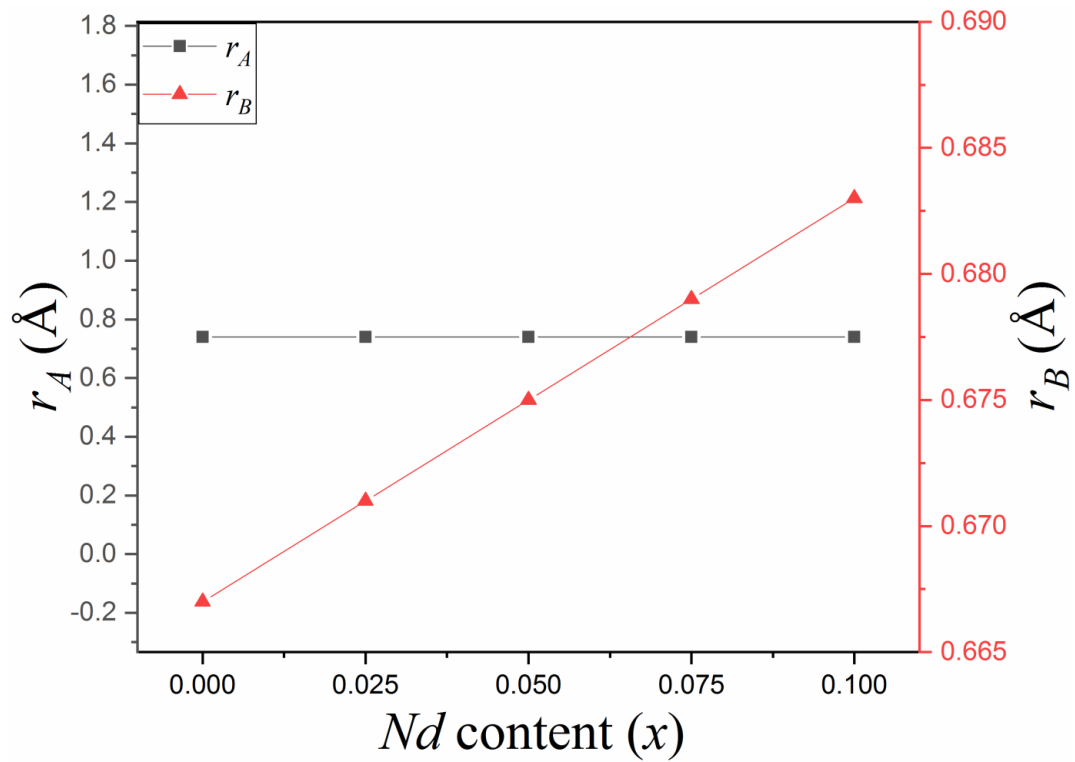


Figure 5.3: Plot of  $r_A$  &  $r_B$  with Nd content ( $x$ ).

## Cation distribution and magnetic study of La<sup>3+</sup>, Gd<sup>3+</sup> & Nd<sup>3+</sup> doped Mn-Zn nano ferrites

---

The values of lattice parameter ( $a_{th}$ ) has been calculated theoretically by using the average cation radius values corresponding to A-sites and B-sites [11];

$$a_{th} = \frac{8}{3\sqrt{3}} [(r_A + R_o) + \sqrt{3}(r_B + R_o)] \quad (3)$$

where  $R_o$  represents oxygen ion radius (1.32Å). Table 5.2, 5.3 & 5.4 shows the computed values of  $a_{th}$ . It has been observed that there is an increment in the  $a_{th}$  values on doping of  $RE^{3+}$  ions in manganese-zinc ferrites. Since the difference between ionic radii of  $RE^{3+}$  ion and  $Fe^{3+}$  (ferric) ion is large, so to substitute ferric ions with  $RE^{3+}$  ions in the lattice positions is not easy. This may lead to a bit of the  $RE^{3+}$  ions stay on the grain boundaries with transposition of the  $Fe^{3+}$  ions by  $RE^{3+}$  ions. Due to this reason there is difference pertaining to measures of theoretical lattice parameter and experimental lattice parameter.

In ferrites, the oxygen positional parameter ( $U$ ) is quantifiable proportion of uprooting of  $O^{2-}$  ions encompassing A-sites are little to engage metal ions. In majority of the ferrite spinels, the  $O^{2-}$  ions are evidently bigger in comparison to their corresponding metal ions. The inversion parameter ( $\delta$ ) is the deviation of structural factors from the original one on doping. The basic factors that decide the inversion parameter of a specific spinel are the ionic and/or covalent character, the particle size, and above all the crystal field stabilisation. The values of  $U$  and  $\delta$  have been computed by employing the equations [11];  $U = (1/a_{th}\sqrt{3})(r_A + R_o) + 1/4$  and  $\delta = U - U_{ideal}$ , where  $U_{ideal}$  (= 0.375) is the oxygen positional parameter's ideal value for spinel ferrites. Since the physical magnitude of tetrahedral location is comparatively littler than the octahedral location and the oxygen anions have to make connection with the cations occupying A-sites and B-sites. Due to little size of A- site the metal ions can't engage it easily. So the movement of oxygen ions is there to make some adjustments. These adjustments of oxygen ions are described as oxygen positional parameter will lead to some expansion and/or shrinkage between tetrahedral and octahedral sites. Figure 5.4, 5.5 & 5.6 show the change in  $a_{th}$  and  $U$  with varying the dopant i.e.  $RE^{3+}$  ions ( $La^{3+}$ ,  $Gd^{3+}$ ,  $Nd^{3+}$ ) concentration respectively. It has been observed that the values of  $U$  and  $\delta$  decrements with the increment of  $RE^{3+}$  ions concentration (Table 5.2, 5.3 & 5.4).

**Table 5.2:** Values of various theoretical parameters calculated from proposed cation distribution for  $L\alpha^{3+}$  doped manganese-zinc ferrites.

$x$	$r_A$ (Å)	$r_B$ (Å)	$a_{th}$ (Å)	$U$	$\delta$	$R_A$ (Å)	$R_B$ (Å)	$R_x$	$R_{x'}$	$R_{x''}$
0	0.740	0.667	8.470	0.3904	0.0154	2.063	1.998	3.368	2.628	3.010
0.025	0.740	0.672	8.483	0.3902	0.0152	2.054	1.994	3.353	2.626	3.001
0.050	0.740	0.677	8.496	0.3899	0.0149	2.045	1.991	3.340	2.625	2.994
0.075	0.740	0.682	8.510	0.3897	0.0147	2.052	2.002	3.351	2.643	3.007
0.1	0.740	0.687	8.523	0.3895	0.0145	2.046	2.001	3.341	2.645	3.004

**Table 5.3:** Values of various theoretical parameters calculated from proposed cation distribution for Gd<sup>3+</sup> doped manganese-zinc ferrites.

$x$	$r_A$ (Å)	$r_B$ (Å)	$a_{th}$ (Å)	$U$	$\delta$	$R_d$ (Å)	$R_B(\text{Å})$	$R_x$	$R_{x'}$	$R_{x''}$
0	0.740	0.667	8.470	0.3904	0.0154	2.063	1.998	3.368	2.628	3.010
0.025	0.740	0.670	8.478	0.3902	0.0152	2.051	1.990	3.350	2.620	2.996
0.050	0.740	0.674	8.488	0.3901	0.0151	2.060	2.002	3.363	2.638	3.012
0.075	0.740	0.677	8.496	0.3899	0.0149	2.047	1.992	3.343	2.627	2.996
0.1	0.740	0.681	8.507	0.3898	0.0148	2.044	1.994	3.338	2.631	2.996

**Table 5.4:** Values of various theoretical parameters calculated from proposed cation distribution for  $Nd^{2+}$  doped manganese-zinc ferrites.

$x$	$r_A$ (Å)	$r_B$ (Å)	$a_{th}$ (Å)	$U$	$\delta$	$R_A$ (Å)	$R_B$ (Å)	$R_x$	$R_{x'}$	$R_{x''}$
0	0.740	0.667	8.470	0.3904	0.0154	2.063	1.998	3.368	2.628	3.010
0.025	0.740	0.671	8.480	0.3902	0.0152	2.059	1.998	3.362	2.631	3.008
0.050	0.740	0.675	8.491	0.3900	0.0150	2.050	1.993	3.347	2.627	2.998
0.075	0.740	0.679	8.502	0.3898	0.0148	2.028	1.976	3.312	2.607	2.970
0.1	0.740	0.683	8.512	0.3897	0.0147	2.032	1.983	3.317	2.618	2.979

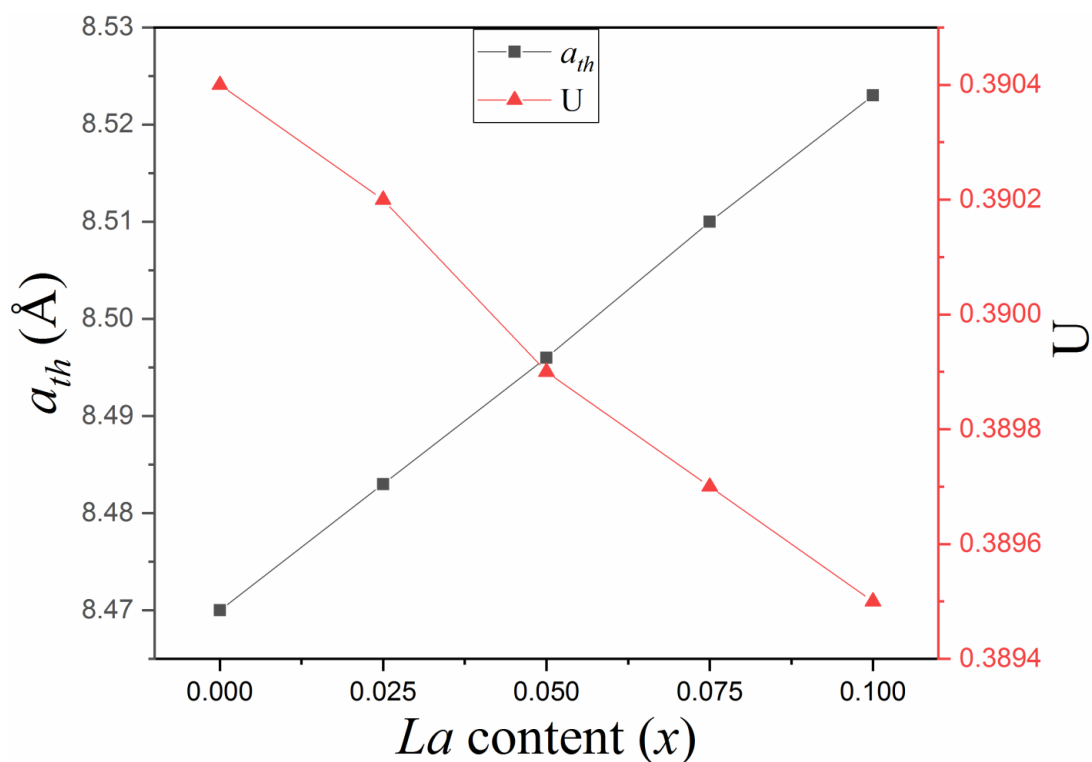


Figure 5.4: Variation of  $a_{th}$  and  $U$  with  $La$  content ( $x$ ) in manganese – zinc ferrites.

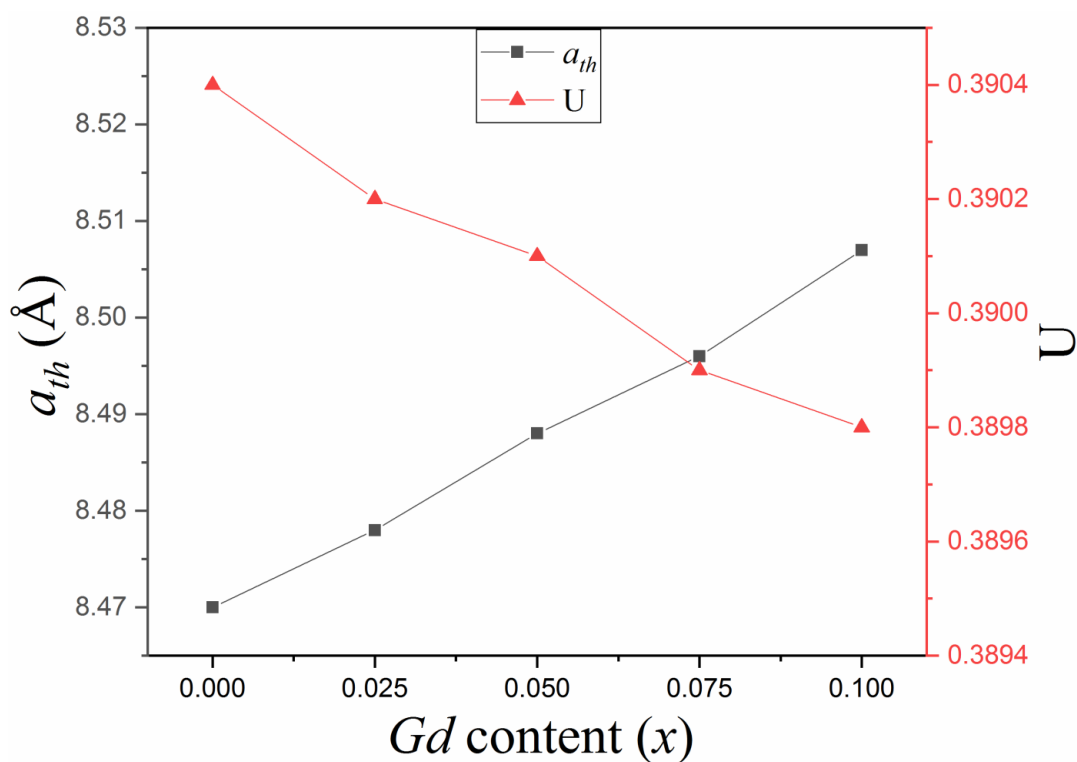
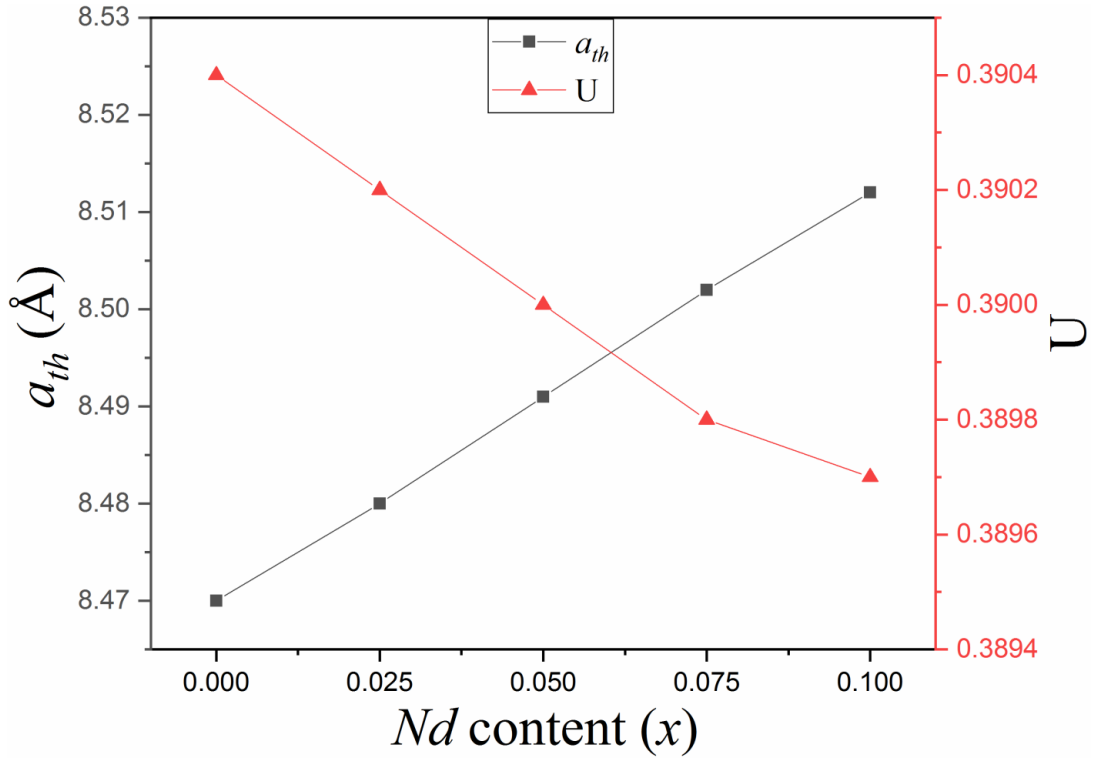


Figure 5.5: Variation of  $a_{th}$  and  $U$  with  $Gd$  content ( $x$ ) in manganese – zinc ferrites.



**Figure 5.6:** Variation of  $a_{th}$  and  $U$  with  $Nd$  content ( $x$ ) in manganese – zinc ferrites.

Bond length amongst cation - anion on the A site is illustrated by  $R_A$  and bond length amongst cation - anion on the B site is illustrated by  $R_B$ . The values of these bond lengths have been computed by employing the relations [11];  $R_A = a\sqrt{3}(\delta + 1/8)$  and  $R_B = a\sqrt{0.0625 - 0.5\delta + 3\delta^2}$ , here  $a$  represents the observational measure of lattice parameter. Tables 5.2, 5.3 & 5.4 contain the quantities of  $R_A$  &  $R_B$  corresponding to  $RE^{3+}$  ions concentration. It is remarked that the change in the values of  $R_A$  as well as  $R_B$  with  $RE^{3+}$  ions doping is in conformity with data-based lattice parameter (figure 5.7, 5.8 & 5.9).

Magnetic interactions among the ions at tetrahedral (A) and octahedral (B) destinations in other words (A-B) interactions, or magnetic interactions among the ions at individual sites, in other words (A-A) interactions and (B-B) interactions have been influenced through the variation in bond distances amongst the cation-cation & cation-anion [12]. The tetrahedral edge length ( $R_x$ ), shared octahedral length ( $R_{x'}$ ) and unshared octahedral edge length ( $R_{x''}$ ) are computed by employing the relations [10]:  $R_x = a\sqrt{2}(2U - 0.5)$ ,  $R_{x'} = a\sqrt{2}(1 - 2U)$ ,  $R_x = a\sqrt{2}(1 - 2u)$  and  $R_{x''} = a(4U^2 - 3U + 11/16)^{0.5}$ .

**Cation distribution and magnetic study of  $\text{La}^{3+}$ ,  $\text{Gd}^{3+}$  &  $\text{Nd}^{3+}$  doped Mn-Zn nano ferrites**

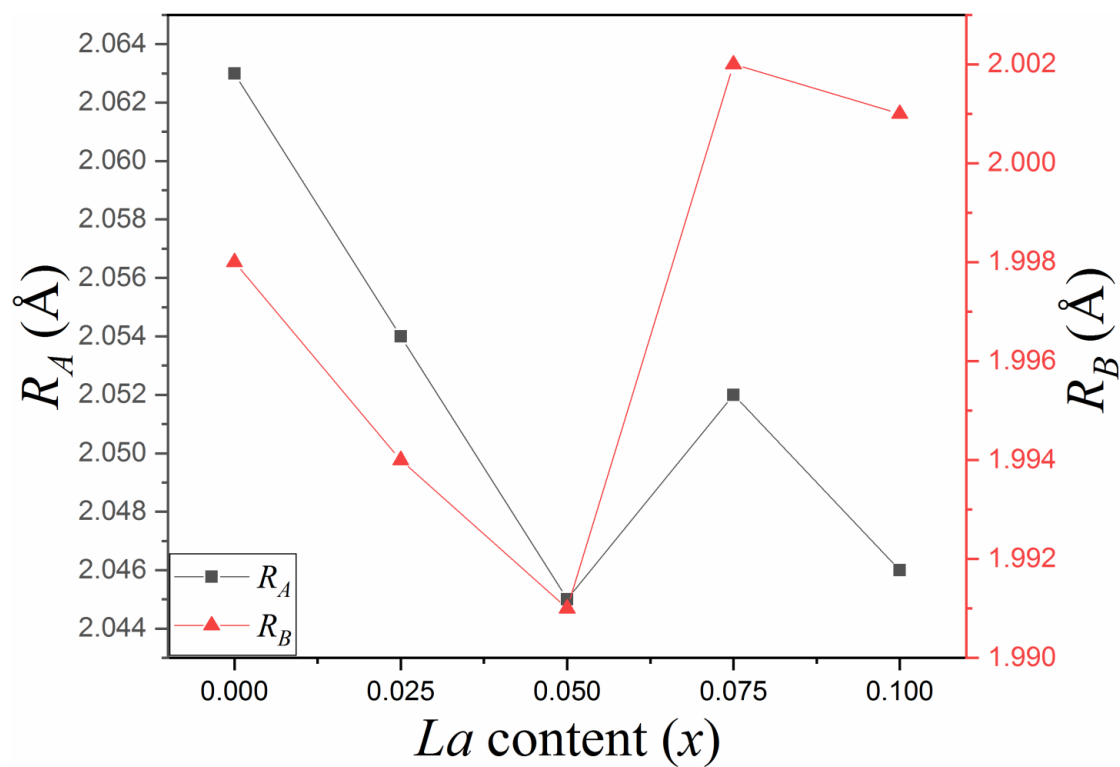


**Figure 5.7:** Graph of  $R_A$  and  $R_B$  with  $La$  content in Mn-Zn ferrites.

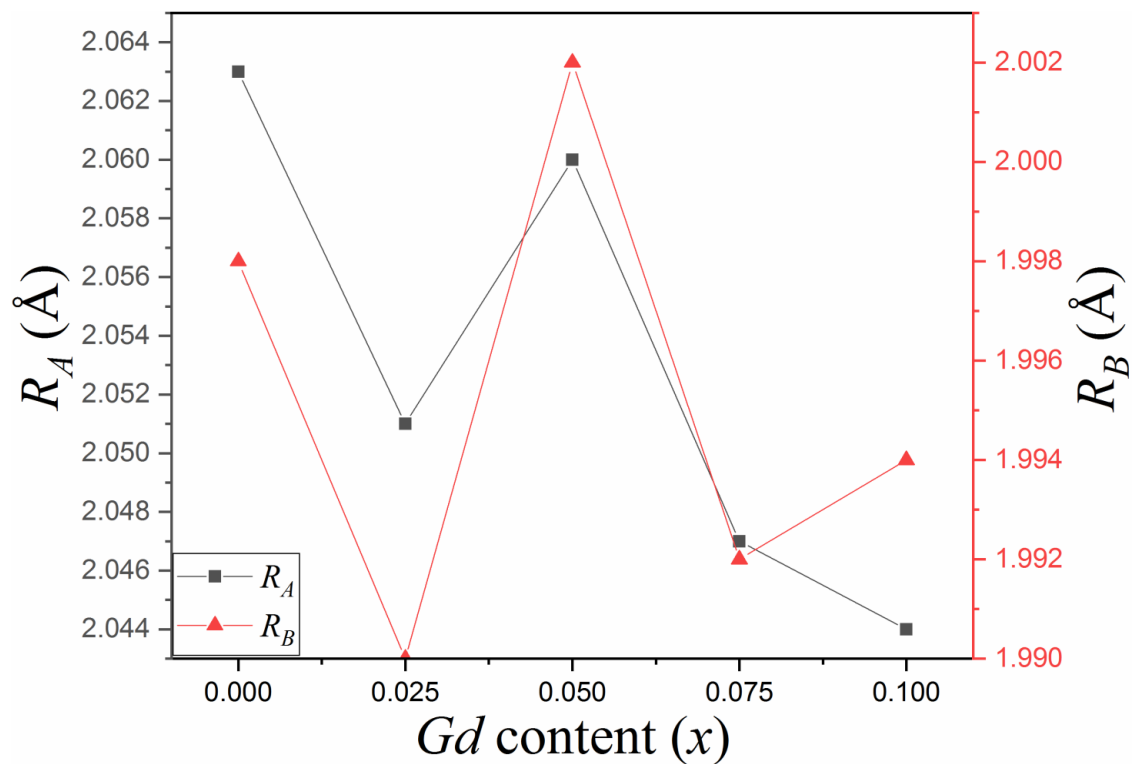


**Figure 5.8:** Graph of  $R_A$  and  $R_B$  with  $Gd$  content in Mn-Zn ferrites.

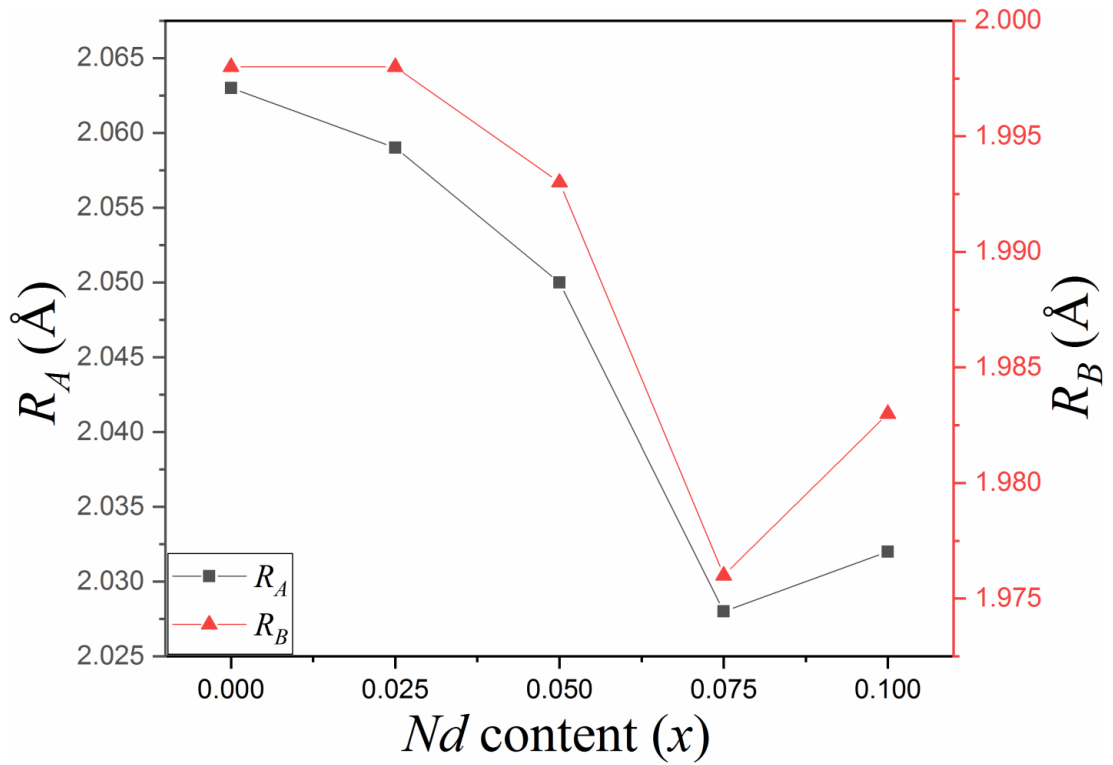


Figure 5.9: Graph of  $R_A$  and  $R_B$  with Nd content in Mn-Zn ferrites.

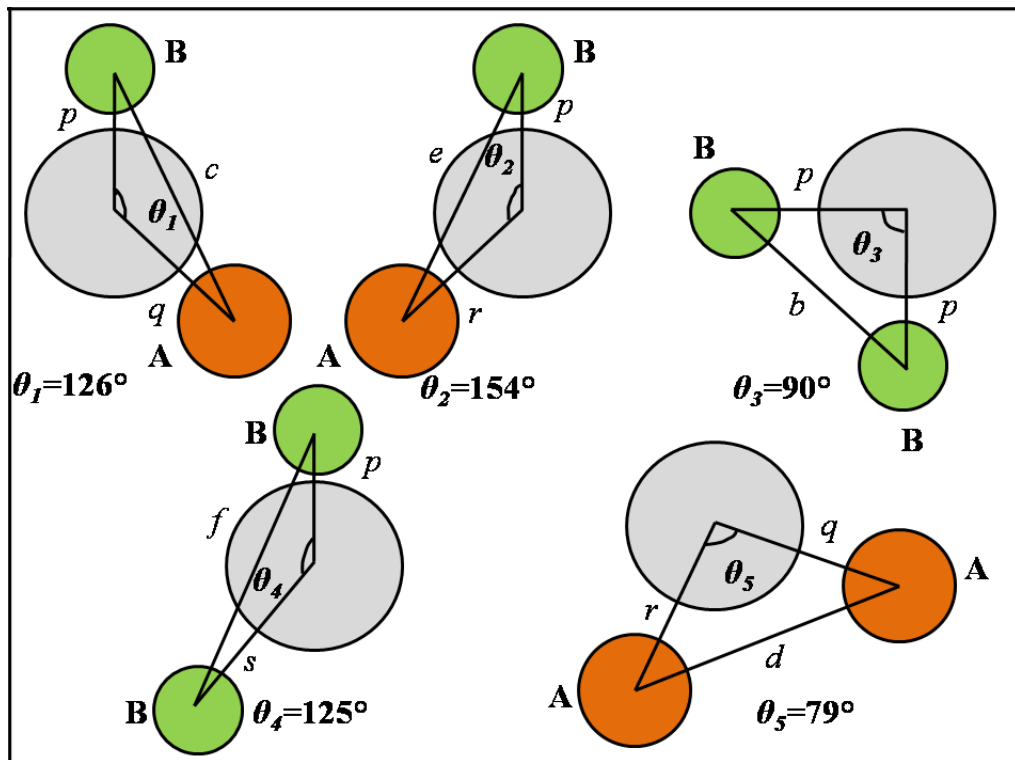


Figure 5.10: Interionic lengths and the angles amongst the ions in spinel ferrites.

## Cation distribution and magnetic study of $La^{3+}$ , $Gd^{3+}$ & $Nd^{3+}$ doped Mn-Zn nano ferrites

The computed values of  $R_x$ ,  $R_x'$  and  $R_{x''}$  are given in table 5.2, 5.3 and 5.4 for  $RE^{3+} = La^{3+}$ ,  $Gd^{3+}$ ,  $Nd^{3+}$  ions doping. It has been observed that the variation in the values of  $R_x$ ,  $R_x'$  and  $R_{x''}$  depend on the  $RE^{3+}$  ( $= La^{3+}$ ,  $Gd^{3+}$ ,  $Nd^{3+}$ ) ions concentration in Mn-Zn ferrites and the experimentally obtained lattice parameter values. Magnetic interactions play a more efficient function at some distances as well as angles between the ions. In general, for spinel ferrites these bond angles and interionic distances which affect the magnetic characteristics are shown in figure 5.10 [11, 12].

The interionic distances between the ions that is to say cation-anion lengths ( $p$ ,  $q$ ,  $r$  &  $s$ ) and cation-cation lengths ( $b$ ,  $c$ ,  $d$ ,  $e$  &  $f$ ) are computed by utilizing the equations [10];

$$p = a \left( \frac{5}{8} - U \right) \quad (4)$$

$$q = a \left( U - \frac{1}{4} \right) \sqrt{3} \quad (5)$$

$$r = a \left( U - \frac{1}{4} \right) \sqrt{11} \quad (6)$$

$$s = a \left( \frac{1}{3} U + \frac{1}{8} \right) \sqrt{3} \quad (7)$$

$$b = \left( \frac{a}{4} \right) \sqrt{2} \quad (8)$$

$$c = \left( \frac{a}{8} \right) \sqrt{11} \quad (9)$$

$$d = \left( \frac{a}{4} \right) \sqrt{3} \quad (10)$$

$$e = \left( \frac{3a}{8} \right) \sqrt{3} \quad (11)$$

$$f = \left( \frac{a}{4} \right) \sqrt{6} \quad (12)$$

The computed values of interionic distances are tabulated in table 5.5, 5.6 & 5.7 for  $RE^{3+} = La^{3+}$ ,  $Gd^{3+}$  &  $Nd^{3+}$  ions doping in Mn-Zn ferrites respectively. The trend of lattice parameter on  $RE^{3+}$  doping into Mn-Zn ferrite has been followed by the values of interionic distances. The bond angles  $\theta_1$ ,  $\theta_2$ ,  $\theta_3$ ,  $\theta_4$  &  $\theta_5$  have been computed by means of these interionic distances [10, 12]:

$$\theta_1 = \cos^{-1} \left[ \frac{p^2 + q^2 - c^2}{2pq} \right] \quad (13)$$

$$\theta_2 = \cos^{-1} \left[ \frac{p^2 + r^2 - e^2}{2pr} \right] \quad (14)$$

$$\theta_3 = \cos^{-1} \left[ \frac{2p^2 - b^2}{2p^2} \right] \quad (15)$$

$$\theta_4 = \cos^{-1} \left[ \frac{p^2 + s^2 - f^2}{2ps} \right] \quad (16)$$

$$\theta_5 = \cos^{-1} \left[ \frac{r^2 + q^2 - d^2}{2rq} \right] \quad (17)$$

The computed values of bond angles  $\theta_1, \theta_2, \theta_3, \theta_4$  &  $\theta_5$  are tabulated in table 5.8, 5.9 & 5.10 for  $RE^{3+} = La^{3+}, Gd^{3+}$  &  $Nd^{3+}$  ions doping in Mn-Zn ferrites respectively.

**Table 5.5:** The interionic distances of cation-anion ( $p, q, r$  &  $s$ ) and cation-cation ( $b, c, d, e$  &  $f$ ) for  $La^{3+}$  doped  $Mn_{0.5}Zn_{0.5}La_xFe_{2-x}O_4$  spinel ferrites.

$x$	$p$	$q$	$r$	$s$	$b$	$c$	$d$	$e$	$f$
0	1.989	2.063	3.950	3.748	2.998	3.516	3.673	5.509	5.174
0.025	1.986	2.054	3.932	3.737	2.990	3.506	3.662	5.494	5.160
0.050	1.983	2.045	3.916	3.726	2.983	3.497	3.653	5.480	5.147
0.075	1.994	2.052	3.929	3.743	2.997	3.514	3.671	5.506	5.171
0.1	1.994	2.046	3.918	3.738	2.993	3.510	3.666	5.500	5.165

**Table 5.6:** The interionic distances of cation-anion ( $p, q, r$  &  $s$ ) and cation-cation ( $b, c, d, e$  &  $f$ ) for  $Gd^{3+}$  doped  $Mn_{0.5}Zn_{0.5}Gd_xFe_{2-x}O_4$  spinel ferrites.

$x$	$p$	$q$	$r$	$s$	$b$	$c$	$d$	$e$	$f$
0	1.989	2.063	3.950	3.748	2.998	3.516	3.673	5.509	5.174
0.025	1.982	2.051	3.928	3.731	2.985	3.500	3.656	5.485	5.151
0.050	1.993	2.060	3.944	3.749	3.000	3.518	3.675	5.513	5.178
0.075	1.984	2.047	3.919	3.729	2.985	3.500	3.656	5.485	5.151
0.1	1.986	2.044	3.915	3.728	2.985	3.500	3.656	5.485	5.151

**Table 5.7:** The interionic distances of cation-anion ( $p, q, r$  &  $s$ ) and cation-cation ( $b, c, d, e$  &  $f$ ) for  $Nd^{3+}$  doped  $Mn_{0.5}Zn_{0.5}Nd_xFe_{2-x}O_4$  spinel ferrites.

$x$	$p$	$q$	$r$	$s$	$b$	$c$	$d$	$e$	$f$
0	1.989	2.063	3.950	3.748	2.998	3.516	3.673	5.509	5.174
0.025	1.990	2.059	3.943	3.745	2.997	3.514	3.671	5.506	5.172
0.050	1.985	2.050	3.925	3.733	2.987	3.503	3.659	5.489	5.155
0.075	1.968	2.028	3.883	3.697	2.959	3.470	3.625	5.437	5.107
0.1	1.975	2.032	3.890	3.707	2.968	3.480	3.635	5.453	5.122

## Cation distribution and magnetic study of La<sup>3+</sup>, Gd<sup>3+</sup> & Nd<sup>3+</sup> doped Mn-Zn nano ferrites

**Table 5.8:** Bond angles ( $\theta_1$ ,  $\theta_2$ ,  $\theta_3$ ,  $\theta_4$  and  $\theta_5$ ), saturation magnetization ( $M_s$ ) and magnetic moment ( $n_B$ ) for La<sup>3+</sup> doped  $Mn_{0.5}Zn_{0.5}La_xFe_{2-x}O_4$  spinel ferrites.

$x$	$\theta_1$	$\theta_2$	$\theta_3$	$\theta_4$	$\theta_5$	$M_s$ (emu/g)	$n_B$ ( $\mu_B$ )
0	120.337	133.366	97.784	125.977	67.005	4.69	0.198
0.025	120.406	133.609	97.661	125.953	67.167	26.5	1.128
0.050	120.475	133.853	97.538	125.929	67.330	31.08	1.335
0.075	120.543	134.096	97.417	125.905	67.492	17.96	0.778
0.1	120.612	134.340	97.296	125.881	67.654	2.89	0.126

**Table 5.9:** Bond angles ( $\theta_1$ ,  $\theta_2$ ,  $\theta_3$ ,  $\theta_4$  and  $\theta_5$ ), saturation magnetization ( $M_s$ ) and magnetic moment ( $n_B$ ) for Gd<sup>3+</sup> doped  $Mn_{0.5}Zn_{0.5}Gd_xFe_{2-x}O_4$  spinel ferrites.

$x$	$\theta_1$	$\theta_2$	$\theta_3$	$\theta_4$	$\theta_5$	$M_s$ (emu/g)	$n_B$ ( $\mu_B$ )
0	120.337	133.366	97.784	125.977	67.005	4.69	0.198
0.025	120.378	133.512	97.710	125.962	67.102	28.88	1.232
0.050	120.433	133.707	97.612	125.943	67.232	19.03	0.820
0.075	120.475	133.853	97.538	125.929	67.330	26.01	1.133
0.1	120.530	134.048	97.441	125.910	67.459	12.55	0.552

**Table 5.10:** Bond angles ( $\theta_1$ ,  $\theta_2$ ,  $\theta_3$ ,  $\theta_4$  and  $\theta_5$ ), saturation magnetization ( $M_s$ ) and magnetic moment ( $n_B$ ) for Nd<sup>3+</sup> doped  $Mn_{0.5}Zn_{0.5}Nd_xFe_{2-x}O_4$  spinel ferrites.

$x$	$\theta_1$	$\theta_2$	$\theta_3$	$\theta_4$	$\theta_5$	$M_s$ (emu/g)	$n_B$ ( $\mu_B$ )
0	120.337	133.366	97.784	125.977	67.005	4.69	0.198
0.025	120.392	133.561	97.686	125.957	67.135	3.64	0.155
0.050	120.447	133.755	97.587	125.938	67.265	23.65	1.017
0.075	120.502	133.950	97.490	125.919	67.394	18.93	0.821
0.1	120.557	134.145	97.392	125.900	67.524	23.65	1.036

Strong A-A and A-B interactions are observed as is indicated by the gain in the computed values of  $\theta_1$ ,  $\theta_2$  and  $\theta_5$ . Weak B-B interactions are observed as is showed by the fall in the computed values of  $\theta_3$  and  $\theta_4$ .

### 5.3.2 Magnetic study of $\text{La}^{3+}$ , $\text{Gd}^{3+}$ & $\text{Nd}^{3+}$ doped Mn-Zn spinel ferrites

Magnetic study of  $\text{RE}^{3+}$  ( $= \text{La}^{3+}$ ,  $\text{Gd}^{3+}$  &  $\text{Nd}^{3+}$ ) doped  $\text{Mn}_{0.5}\text{Zn}_{0.5}\text{RE}_x\text{Fe}_{2-x}\text{O}_4$  spinel ferrite has been performed in  $-10 \text{ kOe}$  to  $+10 \text{ kOe}$  magnetic range at room temperature. Figure 5.11.1 & 5.11.2, figure 5.12.1 & 5.12.2 and figure 5.13.1 & 5.13.2 show the magnetic characterization plots for  $\text{RE}^{3+} = \text{La}^{3+}$ ,  $\text{Gd}^{3+}$  and  $\text{Nd}^{3+}$  doped  $\text{Mn}_{0.5}\text{Zn}_{0.5}\text{RE}_x\text{Fe}_{2-x}\text{O}_4$  spinel nano ferrites respectively. All the samples under investigation show paramagnetic and superparamagnetic nature.

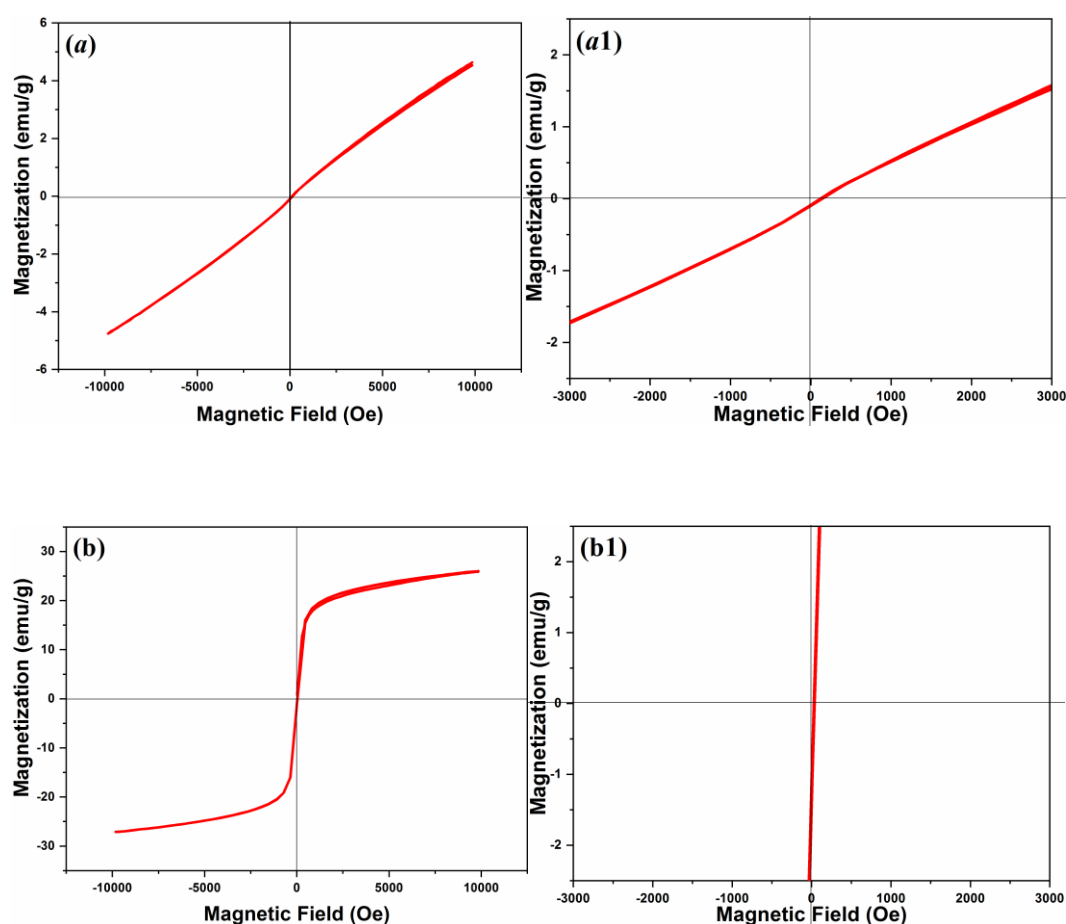


**Figure 5.11.1:** (a) Magnetic hysteresis curve of  $\text{Mn}_{0.5}\text{Zn}_{0.5}\text{Fe}_2\text{O}_4$  spinel nanoferrite; (a1) Zoomed Magnetic hysteresis curve of  $\text{Mn}_{0.5}\text{Zn}_{0.5}\text{Fe}_2\text{O}_4$  spinel nanoferrite; (b) M-H curve of  $\text{Mn}_{0.5}\text{Zn}_{0.5}\text{La}_{0.025}\text{Fe}_{1.975}\text{O}_4$  spinel ferrite; (b1) Zoomed M-H curve of  $\text{Mn}_{0.5}\text{Zn}_{0.5}\text{La}_{0.025}\text{Fe}_{1.975}\text{O}_4$  spinel ferrite.

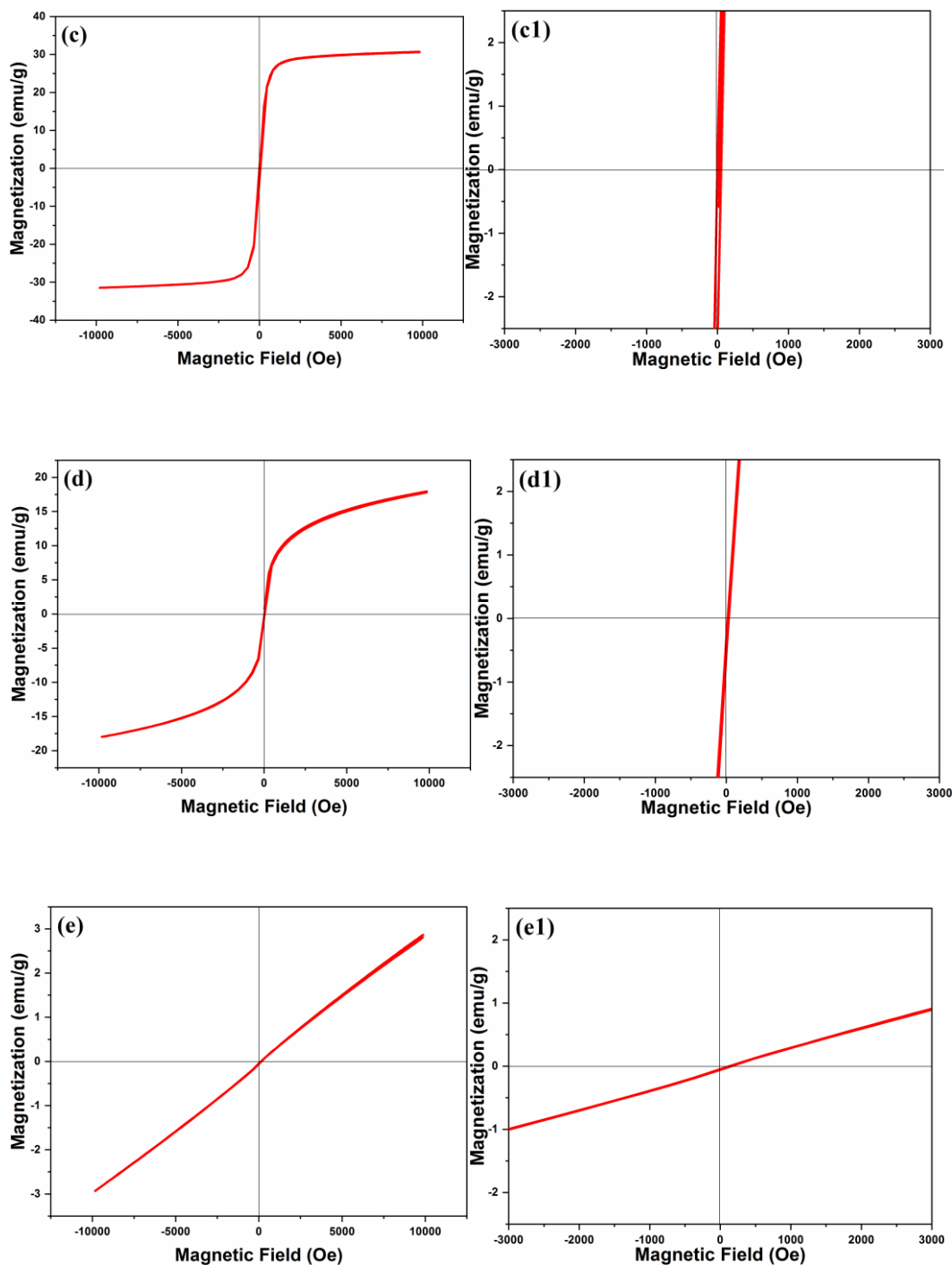


**Figure 5.11.2:** (c) M-H curve of  $\text{Mn}_{0.5}\text{Zn}_{0.5}\text{La}_{0.050}\text{Fe}_{1.950}\text{O}_4$  spinel ferrite; (c1) Zoomed M-H curve of  $\text{Mn}_{0.5}\text{Zn}_{0.5}\text{La}_{0.050}\text{Fe}_{1.950}\text{O}_4$  spinel ferrite; (d) M-H curve of  $\text{Mn}_{0.5}\text{Zn}_{0.5}\text{La}_{0.075}\text{Fe}_{1.925}\text{O}_4$  spinel ferrite; (d1) Zoomed M-H curve of  $\text{Mn}_{0.5}\text{Zn}_{0.5}\text{La}_{0.075}\text{Fe}_{1.925}\text{O}_4$  spinel ferrite; (e) M-H curve of  $\text{Mn}_{0.5}\text{Zn}_{0.5}\text{La}_{0.1}\text{Fe}_{1.9}\text{O}_4$  spinel ferrite; (e1) Zoomed M-H curve of  $\text{Mn}_{0.5}\text{Zn}_{0.5}\text{La}_{0.1}\text{Fe}_{1.9}\text{O}_4$  spinel ferrite.

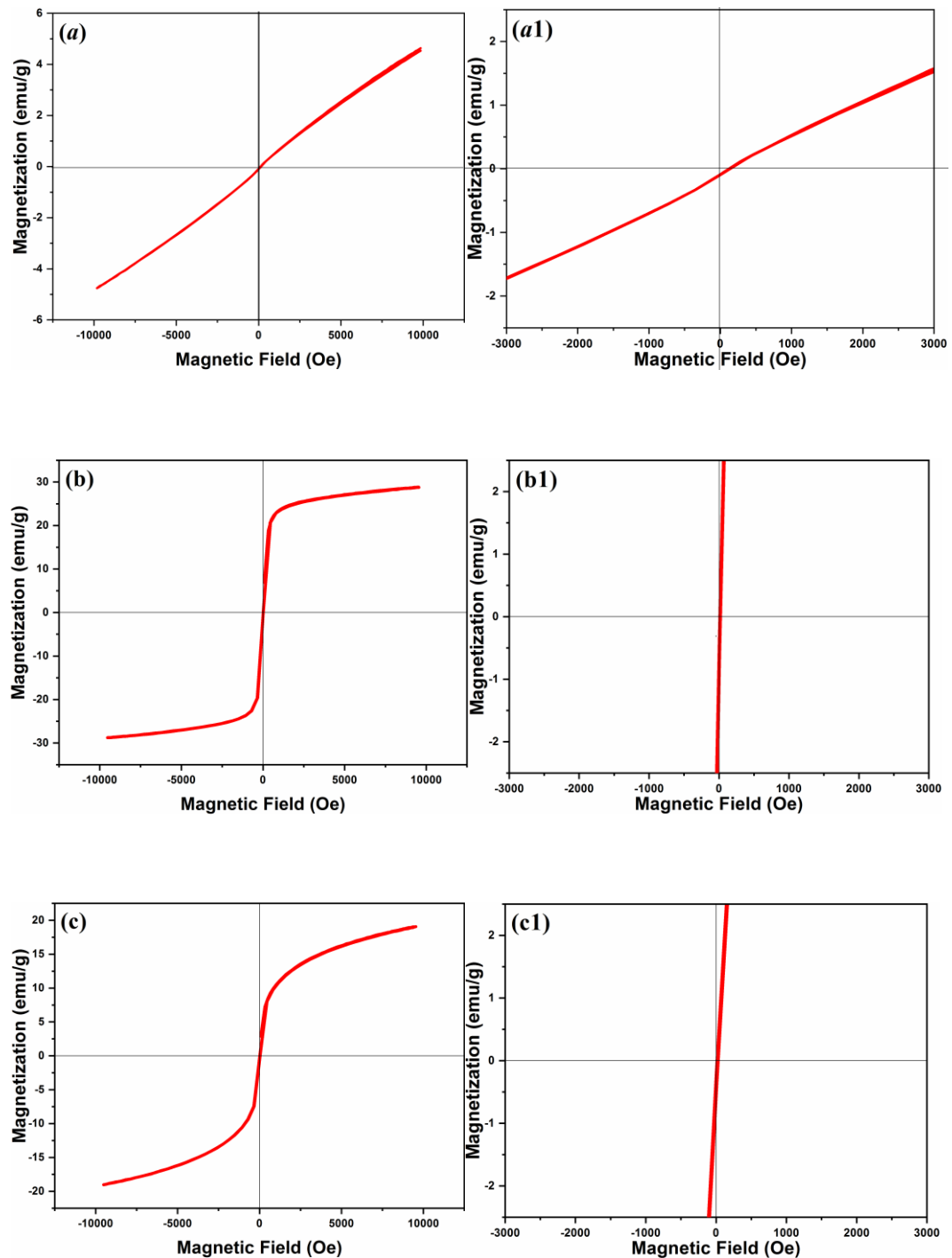


**Figure 5.12.1:** (a) Magnetic hysteresis curve of  $Mn_{0.5}Zn_{0.5}Fe_2O_4$  spinel nanoferrite; (a1) Zoomed Magnetic hysteresis curve of  $Mn_{0.5}Zn_{0.5}Fe_2O_4$  spinel nanoferrite; (b) M-H curve of  $Mn_{0.5}Zn_{0.5}Gd_{0.025}Fe_{1.975}O_4$  spinel ferrite; (b1) Zoomed M-H curve of  $Mn_{0.5}Zn_{0.5}Gd_{0.025}Fe_{1.975}O_4$  spinel ferrite; (c) M-H curve of  $Mn_{0.5}Zn_{0.5}Gd_{0.050}Fe_{1.950}O_4$  spinel ferrite; (c1) Zoomed M-H curve of  $Mn_{0.5}Zn_{0.5}Gd_{0.050}Fe_{1.950}O_4$  spinel ferrite.

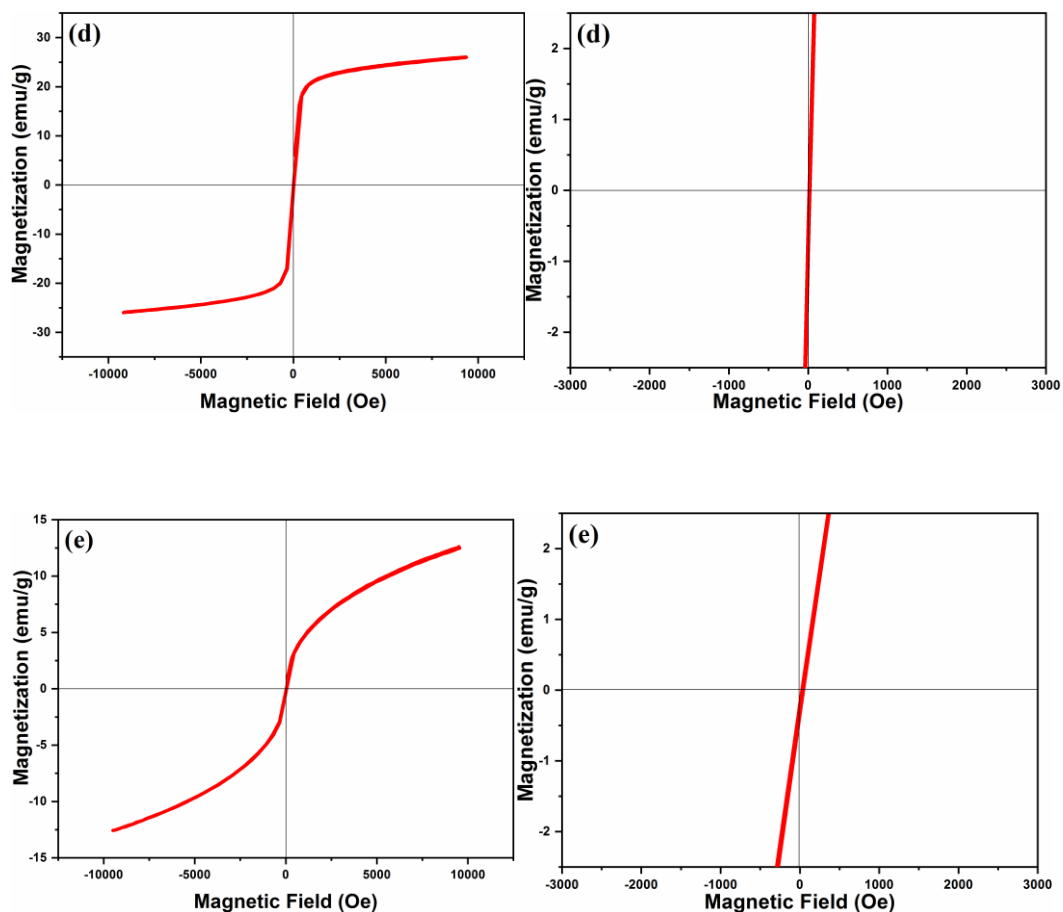


**Figure 5.12.2:** (d) M-H curve of  $\text{Mn}_{0.5}\text{Zn}_{0.5}\text{Gd}_{0.075}\text{Fe}_{1.925}\text{O}_4$  spinel ferrite; (d1) Zoomed M-H curve of  $\text{Mn}_{0.5}\text{Zn}_{0.5}\text{Gd}_{0.075}\text{Fe}_{1.925}\text{O}_4$  spinel ferrite; (e) M-H curve of  $\text{Mn}_{0.5}\text{Zn}_{0.5}\text{Gd}_{0.1}\text{Fe}_{1.9}\text{O}_4$  spinel ferrite; (e1) Zoomed M-H curve of  $\text{Mn}_{0.5}\text{Zn}_{0.5}\text{Gd}_{0.1}\text{Fe}_{1.9}\text{O}_4$  spinel ferrite.

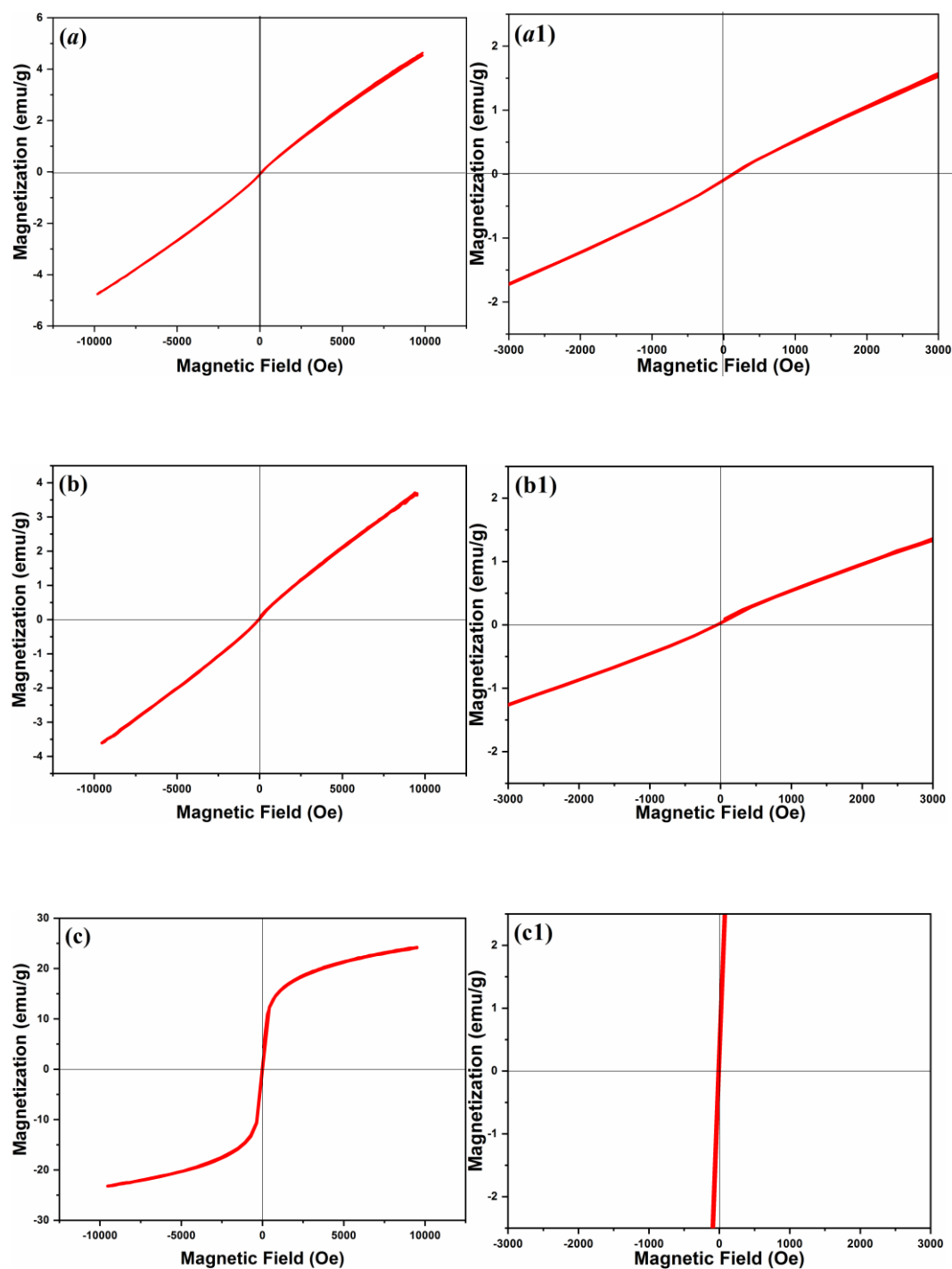


**Figure 5.13.1:** (a) Magnetic hysteresis curve of  $Mn_{0.5}Zn_{0.5}Fe_2O_4$  spinel nanoferrite; (a1) Zoomed Magnetic hysteresis curve of  $Mn_{0.5}Zn_{0.5}Fe_2O_4$  spinel nanoferrite; (b) M-H curve of  $Mn_{0.5}Zn_{0.5}Nd_{0.025}Fe_{1.975}O_4$  spinel ferrite; (b1) Zoomed M-H curve of  $Mn_{0.5}Zn_{0.5}Nd_{0.025}Fe_{1.975}O_4$  spinel ferrite; (c) M-H curve of  $Mn_{0.5}Zn_{0.5}Nd_{0.050}Fe_{1.950}O_4$  spinel ferrite; (c1) Zoomed M-H curve of  $Mn_{0.5}Zn_{0.5}Nd_{0.050}Fe_{1.950}O_4$  spinel ferrite.

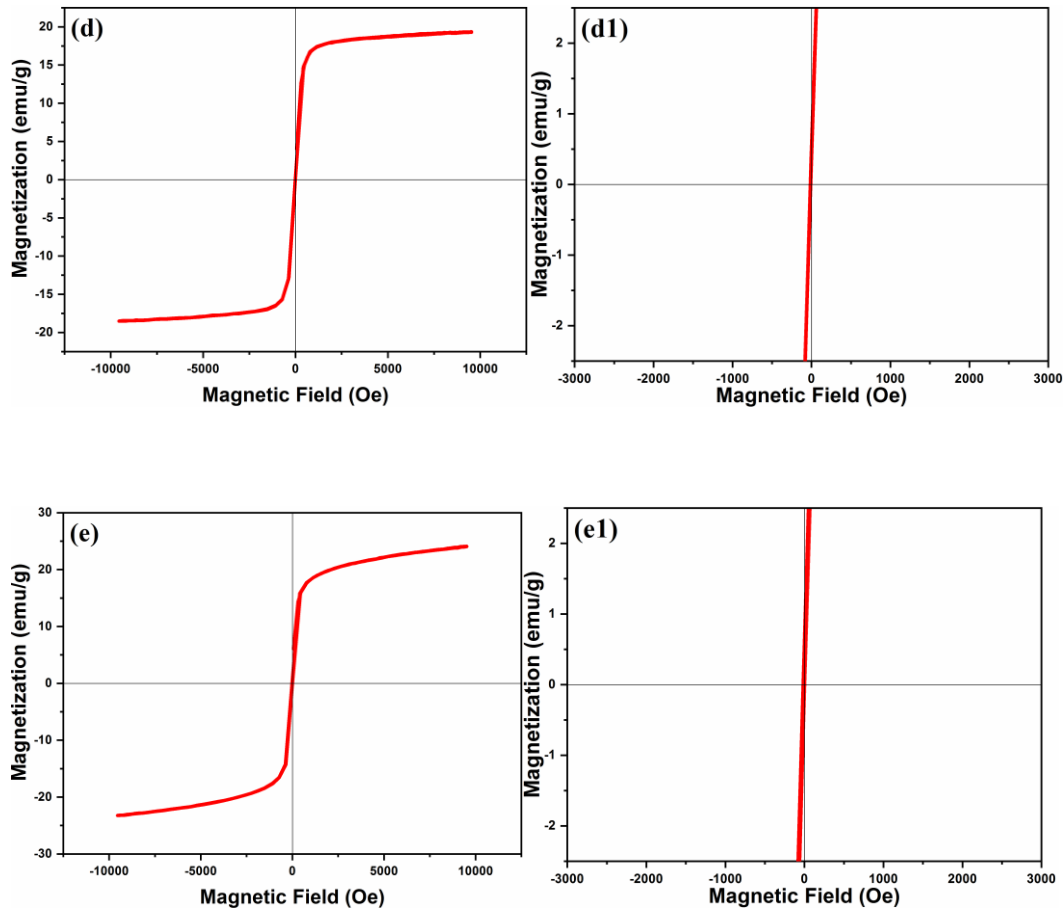


**Figure 5.13.2:** (d) M-H curve of  $\text{Mn}_{0.5}\text{Zn}_{0.5}\text{Nd}_{0.075}\text{Fe}_{1.925}\text{O}_4$  spinel ferrite; (d1) Zoomed M-H curve of  $\text{Mn}_{0.5}\text{Zn}_{0.5}\text{Nd}_{0.075}\text{Fe}_{1.925}\text{O}_4$  spinel ferrite; (e) M-H curve of  $\text{Mn}_{0.5}\text{Zn}_{0.5}\text{Nd}_{0.1}\text{Fe}_{1.9}\text{O}_4$  spinel ferrite; (e1) Zoomed M-H curve of  $\text{Mn}_{0.5}\text{Zn}_{0.5}\text{Nd}_{0.1}\text{Fe}_{1.9}\text{O}_4$  spinel ferrite.

Magnetic moment ( $n_B$ ) has been computed by employing the equation [13];  $n_B = (M \times M_s) / 5585$ , here  $M$  and  $M_s$  denote molecular weight of  $RE^{3+}$  ( $= La^{3+}$ ,  $Gd^{3+}$  &  $Nd^{3+}$ ) doped  $Mn_{0.5}Zn_{0.5}RE_xFe_{2-x}O_4$  spinel nanoferrites and saturation magnetization of respective composition. The computed quantities of  $n_B$  and  $M_s$  are given in table 5.8, 5.9 & 5.10 for  $RE^{3+} = La^{3+}$ ,  $Gd^{3+}$  &  $Nd^{3+}$  ions doping in Mn-Zn ferrites respectively. Figure 5.14, figure 5.15 and figure 5.16 show the variation of  $n_B$  and  $M_s$  with  $RE^{3+}$  content ( $x$ ). Further, it has been revealed that in the lack of magnetic field all the investigated samples have shown zero retentivity ( $Mr$ ) and zero coercivity ( $H_c$ ). This shows that investigated samples have either superparamagnetic or paramagnetic behaviour.

Super paramagnetic nature of  $Mn_{0.5}Zn_{0.5}RE_xFe_{2-x}O_4$  nanoferrites is proposed by an undivided domain structure. It has been observed that there is transformation of paramagnetic nature to superparamagnetic nature with the addition of  $RE^{3+}$  to Mn-Zn nano ferrites {see figures (5.11.1 to 5.13.2)}. This may be correlated to the decrease of crystallite with the addition of  $RE^{3+}$  to Mn-Zn nano ferrites (table 4.1).

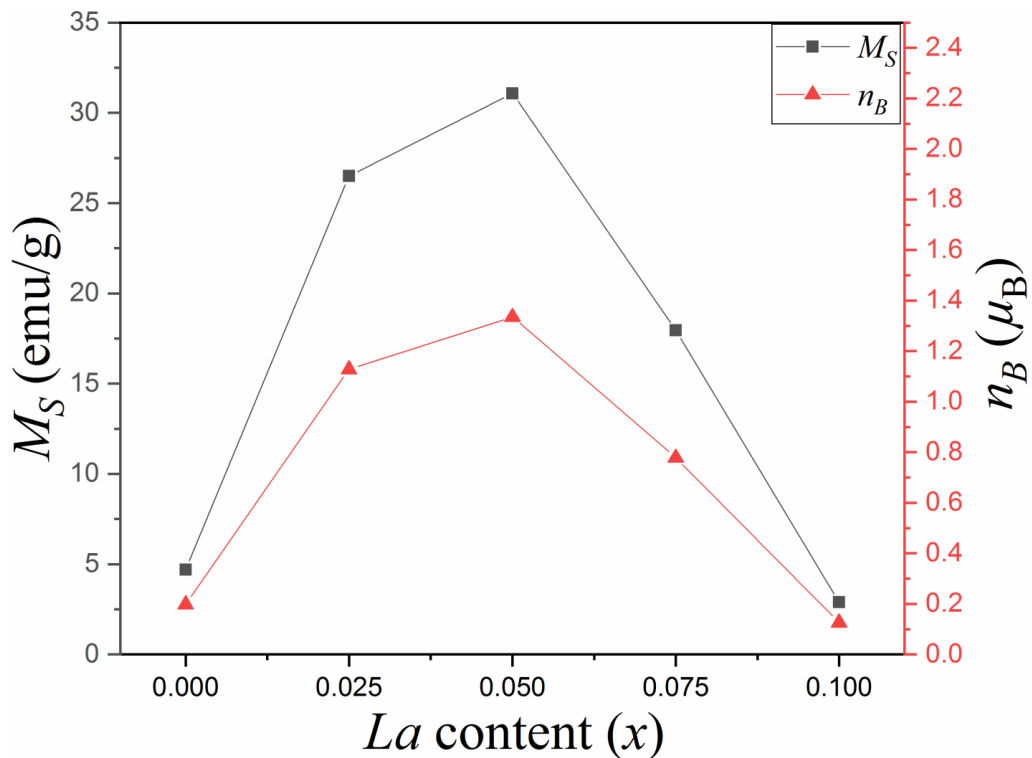


**Figure 5.14:** A plot of magnetic parameters  $M_s$  and  $n_B$  with  $La$  content ( $x$ ).

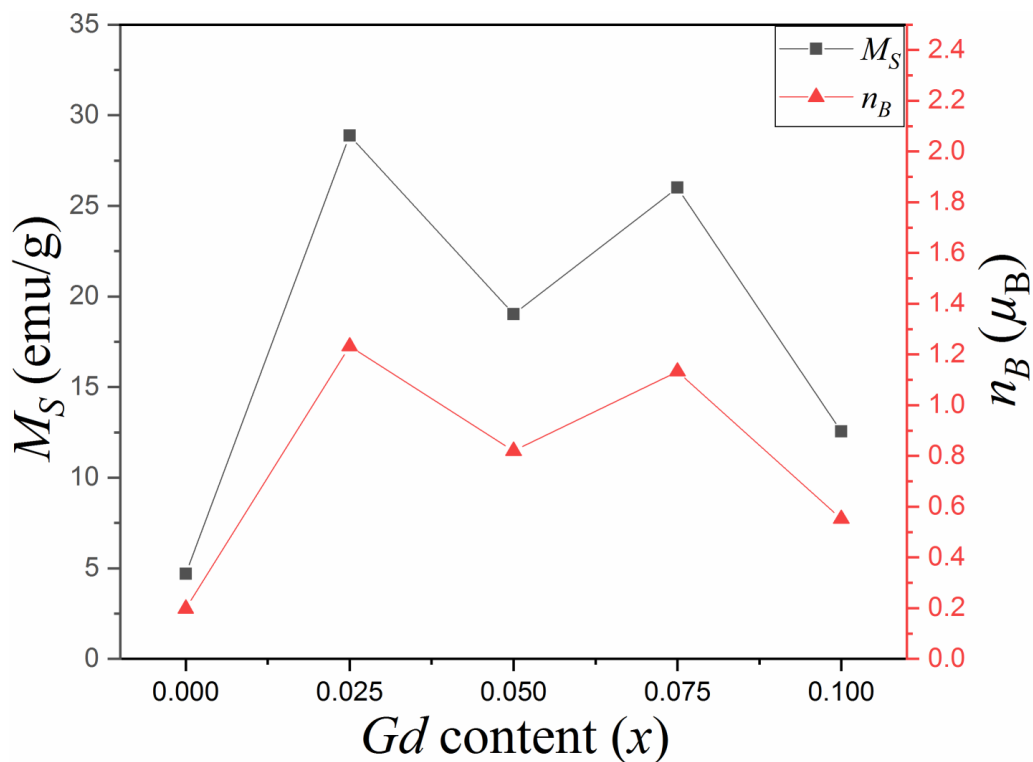


Figure 5.15: A plot of magnetic parameters  $M_S$  and  $n_B$  with Gd content ( $x$ ).

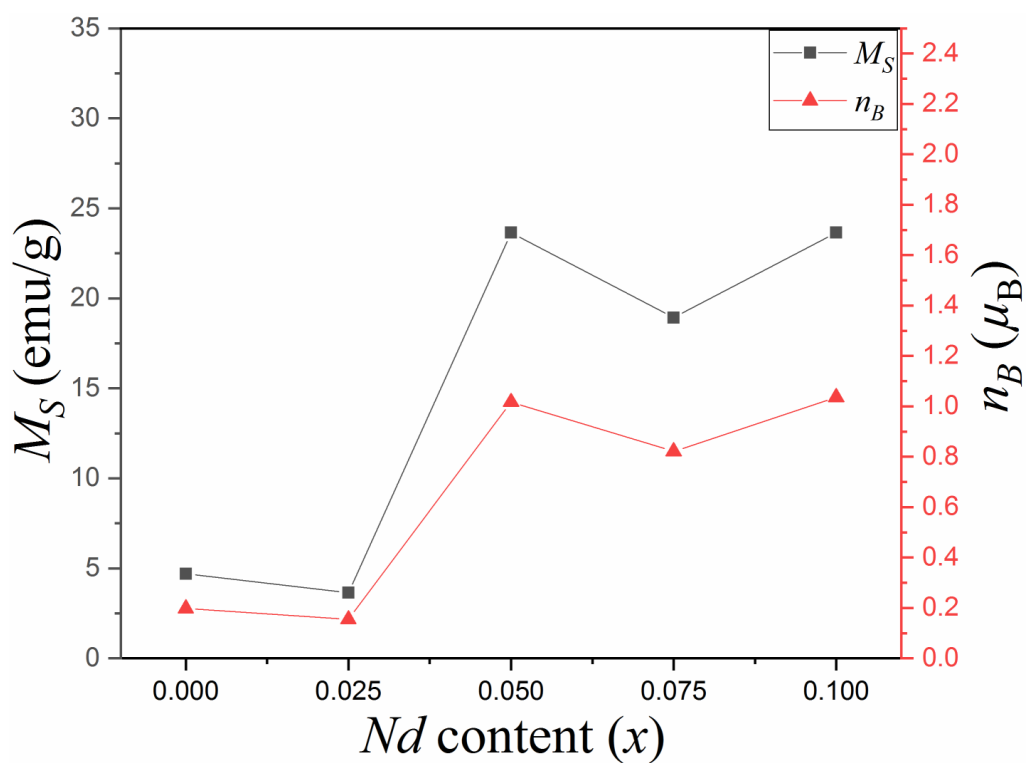


Figure 5.16: A plot of magnetic parameters  $M_S$  and  $n_B$  with Nd content ( $x$ ).

The decrease in size may be correlated to the transformation from multi-domain structure to single domain structure with the addition of  $RE^{3+}$  to Mn-Zn nano ferrites. Further from the proposed cation distribution, at the tetrahedral locations zinc ions and ferric ions feature A-A exchange interactions whereas in octahedral locations manganese ions, ferric ions and  $RE^{3+}$  ( $= La^{3+}$ ,  $Gd^{3+}$  &  $Nd^{3+}$ ) ions feature B-B interactions. At tetrahedral locations and octahedral locations, both bivalent ( $Zn^{2+}$  &  $Mn^{2+}$ ) and trivalent ( $Fe^{3+}$  &  $RE^{3+}$ ) metal ions bear A-B super exchange interactions. A-B super exchange interactions are practically superior to A-A and B-B interactions at respective sites [14]. There may be an improvement of A-B super exchange interactions with the addition of  $RE^{3+}$  concentration ( $x$ ) in  $Mn_{0.5}Zn_{0.5}RE_xFe_{2-x}O_4$  spinel nanoferrites. This improvement in A-B interaction suggests an increase in the measures of saturation magnetization and magnetic moment. In present work, the values of magnetic parameters ( $M_S$  and  $n_B$ ) have an increasing trend with the addition of  $RE^{3+}$  in  $Mn_{0.5}Zn_{0.5}RE_xFe_{2-x}O_4$  spinel ferrites. This increase in magnetic parameters can be correlated with the bond angles (Table 5.8, 5.9 & 5.10). There is an increment in the values of  $\theta_1$ ,  $\theta_2$ ,  $\theta_5$  suggesting firm A-A and A-B interactions whereas a decrement in the quantities of  $\theta_3$  &  $\theta_4$  indicates feeble B-B interactions. Finite solubility of large  $RE^{3+}$  ( $La^{3+}$ ,  $Gd^{3+}$  &  $Nd^{3+}$ ) ions in B- locations might be causative for the change in magnetic behavior of  $Mn_{0.5}Zn_{0.5}RE_xFe_{2-x}O_4$  nano ferrites (figure 5.14, 5.15 & 5.16). For  $La^{3+}$  ( $x = 0.050$ ),  $Gd^{3+}$  ( $x = 0.025$ ) and  $Nd^{3+}$  ( $x = 0.1$ ) there may be maximum tendency of  $RE^{3+}$  ( $= La^{3+}$ ,  $Gd^{3+}$  &  $Nd^{3+}$ ) ions to substitute ferric ions in octahedral sites. This may be the reason that there is maximum value of  $M_S$  and  $n_B$  at these lanthanide concentrations. For other lanthanide  $x$ -values, few of the  $RE^{3+}$  ions might have resided on the grain boundaries leading to a weak magnetic behaviour. Moreover, the magnetic parameters of spinel ferrites depends upon various components, for example synthesis technique, sintering temperature, crystallite size, grain size and redistribution of cations amongst A and B locations [1,15]

Kumar *et al.* observed the influence of gadolinium ( $Gd^{3+}$ ) doping on the magnetic characteristics of Mg–Mn nanoferrite devised by self-ignited solution combustion technique [12]. Superparamagnetic nature has been observed for all prepared samples. The consequence of heat treatment upon magnetic characteristics of Mn-Zn ferrite prepared through nitrate–citrate auto-combustion technique has been reported by Hu *et al.* [16]. Sample annealed at 600 °C in air have pointed very low value of  $M_S$  (1.552 emu g<sup>-1</sup>), coercivity (29 Oe) and remanence (0.03489 emu g<sup>-1</sup>) showing

## **Cation distribution and magnetic study of La<sup>3+</sup>, Gd<sup>3+</sup> & Nd<sup>3+</sup> doped Mn-Zn nano ferrites**

---

behaviour almost near to paramagnetism and superparamagnetism. Chaudhuri *et al.* [17] reported the outcome of lanthanum doping on magnetic characteristics of bismuth ferrite prepared by hydrothermal technique [17]. Using room temperature VSM characterization, for lower content of La ( $x=0, 0.05$ ) paramagnetic behaviour has been observed. Again for undoped sample at 560 °C paramagnetic behaviour has been observed using high temperature VSM characterization. Moussaoui *et al.* have observed the effect of transition metal (Co, Ni, Mn) doping on magnetic characteristics of neodymium spinel ferrites [18]. Superparamagnetic behaviour is remarked for both nickel (Ni) and manganese (Mn) doped neodymium (Nd) spinel ferrites and ferrimagnetic for cobalt (Co) doped neodymium spinel ferrites. Naik *et al.* described the result of neodymium (Nd<sup>3+</sup>) substitution the magnetic characteristics of Mn-Zn nanoferrites [6]. Superparamagnetic behaviour has been reported for prepared samples. Saturation magnetization and magnetic moment found to be decrease with Nd<sup>3+</sup> doping upto  $x=0.04$  and then increased upto  $x=0.1$ . Our results for spinel ferrites are in agreeable conformity with the results described in literature by several researchers [6,12,16-18].

Superparamagnetic nanoparticles (SPNs) have several applications in biomedicine like drug delivery, gene delivery, MRI Contrast Enhancement, hyperthermia, radionuclide delivery *etc.* [19-21]. SPNs have also shown their competence in magnetic recording [22, 23].

### **5.4. Conclusion**

From the proposed cation distribution, at the A-sites zinc ions and ferric ions cause A-A exchange interactions whereas in B-sites manganese ions, ferric ions and RE<sup>3+</sup> ( $= La^{3+}, Gd^{3+} \& Nd^{3+}$ ) ions experience B-B interactions. At the A- and B-sites both bivalent ( $Zn^{2+} \& Mn^{2+}$ ) and trivalent ( $Fe^{3+} \& RE^{3+}$ ) metal ions experience A-B super exchange interactions. This has been further confirmed by the bond angles between the metal ions. There is an increase in the values of  $\theta_1, \theta_2, \theta_5$  suggesting firm A-A and A-B interactions whereas decrement in the quantities of  $\theta_3 \& \theta_4$  indicates feeble B-B interactions. Magnetic characterizations show superparamagnetic and paramagnetic behaviour of RE<sup>3+</sup> ( $= La^{3+}, Gd^{3+}, Nd^{3+}$ ) doped Mn-Zn spinel ferrite. For samples under investigation, the absence of retentivity and coercivity have been noticed at no magnetic field. Increase in magnetic parameters ( $M_S$  and  $n_B$ ) with RE<sup>3+</sup> doping is correlated with

the bond angles. For  $La^{3+}$  ( $x = 0.050$ ),  $Gd^{3+}$  ( $x = 0.025$ ) and  $Nd^{3+}$  ( $x = 0.1$ ) compositions, a maximum value of magnetic parameters have been observed.



# **CHAPTER-6**

---

**Summary and future scope**



Spinel ferrites have shown their competence in various technological applications like high-frequency devices, catalysis, microwave devices *etc.* These materials have also shown their usefulness in biomedical applications particularly for hyperthermia and drug delivery. Spinel ferrites exist in  $AB_2O_4$  form with  $A$  as bivalent metal ions (*e.g.*  $Mn^{2+}$ ,  $Co^{2+}$ ,  $Zn^{2+}$ ,  $Mg^{2+}$ ,  $Ni^{2+}$  *etc.*) and  $B$  as trivalent metal ions {*e.g.* rare earth metals ( $La^{3+}$ ,  $Gd^{3+}$  *etc.*),  $In^{3+}$ ,  $Al^{3+}$  *etc.*}. The places occupied by  $A$  ions are known as tetrahedral sites and the places occupied by  $B$  ions are known as octahedral sites. The distribution of ions in these sites is accountable for the different conceptions of spinel ferrites. The structural and magnetic behaviour of spinel ferrites are being decided by their chemical configuration, synthesis technique, sintering temperature, type of dopant and particle size. Among various soft ferrites, manganese-zinc spinel ferrites have shown their importance due to their application in high frequency devices and property of high initial magnetic permeability. Different synthesis techniques *viz.* sol-gel, sol-gel autocombustion, hydrothermal, co-precipitation *etc.* have been employed by various researchers to prepare manganese-zinc spinel ferrites. Evolution of microstructure and homogeneous compositions on mixing the precursors at molecular stage are the primary advantages of these synthesis techniques. In this work, lanthanide ( $RE^{3+} = La^{3+}$ ,  $Gd^{3+}$  and  $Nd^{3+}$ ) doped manganese-zinc ferrites has been studied. The samples of ferrites has been synthesized using co-precipitation technique. First, the sintering temperature has been optimized for the manganese-zinc ferrites. Second, the addition of lanthanides ( $La^{3+}$ ,  $Gd^{3+}$  &  $Nd^{3+}$ ) to manganese-zinc cubic spinel ferrites synthesized using co-precipitation technique have been studied for the structural, morphological and magnetic properties. Various characterization techniques *viz.* XRD, FTIR, EDS, FE-SEM and VSM have been employed to study the above mentioned properties. To understand the magnetic behaviour of lanthanide ( $RE^{3+} = La^{3+}$ ,  $Gd^{3+}$  and  $Nd^{3+}$ ) doped manganese-zinc ferrites a theoretical cation distribution has also been suggested.

The co-precipitation synthesis technique has been used for the preparation of  $Mn_{0.5}Zn_{0.5}Fe_2O_4$  nanoferrite. The synthesized ferrite has been subjected to sintering sample at three temperatures that is to say 973 K, 1173 K and 1373 K. From the structural analysis using XRD at three sintering temperatures, a single phase cubical spinel is remarked at 1373 K whereas a secondary phase  $Fe_2O_3$  is observed at lower sintering temperatures. The average crystallite size is noticed to increase (11.38 nm to 67.42 nm) with the increasing sintering temperature (973 K to 1373 K). The presence

of two absorption bands that is to say at  $421\text{ cm}^{-1}$  to  $491\text{ cm}^{-1}$  and  $516\text{ cm}^{-1}$  to  $592\text{ cm}^{-1}$  in FTIR spectra has supported the formation of spinel ferrite. FE-SEM images have shown the development of homogeneous crystalline nanoparticles with increment in sintering temperature. For  $\text{RE}^{3+}$  doped Mn-Zn ferrites, we have taken the sintering temperature as  $1373\text{ K}$  for further investigation after considering the optimized sintering results.

Structural investigations show a cubic spinel phase for  $\text{Mn}_{0.5}\text{Zn}_{0.5}\text{RE}_x\text{Fe}_{2-x}\text{O}_4$ , where  $x = 0, 0.025, 0.050, 0.075$  and  $0.1$  for nanoferrites synthesized through co-precipitation synthesis technique, where  $\text{RE} = \text{La}, \text{Gd} \& \text{Nd}$ . For the three dopants used in Mn-Zn ferrites, the structural parameters ( $D, a, d$  and  $P$ ) have been observed to decrease generally. The occurrence of spinel structure in all the investigated samples has also been confirmed from FTIR spectroscopy. A clear change in the location of absorption bands on  $\text{RE} (= \text{La}, \text{Gd} \& \text{Nd})$  doping has also been observed. FE-SEM micrographs of  $\text{Mn}_{0.5}\text{Zn}_{0.5}\text{RE}_x\text{Fe}_{2-x}\text{O}_4$  (where  $\text{RE} = \text{La}, \text{Gd}, \text{Nd}$ ) ferrites show sharp crystalline structures. EDS spectroscopy confirms the presence of constituents that is to say  $\text{Mn}, \text{Zn}, \text{RE} (= \text{La}, \text{Gd} \& \text{Nd}), \text{Fe}, \text{O}$  for every investigated sample.

From the proposed cation distribution, at the tetrahedral locations zinc ions and ferric ions cause A-A exchange interactions whereas at the octahedral locations manganese ions, ferric ions and  $\text{RE}^{3+} (= \text{La}^{3+}, \text{Gd}^{3+} \& \text{Nd}^{3+})$  ions feature B-B interactions. At the tetrahedral and octahedral locations both bivalent ( $\text{Zn}^{2+} \& \text{Mn}^{2+}$ ) and trivalent ( $\text{Fe}^{3+} \& \text{RE}^{3+}$ ) metal ions cause A-B super exchange interactions. This has been further confirmed by the bond angles between the metal ions. There is an increment for quantities of  $\theta_1, \theta_2, \theta_5$  suggesting firm A-A and A-B interactions whereas a decrement for quantities of  $\theta_3 \& \theta_4$  indicates feeble B-B interactions. Magnetic characterizations show superparamagnetic and paramagnetic behaviour of  $\text{RE}^{3+} (= \text{La}^{3+}, \text{Gd}^{3+}, \text{Nd}^{3+})$  doped Mn-Zn spinel ferrite. The absence of retentivity and coercivity at no magnetic field has been noticed for samples under investigation. Increase in magnetic parameters ( $M_S$  and  $n_B$ ) with  $\text{RE}^{3+}$  doping is correlated with the bond angles. For  $\text{La}^{3+}$  ( $x = 0.050$ ),  $\text{Gd}^{3+}$  ( $x = 0.025$ ) and  $\text{Nd}^{3+}$  ( $x = 0.1$ ) compositions, a maximum value of magnetic parameters have been observed.

The ferrite nanoparticles having superparamagnetic behaviour may have several applications in biomedicine like drug delivery, gene delivery, MRI contrast enhancement, hyperthermia, radionuclide delivery *etc.* The future work will comprise to check the biocompatibility (*i.e.* cytotoxicity on cell lines) of bare and encapsulated

(*i.e.* coated with polyvinyl alcohol) ferrite superparamagnetic nanoparticle. Thereafter considering the results the bare and/or encapsulated ferrite superparamagnetic nanoparticle will be studied for possible drug delivery applications. On the part of fundamentals behind magnetization of the studied samples Mossbauer spectroscopy and temperature dependent VSM investigations will also be performed.



# **BIBLIOGRAPHY**

---



**Bibliography****Chapter - 1**

- [1] Dattagupta, S., Arun M. Jayannavar, and Narendra Kumar. "Landau diamagnetism revisited." *Current science* 80 (2001): 861-863.
- [2] Miessler, G. L. and Tarr, D. A. *Inorganic Chemistry* 3rd ed., Pearson/Prentice Hall publisher, (2010) ISBN 0-13-035471-6.
- [3] Deshpande, C. E. "Recent developments in processing of Mn-Zn ferrites-An overview." *Indian Journal of Chemistry* Vol 35A, May 1996, pp. 353-365.
- [4] Chikazumi, Soshin, and Chad D. Graham. *Physics of Ferromagnetism 2e*. Vol. 94. Oxford University Press on Demand, 2009.
- [5] Richard M. Bozorth, *Ferromagnetism*, first published 1951, reprinted 1993 by IEEE Press, New York as a "Classic Reissue." ISBN 0-7803-1032-2.
- [6] Néel, M. Louis. "Propriétés magnétiques des ferrites; ferrimagnétisme et antiferromagnétisme." In *Annales de Physique*, vol. 12, pp. 137-198. 1948.
- [7] Stanciu, C. D., A. V. Kimel, F. Hansteen, A. Tsukamoto, A. Itoh, A. Kirilyuk, and Th Rasing. "Ultrafast spin dynamics across compensation points in ferrimagnetic GdFeCo: The role of angular momentum compensation." *Physical Review B* 73, no. 22 (2006): 220402.
- [8] Carter, C. Barry, and M. Grant Norton. *Ceramic materials: science and engineering*. Springer Science & Business Media, 2007.
- [9] Maharshi Bharadwaaja "The Vaimanika Shastra." *Ancient manuscripts on the construction and use of UFOs-Forgotten Books* (1973) (propounded by Subbaraya Shastry, Translated into English and Edited, Printed and Published by G.R. JOSYER) Coronation Press, Mysore-4, India.
- [10] Shivananda Lahari and Adi Shankaracharya, Staza. No. 61.
- [11] Wohlfarth, E. P. "The magnetic field dependence of the susceptibility peak of some spin glass materials." *Journal of Physics F: Metal Physics* 10, no. 9 (1980): L241.
- [12] Néel, Louis. "Some theoretical aspects of rock-magnetism." *Advances in physics* 4, no. 14 (1955): 191-243.
- [13] Néel, Louis. "Antiferromagnetism and ferrimagnetism." *Proceedings of the Physical Society. Section A* 65, no. 11 (1952): 869.

- [14] Srivastava, Richa, and B. C. Yadav. "Ferrite materials: introduction, synthesis techniques, and applications as sensors." *International Journal of Green Nanotechnology* 4, no. 2 (2012): 141-154.
- [15] Okamoto, Akira. "The invention of ferrites and their contribution to the miniaturization of radios." In *GLOBECOM Workshops, 2009 IEEE*, pp. 1-6. IEEE, 2009.
- [16] Shriver, D. F.; Atkins, P. W.; Overton, T. L.; Rourke, J. P.; Weller, M. T.; Armstrong, F. A. (2006). *Inorganic Chemistry*. New York: W. H. Freeman. ISBN 0-7167-4878-9.
- [17] Ullah, Zaka, Shahid Atiq, and Shahzad Naseem. "Influence of Pb doping on structural, electrical and magnetic properties of Sr-hexaferrites." *Journal of Alloys and Compounds* 555 (2013): 263-267.
- [18] Kools, F. X. N. M., and D. Stoppels. "Ferrites." *Kirk-Othmer Encyclopedia of Chemical Technology* Vol. 11(2000) pp. 55-91.
- [19] Chen, Yajie, Anton L. Geiler, Taiyang Chen, Tomokazu Sakai, C. Vittoria, and V. G. Harris. "Low-loss barium ferrite quasi-single-crystals for microwave application." *Journal of applied physics* 101, no. 9 (2007): 09M501.
- [20] Lee, Jae-Gwang, Jae Yun Park, Young-Jei Oh, and Chul Sung Kim. "Magnetic properties of CoFe<sub>2</sub>O<sub>4</sub> thin films prepared by a sol-gel method." *Journal of Applied Physics* 84, no. 5 (1998): 2801-2804.
- [21] Bragg, William Henry. "XXX. The structure of the spinel group of crystals." *The London, Edinburgh, and Dublin Philosophical Magazine and Journal of Science* 30, no. 176 (1915): 305-315.
- [22] Braun, P. B. "A superstructure in spinels." *Nature* 170, no. 4339 (1952): 1123-1123.
- [23] Collins, T., and A. E. Brown. "Low-Loss Lithium Ferrites for Microwave Latching Applications." *Journal of Applied Physics* 42, no. 9 (1971): 3451-3454.
- [24] Hanif, Mehwish, U. Rafiq, M. Anis-ur-Rehman, and A. ul Haq. "Structural and Dielectric Properties of Rare Earth Doped Lithium Nanoferrites for Sensing Applications." *Journal of Superconductivity and Novel Magnetism* 30, no. 12 (2017): 3573-3576.
- [25] Sawant, V. S., and K. Y. Rajpure. "The effect of Co substitution on the structural and magnetic properties of lithium ferrite synthesized by an autocombustion method." *Journal of Magnetism and Magnetic Materials* 382 (2015): 152-157.

- [26] Gilani, Zaheer Abbas, Muhammad Shahzad Shifa, Muhammad Azhar Khan, Muhammad Naeem Anjum, Muhammad Nauman Usmani, Rajjab Ali, and Muhammad Farooq Warsi. "New  $\text{LiCo}_{0.5}\text{PrxFe}_{2-x}\text{O}_4$  nanoferrites: Prepared via low cost technique for high density storage application." *Ceramics International* 44, no. 2 (2018): 1881-1885.
- [27] Hussein, Shaban I., Ashraf S. Elkady, M. M. Rashad, A. G. Mostafa, and R. M. Megahid. "Structural and magnetic properties of magnesium ferrite nanoparticles prepared via EDTA-based sol–gel reaction." *Journal of Magnetism and Magnetic Materials* 379 (2015): 9-15.
- [28] Choodamani, C., B. Rudraswamy, and G. T. Chandrappa. "Structural, electrical, and magnetic properties of Zn substituted magnesium ferrite." *Ceramics International* 42, no. 9 (2016): 10565-10571.
- [29] Zaki, H. M., S. H. Al-Heniti, and T. A. Elmosalami. "Structural, magnetic and dielectric studies of copper substituted nano-crystalline spinel magnesium zinc ferrite." *Journal of Alloys and Compounds* 633 (2015): 104-114.
- [30] Naseri, Mahmoud Goodarz, Mohammad Hossein Majles Ara, Elias B. Saion, and Abdul Halim Shaari. "Superparamagnetic magnesium ferrite nanoparticles fabricated by a simple, thermal-treatment method." *Journal of Magnetism and Magnetic Materials* 350 (2014): 141-147.
- [31] Gagan Kumar, Jyoti Shah, R.K. Kotnala, VirenderPratap Singh, Sarveena, Godawari Garg, Sagar E. Shirsath, Khalid M. Bato, Mahavir Singh, Superparamagnetic behaviour and evidence of weakening in super-exchange interactions with the substitution of  $\text{Gd}^{3+}$  ions in the Mg–Mn nanoferrite matrix, *Materials Research Bulletin* 63 (2015) 216–225.
- [32] Modi, K. B., N. H. Vasoya, V. K. Lakhani, and T. K. Pathak. "Magnetic phase evolution and particle size estimation study on nanocrystalline Mg–Mn ferrites." *Applied Nanoscience* 5, no. 1 (2015): 11-17.
- [33] Baba, P. D., G. Argentina, W. Courtney, G. Dionne, and D. Temme. "Fabrication and properties of microwave lithium ferrites." *IEEE Transactions on Magnetism* 8, no. 1 (1972): 83-94.
- [34] Heiba, Zein K., Mohamed Bakr Mohamed, Adel Maher Wahba, and L. Arda. "Magnetic and structural properties of nanocrystalline cobalt-substituted magnesium–manganese ferrite." *Journal of Superconductivity and Novel Magnetism* 28, no. 8 (2015): 2517-2524.

- [35] S. A. Morrison, C. L. Cahill, E. E. Carpenter, S. Calvin, R. Swaminathan, M. E. McHenry, "Magnetic and structural properties of nickel zinc ferrite nanoparticles synthesized at room temperature", *J. Appl. Phys.* 95 (11) (2004) 6392.
- [36] Verma, A., T. C. Goel, R. G. Mendiratta, and P. Kishan. "Magnetic properties of nickel–zinc ferrites prepared by the citrate precursor method." *Journal of Magnetism and Magnetic materials* 208, no. 1-2 (2000): 13-19.
- [37] Ghodake, J. S., Rahul C. Kambale, T. J. Shinde, P. K. Maskar, and S. S. Suryavanshi. "Magnetic and microwave absorbing properties of Co<sup>2+</sup> substituted nickel–zinc ferrites with the emphasis on initial permeability studies." *Journal of Magnetism and Magnetic Materials* 401 (2016): 938-942.
- [38] Sun, Ke, Hai Liu, Yan Yang, Zhong Yu, Chuan Chen, Guohua Wu, Xiaona Jiang, Zhongwen Lan, and Lezhong Li. "Contribution of magnetization mechanisms in nickel–zinc ferrites with different grain sizes and its temperature relationship." *Materials Chemistry and Physics* 175 (2016): 131-137.
- [39] Phan, C. H., M. Mariatti, and Y. H. Koh. "Electromagnetic interference shielding performance of epoxy composites filled with multiwalled carbon nanotubes/manganese zinc ferrite hybrid fillers." *Journal of Magnetism and Magnetic Materials* 401 (2016): 472-478.
- [40] Monfared, A. H., A. Zamanian, M. Beygzadeh, I. Sharifi, and M. Mozafari. "A rapid and efficient thermal decomposition approach for the synthesis of manganese-zinc/oleylamine core/shell ferrite nanoparticles." *Journal of Alloys and Compounds* 693 (2017): 1090-1095.
- [41] Angadi, V. Jagadeesha, B. Rudraswamy, K. Sadhana, and K. Praveena. "Structural and magnetic properties of manganese zinc ferrite nanoparticles prepared by solution combustion method using mixture of fuels." *Journal of Magnetism and Magnetic Materials* 409 (2016): 111-115.
- [42] Jishkariani, Davit, Jennifer D. Lee, Hongseok Yun, Taejong Paik, James M. Kikkawa, Cherie R. Kagan, Bertrand Donnio, and Christopher B. Murray. "The dendritic effect and magnetic permeability in dendron coated nickel and manganese zinc ferrite nanoparticles." *Nanoscale* 9, no. 37 (2017): 13922-13928.
- [43] Kurian, Manju, and Divya S. Nair. "Manganese zinc ferrite nanoparticles as efficient catalysts for wet peroxide oxidation of organic aqueous wastes." *Journal of Chemical Sciences* 127, no. 3 (2015): 537-546.

- [44] Szczygieł, Irena, and Katarzyna Winiarska. "Synthesis and characterization of manganese–zinc ferrite obtained by thermal decomposition from organic precursors." *Journal of Thermal Analysis and Calorimetry* 115, no. 1 (2014): 471-477.
- [45] Sun, Bing, Fugang Chen, Wenda Yang, Hongqing Shen, and Dan Xie. "Effects of nano-TiO<sub>2</sub> and normal size TiO<sub>2</sub> additions on the microstructure and magnetic properties of manganese–zinc power ferrites." *Journal of Magnetism and Magnetic Materials* 349 (2014): 180-187.
- [46] Thota, Suneetha, Subhash C. Kashyap, Shiv K. Sharma, and V. R. Reddy. "Micro Raman, Mossbauer and magnetic studies of manganese substituted zinc ferrite nanoparticles: Role of Mn." *Journal of Physics and Chemistry of Solids* 91 (2016): 136-144.
- [47] Kumar, Surender, Tukaram J. Shinde, Pramod N. Vasambekar, and Kapil Bhatt. "Chemical Synthesis and Magnetic Properties of Indium-Substituted Manganese-Zinc Nanoferrites." *IEEE Transactions on Magnetics* 51, no. 4 (2015): 1-8.
- [48] Lin, Zhou, Peng Xiaoling, Wang Xinqing, Ge Hongliang, Zhang Jing, and Xu Yunwei. "Preparation and Characterization of Manganese-Zinc Ferrites by a Solvothermal Method." *Rare Metal Materials and Engineering* 44, no. 5 (2015): 1062-1066.
- [49] Pashchenko, V. P., A. A. Khor'yakov, A. V. Pashchenko, Yu S. Prilipko, and A. A. Shemyakov. "Effect of oxygen nonstoichiometry on the structure, 55 Mn and 57 Fe NMR, electromagnetic properties, and magnetoresistance of manganese zinc ferrites." *Inorganic Materials* 50, no. 2 (2014): 191-196.
- [50] Karthick, R., and R. Srinivasan. "A study on impact of zinc substitution on magneto-optic properties of manganese ferrite nanoferrofluids." *Journal of Magnetism and Magnetic Materials* 441 (2017): 443-447.
- [51] Ding, Chuan, Wenhui Yin, Liangliang Cao, and Yanwei Zeng. "Synthesis of manganese–zinc ferrite nanopowders prepared by a microwave-assisted auto-combustion method: Influence of sol–gel chemistry on microstructure." *Materials Science in Semiconductor Processing* 23 (2014): 50-57.
- [52] M. J. Nasr Isfahani and M. Myndyk, et al., "Magnetic properties of nanostructured MnZn ferrite", *J. Magn. Magn. Mater.*, 321(2009)152–156.
- [53] D. Varshney, K. Verma, A. Kumar, "Structural and vibrational properties of Zn<sub>x</sub>Mn<sub>1-x</sub>Fe<sub>2</sub>O<sub>4</sub> (x= 0.0, 0.25, 0.50, 0.75, 1.0) mixed ferrites", *Mater. Chem. Phys.*, 131(2011) 413–419

- [54] D. Zhang, X. Zhang, et al., "Low-temperature fabrication of MnFe<sub>2</sub>O<sub>4</sub> octahedrons: Magnetic and electrochemical properties", *Chem. Phys. Lett.*, 426(2006)120–123.
- [55] P. Hu, H. Yang, et al., "Heat treatment effects on microstructure and magnetic properties of Mn–Zn ferrite powders", *J. Magn. Magn. Mater.*, 322(2010)173–177.
- [56] C.C. Agrafiotis, V.T. Zaspalis, "Self-propagating high-temperature synthesis of MnZn ferrites for inductor applications" *J. Magn. Magn. Mater.*, 283(2004)364–374.
- [57] Zahraei, Maryam, Ahmad Monshi, Maria del Puerto Morales, Daryoush Shahbazi-Gahrouei, Mehdi Amirnasr, and Behshid Behdadfar. "Hydrothermal synthesis of fine stabilized superparamagnetic nanoparticles of Zn<sup>2+</sup> substituted manganese ferrite." *Journal of magnetism and magnetic materials* 393 (2015): 429-436.
- [58] Chiang, Chao-Lung, Kuen-Song Lin, Pei-Ju Hsu, and Yan-Gu Lin. "Synthesis and characterization of magnetic zinc and manganese ferrite catalysts for decomposition of carbon dioxide into methane." *international journal of hydrogen energy* 42, no. 34 (2017): 22123-22137.
- [59] Das, Sukanta, G. C. Nayak, S. K. Sahu, P. C. Routray, A. K. Roy, and H. Baskey. "Microwave absorption properties of double-layer composites using CoZn/NiZn/MnZn-ferrite and titanium dioxide." *Journal of Magnetism and Magnetic Materials* 377 (2015): 111-116.
- [60] Gabal, M. A., R. S. Al-Luhaibi, and Y. M. Al Angari. "Recycling spent zinc–carbon batteries through synthesizing nano-crystalline Mn–Zn ferrites." *Powder Technology* 258 (2014): 32-37.
- [61] Baykal, Abdülhadi, Sadik Güner, and Ayşe Demir. "Synthesis and magneto-optical properties of triethylene glycol stabilized Mn<sub>1-x</sub>Zn<sub>x</sub>Fe<sub>2</sub>O<sub>4</sub> nanoparticles." *Journal of Alloys and Compounds* 619 (2015): 5-11.
- [62] Ying, Yao, Yuzhao Gong, Dong Liu, Wangchang Li, Jing Yu, Liqiang Jiang, and Shenglei Che. "Effect of MoO<sub>3</sub> addition on the magnetic properties and complex impedance of Mn–Zn ferrites with high B<sub>s</sub> and high initial permeability." *Journal of Superconductivity and Novel Magnetism* 30, no. 8 (2017): 2129-2134.
- [63] Hosoya, Takashi, Wataru Sakamoto, and Toshinobu Yogo. "In situ synthesis of manganese zinc ferrite nanoparticle/polymer hybrid nanocomposite from metal organics." *Journal of materials science* 49, no. 14 (2014): 5093-5099.

- [64] Moučka, Robert, N. Kazantseva, and Irina Sapurina. "Electric properties of MnZn ferrite/polyaniline composites: the implication of polyaniline morphology." *Journal of Materials Science* 53, no. 3 (2018): 1995-2004.
- [65] Kumar, E. Ranjith, and R. Jayaprakash. "The role of fuel concentration on particle size and dielectric properties of manganese substituted zinc ferrite nanoparticles." *Journal of Magnetism and Magnetic Materials* 366 (2014): 33-39.
- [66] Baykal, Abdülhadi, Sadik Güner, Ayse Demir, Sinem Esir, and Fazilet Genç. "Effect of zinc substitution on magneto-optical properties of Mn<sub>1-x</sub>Zn<sub>x</sub>Fe<sub>2</sub>O<sub>4</sub>/SiO<sub>2</sub> nanocomposites." *Ceramics International* 40, no. 8 (2014): 13401-13408.
- [67] Kumar, E. Ranjith, T. Arunkumar, and T. Prakash. "Heat treatment effects on structural and dielectric properties of Mn substituted CuFe<sub>2</sub>O<sub>4</sub> and ZnFe<sub>2</sub>O<sub>4</sub> nanoparticles." *Superlattices and Microstructures* 85 (2015): 530-535.
- [68] Beji, Z., M. Sun, L. S. Smiri, F. Herbst, C. Mangeney, and S. Ammar. "Polyol synthesis of non-stoichiometric Mn–Zn ferrite nanocrystals: structural/microstructural characterization and catalytic application." *RSC Advances* 5, no. 80 (2015): 65010-65022.
- [69] Abbas, Mohamed, Sri Ramulu Torati, B. Parvatheeswara Rao, M. O. Abdel-Hamed, and CheolGi Kim. "Size controlled sonochemical synthesis of highly crystalline superparamagnetic Mn–Zn ferrite nanoparticles in aqueous medium." *Journal of Alloys and Compounds* 644 (2015): 774-782.
- [70] Jalaiah, K., and K. Vijaya Babu. "Structural, magnetic and electrical properties of nickel doped Mn-Zn spinel ferrite synthesized by sol-gel method." *Journal of Magnetism and Magnetic Materials* 423 (2017): 275-280.
- [71] Eltabey, M. M., A. M. Massoud, and Cosmin Radu. "Amendment of saturation magnetization, blocking temperature and particle size homogeneity in Mn-ferrite nanoparticles using Co-Zn substitution." *Materials Chemistry and Physics* 186 (2017): 505-512.
- [72] Masthoff, I-C., A. Gutsche, H. Nirschl, and G. Garnweitner. "Oriented attachment of ultra-small Mn (1-x) Zn x Fe 2 O 4 nanoparticles during the non-aqueous sol-gel synthesis." *Cryst Eng Comm* 17, no. 12 (2015): 2464-2470.
- [73] Xi, Guoxi, Yuebin Xi, Huidao Xu, and Lu Wang. "Study of the preparation of Ni–Mn–Zn ferrite using spent Ni–MH and alkaline Zn–Mn batteries." *Journal of Magnetism and Magnetic Materials* 398 (2016): 196-199.

- [74] Liu, Shiyuan, Lijun Wang, and Kuochih Chou. "Synthesis of metal-doped Mn-Zn ferrite from the leaching solutions of vanadium slag using hydrothermal method." *Journal of Magnetism and Magnetic Materials* 449 (2018): 49-54.
- [75] Li, Mingling, Xiansong Liu, Taotao Xu, Yu Nie, Honglin Li, and Cong Zhang. "Synthesis and characterization of nanosized MnZn ferrites via a modified hydrothermal method." *Journal of Magnetism and Magnetic Materials* 439 (2017): 228-235.
- [76] Chen, Zhenhua, Yi Zhou, Zhitao Kang, and Ding Chen. "Synthesis of Mn-Zn ferrite nanoparticles by the coupling effect of ultrasonic irradiation and mechanical forces." *Journal of Alloys and Compounds* 609 (2014): 21-24.
- [77] R.Lebourgeois, J.P.Ganne and B.Lloret, *J.Phys.IV France* 7, Colleque C1,105 (1997).
- [78] Sridhar, Ch SLN, Ch S. Lakshmi, G. Govindraj, S. Bangarraju, L. Satyanarayana, and D. M. Potukuchi. "Structural, morphological, magnetic and dielectric characterization of nano-phased antimony doped manganese zinc ferrites." *Journal of Physics and Chemistry of Solids* 92 (2016): 70-84.
- [79] Šepelák, V., P. Heitjans, and K. Becker. "Nanoscale spinel ferrites prepared by mechanochemical route: thermal stability and size dependent magnetic properties." *Journal of Thermal Analysis and Calorimetry* 90, no. 1 (2007): 93-97.
- [80] Modak, S., M. Ammar, F. Mazaleyrat, S. Das, and P. K. Chakrabarti. "XRD, HRTEM and magnetic properties of mixed spinel nanocrystalline Ni-Zn-Cu-ferrite." *Journal of alloys and compounds* 473, no. 1-2 (2009): 15-19.
- [81] P. Samoila, L. Sacarescu, A.I. Borhan, D. Timpu, M. Grigoras, N. Lupu, M. Zaltariov, V. Harabagiu, Magnetic properties of nanosized Gd doped Ni-Mn-Cr ferrites prepared using the sol-gel autocombustion technique, *Journal of Magnetism and Magnetic Materials* 378 (2015) 92-97.
- [82] Töpfer, J., W. Schöps, P. Nauber, and D. Kätzel. "Modern developmental trends in the production and application of hard and soft magnetic ferrite materials." In *CFI. Ceramic forum international*, vol. 76, no. 9, (1999) pp. 49-55.
- [83] Waqas, H., and A. H. Qureshi. "Influence of pH on nanosized Mn-Zn ferrite synthesized by sol-gel auto combustion process." *Journal of thermal analysis and calorimetry* 98, no. 2 (2009): 355.

- [84] Costa, A. C. F. M., E. Tortella, M. R. Morelli, and R. H. G. A. Kiminami. "Synthesis, microstructure and magnetic properties of Ni–Zn ferrites." *Journal of magnetism and magnetic materials* 256, no. 1-3 (2003): 174-182.
- [85] Verma, A., T. C. Goel, R. G. Mendiratta, and M. I. Alam. "Dielectric properties of NiZn ferrites prepared by the citrate precursor method." *Materials Science and Engineering: B* 60, no. 2 (1999): 156-162.
- [86] Rath, Chandana, S. Anand, R. P. Das, K. K. Sahu, S. D. Kulkarni, S. K. Date, and N. C. Mishra. "Dependence on cation distribution of particle size, lattice parameter, and magnetic properties in nanosize Mn–Zn ferrite." *Journal of Applied Physics* 91, no. 4 (2002): 2211-2215.
- [87] Rezlescu, E., N. Rezlescu, C. Pasnicu, M. L. Craus, and D. P. Popa. "The influence of additives on the properties of Ni-Zn ferrite used in magnetic heads." *Journal of magnetism and magnetic materials* 117, no. 3 (1992): 448-454.
- [88] Mansour, S. F., M. A. Abdo, and S. M. Alwan. "The role of Cr<sup>3+</sup> ions substitution on structural, magnetic and dielectric modulus of manganese zinc nanoferrites." *Ceramics International* (2018).
- [89] Angadi, V. Jagadeesha, B. Rudraswamy, K. Sadhana, S. Ramana Murthy, and K. Praveena. "Effect of Sm<sup>3+</sup>–Gd<sup>3+</sup> on structural, electrical and magnetic properties of Mn–Zn ferrites synthesized via combustion route." *Journal of Alloys and Compounds* 656 (2016): 5-12.
- [90] G. Chandrasekaran, S. Selvanandan, and K. Manivannane. "Electrical and FTIR studies on Al substituted Mn–Zn mixed ferrites." *Journal of Materials Science: Materials in Electronics* 15, no. 1 (2004): 15-18.
- [91] Humaira Anwar, Asghari Maqsood, and I. H. Gul. "Effect of synthesis on structural and magnetic properties of cobalt doped Mn–Zn nano ferrites." *Journal of Alloys and Compounds* 626 (2015): 410-414.
- [92] I. Szczygieł, K. Winiarska, A. Bien'ko, K. Suracka, D. Gaworska-Koniarek, The effect of the sol–gel autocombustion synthesis conditions on the Mn–Zn ferrite magnetic properties, *Journal of Alloys and Compounds* 604 (2014) 1–7.
- [93] Abdulhadi Baykal, Sadik Guner, Ays\_e Demir, Synthesis and magneto-optical properties of triethylene glycol stabilized Mn<sub>1-x</sub>Zn<sub>x</sub>Fe<sub>2</sub>O<sub>4</sub> nanoparticles, *Journal of Alloys and Compounds* 619 (2015) 5–11.

- [94] Dzmitry Kotsikau, Maria Ivanovskaya, Vladimir Pankov, Yulia Fedotova, Structure and magnetic properties of manganese-zinc-ferrites prepared by spray pyrolysis method, *Solid State Sciences* 39 (2015) 69-73.
- [95] Mohamed Bakr Mohamed and Adel Maher Wahba. "Structural, magnetic, and elastic properties of nanocrystalline Al-substituted  $Mn_{0.5}Zn_{0.5}Fe_2O_4$  ferrite." *Ceramics International* 40, no. 8 (2014): 11773-11780.
- [96] C. F. Zhang, X. C. Zhong, H. Y. Yu, Z. W. Liu, and D. C. Zeng. "Effects of cobalt doping on the microstructure and magnetic properties of Mn–Zn ferrites prepared by the co-precipitation method." *Physica B: Condensed Matter* 404, no. 16 (2009): 2327-2331.
- [97] M. A. Gabal, A. M. Abdel-Daiem, Y. M. Al Angari, and I. M. Ismail. "Influence of Al-substitution on structural, electrical and magnetic properties of Mn–Zn ferrites nanopowders prepared via the sol–gel auto-combustion method." *Polyhedron* 57 (2013): 105-111.
- [98] Surender Kumar, Tukaram J. Shinde, and Pramod N. Vasambekar. "Study of conduction phenomena in indium substituted Mn–Zn nano-ferrites." *Journal of Magnetism and Magnetic Materials* 379 (2015): 179-185.
- [99] Naik, Pranav P., R. B. Tangsali, S. S. Meena, and S. M. Yusuf. "Influence of rare earth ( $Nd^{+3}$ ) doping on structural and magnetic properties of nanocrystalline manganese-zinc ferrite." *Materials Chemistry and Physics* 191 (2017): 215-224.
- [100] Yadav, Nisha, Ashok Kumar, Pawan S. Rana, Dinesh S. Rana, Manju Arora, and R. P. Pant. "Finite size effect on  $Sm^{3+}$  doped  $Mn_{0.5}Zn_{0.5}Sm_xFe_{2-x}O_4$  ( $0 \leq x \leq 0.5$ ) ferrite nanoparticles." *Ceramics International* 41, no. 7 (2015): 8623-8629.
- [101] Winiarska, Katarzyna, Irena Szczygieł, and Roman Klimkiewicz. "Manganese–zinc ferrite synthesis by the sol–gel autocombustion method. Effect of the precursor on the ferrite's catalytic properties." *Industrial & Engineering Chemistry Research* 52, no. 1 (2012): 353-361.
- [102] Raghvendra A. Bohara, Nanasaheb D. Throat, Akhilesh K. Chaurasia, Shivaji H. Pawar, Cancer cells extinction through magnetic fluid hyperthermia treatment produced by superparamagnetic Co-Zn ferrite nanoparticles, *RSC Advances* 5 (2015) 47225-47234.
- [103] K. E. Sapsford, W. R. Algar, L. Berti, K. B. Gemmill, B. J. Casey, E. Oh, M. H. Stewart, I. L. Medintz, Functionalizing nanoparticles with biological molecules:

developing chemistries that facilitate nanotechnology, *Chemical reviews* 113 (2013) 1904–2074.

[104] M. P. Monopoli, C. Aberg, A. Salvati, K. A. Dawson, Biomolecular coronas provide the biological identity of nanosized materials, *Nature nanotechnology* 7 (2012) 779–86.

[105] Ansar Ereath Beerana, Shaiju. S. Nazeerb, Francis Boniface Fernandezc, Krishna Surendra Muvvala, Wilfried Wunderlich, Sukumaran Anild, Sajith Vellappallye, Ramachandra Rao M.S., Annie Johnc, Ramapurath. S. Jayasreeb, Harikrishna Varma P R, An aqueous method for the controlled manganese ( $Mn^{2+}$ ) substitution in superparamagnetic iron oxide nanoparticle for contrast enhancement in MRI, *Physical Chemistry Chemical Physics* 17 (2015) 4609-4619.

[106] M. Mahmoudi, H. Hosseinkhani, M. Hosseinkhani, S. Boutry, A. Simchi, W. S. Journeay, K. Subramani, S. Laurent, Magnetic resonance imaging tracking of stem cells in vivo using iron oxide nanoparticles as a tool for the advancement of clinical regenerative medicine, *Chemical Reviews* 111 (2010) 253-280.

[107] U. Jeong, X. Teng, Y. Wang, H. Yang, Y. Xia, Superparamagnetic colloids: controlled synthesis and niche applications, *Advanced Materials* 19 (2007) 33-60.

[108] N. K. Verma, K. Crosbie-Staunton, A. Satti, S. Gallagher, K. B. Ryan, T. Doody, C. McAtamney, R. MacLoughlin, P. Galvin, C. S. Burke, Y. Volkov, Y. K. Gun'ko, Magnetic core-shell nanoparticles for drug delivery by nebulization, *Journal of nanobiotechnology* 11 (2013) 1.

[109] M. Guo, C. Que, C. Wang, X. Liu, H. Yan, K. Liu, Multifunctional superparamagnetic nanocarriers with folate-mediated and pH-responsive targeting properties for anticancer drug delivery, *Biomaterials* 32 (2011) 185-194.

[110] M. Creixell, A. C. Bohorquez, M. Torres-Lugo, C. Rinaldi, EGFR-targeted magnetic nanoparticle heaters kill cancer cells without a perceptible temperature rise, *ACS nano* 5 (2011) 7124-7129.

[111] A. Kaushik, R. Khan, P. R. Solanki, P. Pandey, J. Alam, S. Ahmad, B. D. Malhotra, Iron oxide nanoparticles–chitosan composite based glucose biosensor, *Biosensors and bioelectronics* 24 (2008) 676-683.

[112] H. B. Na, I. C. Song, T. Hyeon, Inorganic nanoparticles for MRI contrast agents, *Advanced materials* 21 (2009) 2133-2148.

[113] M Zahraei, M Marciello, A Lazaro-Carrillo, A Villanueva, F Herranz, M Talelli, R Costo, A Monshi, D Shahbazi-Gahrouei, M Amirnasr, B Behdadfar and M P Morales,

Versatile theranostics agents designed by coating ferrite nanoparticles with biocompatible polymers, *Nanotechnology* 27 (2016) 255702

[114] Hutchings, M. T., R. J. Birgeneau, and W. P. Wolf. "Magnetic Interactions between Rare-Earth Ions in Insulators. I. Accurate Electron-Paramagnetic-Resonance Determination of Gd<sup>3+</sup> Pair-Interaction Constants in LaCl<sub>3</sub>." *Physical Review* 168, no. 3 (1968): 1026.

[115] McDannald, A., L. Kuna, M. S. Seehra, and M. Jain. "Magnetic exchange interactions of rare-earth-substituted DyCrO<sub>3</sub> bulk powders." *Physical Review B* 91, no. 22 (2015): 224415.

[116] Chaudhari, Vivek, Sagar E. Shirsath, M. L. Mane, R. H. Kadam, S. B. Shelke, and D. R. Mane. "Crystallographic, magnetic and electrical properties of Ni<sub>0.5</sub>Cu<sub>0.25</sub>Zn<sub>0.25</sub>La<sub>x</sub>Fe<sub>2-x</sub>O<sub>4</sub> nanoparticles fabricated by sol-gel method." *Journal of Alloys and Compounds* 549 (2013): 213-220.

[117] Li, Qiaoling, Yongfei Wang, and Chuanbo Chang. "Study of Cu, Co, Mn and La doped NiZn ferrite nanorods synthesized by the coprecipitation method." *Journal of Alloys and Compounds* 505, no. 2 (2010): 523-526.

[118] Kumar, Pawan, S. K. Sharma, M. Knobel, and M. Singh. "Effect of La<sup>3+</sup> doping on the electric, dielectric and magnetic properties of cobalt ferrite processed by coprecipitation technique." *Journal of Alloys and Compounds* 508, no. 1 (2010): 115-118.

## Chapter- 2

[1]. Sakurai, Syoichi, Satoshi Sasaki, Maki Okube, Hiroki Ohara, and Takeshi Toyoda. "Cation distribution and valence state in Mn-Zn ferrite examined by synchrotron X-rays." *Physica B: Condensed Matter* 403, no. 19 (2008): 3589-3595.

[2]. Economos, George. "Magnetic ceramics: I, general methods of magnetic ferrite preparation." *Journal of the American Ceramic Society* 38, no. 7 (1955): 241-244.

[3]. Deshpande, C. E. "Recent developments in processing of Mn-Zn ferrites-An overview." *Indian Journal of Chemistry* 35A (1996) 353-365.

[4]. Murthy, S. R., and B. Ramaiah. "Elastic behavior of polycrystalline Mn-Zn ferrites." *Journal of materials science letters* 19, no. 8 (2000): 703-706.

[5]. Dislich, Helmut. "Sol-gel: science, processes and products." *Journal of non-crystalline solids* 80, no. 1-3 (1986): 115-121.

[6]. Brinker, C. Jeffrey. "Hydrolysis and condensation of silicates: effects on structure." *Journal of Non-Crystalline Solids* 100, no. 1-3 (1988): 31-50.

- [7]. Wu, Shen, Aizhi Sun, Wenhuan Xu, Qian Zhang, Fuqiang Zhai, Philip Logan, and Alex A. Volinsky. "Iron-based soft magnetic composites with Mn–Zn ferrite nanoparticles coating obtained by sol–gel method." *Journal of Magnetism and Magnetic Materials* 324, no. 22 (2012): 3899-3905.
- [8]. Habibi, Mohammad Hossein, and Amir Hossein Habibi. "Effect of the thermal treatment conditions on the formation of zinc ferrite nanocomposite, ZnFe<sub>2</sub>O<sub>4</sub>, by sol–gel method." *Journal of thermal analysis and calorimetry* 113, no. 2 (2013): 843-847.
- [9]. Sutka, Andris, and Gundars Mezinskis. "Sol-gel auto-combustion synthesis of spinel-type ferrite nanomaterials." *Frontiers of Materials Science* 6, no. 2 (2012): 128-141.
- [10]. Liu, Chung-Wen, Cheng-Hsiung Lin, and Yen-Pei Fu. "Mn–Zn Ferrite Powder Preparation by Hydrothermal Process from Used Dry Batteries." *Japanese journal of applied physics* 45, no. 5R (2006): 4040.
- [11]. Mostafa, Nasser Y., M. M. Hessien, and Abdallah A. Shaltout. "Hydrothermal synthesis and characterizations of Ti substituted Mn-ferrites." *Journal of Alloys and Compounds* 529 (2012): 29-33.
- [12]. Kumazawa, H., K. Oki, H-M. Cho, and E. Sada. "Hydrothermal synthesis of ultrafine ferrite particles." *Chemical Engineering Communications* 115, no. 1 (1992): 25-33.
- [13]. Ghone, Deepali M., V. L. Mathe, K. K. Patankar, and S. D. Kaushik. "Microstructure, lattice strain, magnetic and magnetostriction properties of holmium substituted cobalt ferrites obtained by co-precipitation method." *Journal of Alloys and Compounds* 739 (2018) 52-61.
- [14]. Kumar, Pawan, S. K. Sharma, M. Knobel, and M. Singh. "Effect of La<sup>3+</sup> doping on the electric, dielectric and magnetic properties of cobalt ferrite processed by co-precipitation technique." *Journal of Alloys and Compounds* 508, no. 1 (2010): 115-118.
- [15]. Joshi, Seema, Manoj Kumar, Sandeep Chhoker, Geetika Srivastava, Mukesh Jewariya, and V. N. Singh. "Structural, magnetic, dielectric and optical properties of nickel ferrite nanoparticles synthesized by co-precipitation method." *Journal of Molecular Structure* 1076 (2014): 55-62.
- [16]. Rahman, S., K. Nadeem, M. Anis-ur-Rehman, M. Mumtaz, S. Naeem, and I. Letofsky-Papst. "Structural and magnetic properties of ZnMg-ferrite nanoparticles prepared using the co-precipitation method." *Ceramics International* 39, no. 5 (2013): 5235-5239.

- [17]. Sharifi, Ibrahim, and H. Shokrollahi. "Structural, magnetic and Mössbauer evaluation of Mn substituted Co–Zn ferrite nanoparticles synthesized by co-precipitation." *Journal of Magnetism and Magnetic Materials* 334 (2013): 36-40.
- [18]. Cullity, Bernard Dennis. "Elements of X-ray Diffraction." (2001).
- [19]. Griffiths, Peter R., and James A. De Haseth. Fourier transform infrared spectrometry. Vol. 171. John Wiley & Sons, 2007.
- [20]. Brodusch, Nicolas, Demers, Hendrix, Gauvin, Reynald, Field Emission Scanning Electron Microscopy: New Perspectives for Materials Characterization, Springer (2018).
- [21]. Foner, Simon. "Versatile and sensitive vibrating-sample magnetometer." *Review of Scientific Instruments* 30, no. 7 (1959): 548-557.

### Chapter – 3

- [1] P. Hu, H.B. Yang, D.A. Pan, H. Wang, J.J. Tian, S.G. Zhang, X.F. Wang, A.A. Volinsky, Heat treatment effects on microstructure and magnetic properties of Mn–Zn ferrite powders, *Journal of Magnetism and Magnetic Materials* 322 (2010) 173–177.
- [2] G. Ott, J. Wrba, R. Lucke, Recent developments of Mn–Zn ferrites for high permeability applications, *Journal of Magnetism and Magnetic Materials* 254 (2003) 535-537.
- [3] U. Ghazanfar, S.A. Siddiqi, G. Abbas, Structural analysis of the Mn–Zn ferrites using XRD technique, *Materials Science and Engineering: B* 118 (2005) 84.
- [4] A. Thakur, P. Mathur, M. Singh, Study of dielectric behaviour of Mn–Zn nano ferrites, *Journal of Physics and Chemistry of solids* 68 (2007) 378–381.
- [5] S.J. Shukla, K.M. Jadhav, G.K. Bichile, Study of bulk magnetic properties of the mixed spinel  $MgCr_xFe_{2-x}O_4$ , *Indian Journal of Pure and Applied Physics* 39 (2001) 226.
- [6] M.I. Rosales, E. Amano, M.P. Cuautle, R. Valenzuela, Impedance spectroscopy studies of Ni–Zn ferrites, *Materials Science and Engineering: B* 49 (1997) 221.
- [7] J. Smit, H. P. J. Wijn, Ferrites John Wiley, New York, 1959.
- [8] P. Mathur, A. Thakur, M. Singh, Effect of nanoparticles on the magnetic properties of Mn–Zn soft ferrite, *Journal of Magnetism and Magnetic Materials* 320 (2008) 1364–1369.

- [9] E. R. kumar, R. Jayaprakash, M. S. Seehra, T. Prakash, S. Kumar, Effect of  $\alpha$ -Fe<sub>2</sub>O<sub>3</sub> phase on structural, magnetic and dielectric properties of Mn–Zn ferrite nanoparticles, *Journal of Physics and Chemistry of Solids* 74 (2013) 943–949.
- [10] J. Azadmanjiri, Preparation of Mn–Zn ferrite nanoparticles from chemical sol–gel combustion method and the magnetic properties after sintering, *Journal of Non-Crystalline Solids* 353 (2007) 4170–4173.
- [11] A. Thakur, M. Singh, Preparation and characterization of nanosize Mn<sub>0.4</sub>Zn<sub>0.6</sub>Fe<sub>2</sub>O<sub>4</sub> ferrite by citrate precursor method, *Ceramics International* 29 (2003) 505–511.
- [12] B.S. Chauhan, R. Kumar, K.M. Jadhav, M. Singh, Magnetic study of substituted Mg–Mn ferrites synthesized by citrate precursor method, *Journal of Magnetism and Magnetic Materials* 283 (2004) 71–81.
- [13] A. Verma, T.C. Goel, R.G. Mendiratta, Low temperature processing of NiZn ferrite by citrate precursor method and study of properties, *Materials science and technology* 16 (2000) 712–715.
- [14] R. Kumar, H. Kumar, R. R. Singh, P. B. Barman, Variation in magnetic and structural properties of Co-doped Ni–Zn ferrite nanoparticles: a different aspect, *Journal of Sol-Gel Science and Technology* 78 (2016) 566-575.
- [15] M.A.U. Rehman, M. A. Malik, M. Akram, K. Khan, A. Maqsood, Proficient magnesium nanoferrites: synthesis and characterization, *Physica Scripta* 83 (2011) 015602.
- [16] R. Kumar, H. Kumar, M. Kumar, R. R. Singh, P. B. Barman, Enhanced Saturation Magnetization in Cobalt Doped Ni-Zn Ferrite Nanoparticles, *Journal of Superconductivity and Novel Magnetism* 28 (2015) 3557-3564.
- [17] S. Thankachan, B. P. Jacob, S. Xavier, E. M. Mohammed, Effect of neodymium substitution on structural and magnetic properties of magnesium ferrite nanoparticles, *Physica Scripta* 87 (2013) 025701.
- [18] M. B. Mohamed, A. M. Wahba, Structural, magnetic and elastic properties of nanocrystalline Al-substituted Mn<sub>0.5</sub>Zn<sub>0.5</sub>Fe<sub>2</sub>O<sub>4</sub> ferrite, *Ceramics International* 40 (2014) 11773-11780.
- [19] K.A. Mohammed, A.D.A. Rawas, A.M.Gismelseed, A.Sellai, H.M.Widatallah, A.Yousif, M.E. Elzain, M.Shongwe, Infrared and structural studies of Mg<sub>1-x</sub>Zn<sub>x</sub>Fe<sub>2</sub>O<sub>4</sub> ferrites, *Physica B* 407 (2012) 795–804.

### Chapter - 4

- [1] P. Samoila, L. Sacarescu, A.I. Borhan, D. Timpu, M. Grigoras, N. Lupu, M. Zaltariov, V. Harabagiu, Magnetic properties of nanosized Gd doped Ni–Mn–Cr ferrites prepared using the sol–gel autocombustion technique, *Journal of Magnetism and Magnetic Materials* 378 (2015) 92–97.
- [2] G.Dixit, J.P. Singh, R.C. Srivastava, H.M. Agrawal, Magnetic resonance study of Ce and Gd doped NiFe<sub>2</sub>O<sub>4</sub> nanoparticles, *Journal of Magnetism and Magnetic Materials* 324 (2012) 479–483.
- [3] M.A. Iqbal, M.Islam, M.N.Ashiq, I. Ali, A. Iftikhar, H.M. Khan, Effect of Gd-substitution on physical and magnetic properties of Li<sub>1.2</sub>Mg<sub>0.4</sub>Gd<sub>x</sub>Fe<sub>(2-x)</sub>O<sub>4</sub> ferrites, *Journal of Alloys and Compounds* 579 (2013) 181–186.
- [4] P. Samoila, T. Slatineanu, P. Postolache, A.R. Iordan, M.N. Palamaru, The effect of chelating/combustion agent on catalytic activity and magnetic properties of Dy doped Ni–Zn ferrite, *Materials Chemistry and Physics* 136 (2012) 241–246.
- [5] A.I. Borhan, P. Samoila, V. Hulea, A.R. Iordan, M.N. Palamaru, Effect of Al<sup>3+</sup> substituted zinc ferrite on photocatalytic degradation of Orange I azo dye, *Journal of Photochemistry and Photobiology A: Chemistry* 279 (2014) 17–23.
- [6] I.Sharifi, H. Shokrollahi, S. Amiri, Ferrite-based magnetic nano fluids used in hyperthermia applications, *Journal of Magnetism and Magnetic Materials* 324 (2012) 903–915.
- [7] T.N. Brusentsova, V.D. Kuznetsov, Synthesis and investigation of magnetic properties of substituted ferrite nanoparticles of spinel system Mn<sub>1-x</sub>Zn<sub>x</sub>[Fe<sub>2-y</sub>Li<sub>y</sub>]O<sub>4</sub>, *Journal of Magnetism and Magnetic Materials* 311 (2007) 22–25.
- [8] Katarzyna Winiarska, Irena Szczygieł, and Roman Klimkiewicz, Manganese–zinc ferrite synthesis by the sol–gel autocombustion method. Effect of the precursor on the ferrite’s catalytic properties, *Industrial & Engineering Chemistry Research* 52 (2012) 353–361.
- [9] Alex. Goldman, Modern ferrite technology. Springer Science & Business Media, 2006.
- [10] J. Azadmanjiri, Preparation of Mn–Zn ferrite nanoparticles from chemical sol–gel combustion method and the magnetic properties after sintering, *Journal of Non-Crystalline Solids*, 353 (2007) 4170–4173.

- [11] H. Waqas, A. H. Qureshi, Low temperature sintering study of nanosized Mn–Zn ferrites synthesized by sol–gel autocombustion process, *Journal of thermal analysis and calorimetry* 100 (2010) 529-535.
- [12] I. Szczygiel, K. Winiarska, Low-temperature synthesis and characterization of the Mn–Zn ferrite, *Journal of thermal analysis and calorimetry* 104 (2011) 577-583.
- [13] A. C. F. M. Costa, V. J. Silva, C. C. Xin, D. A. Vieira, D. R. Cornejo, R. H. G. A. Kiminami, Effect of urea and glycine fuels on the combustion reaction synthesis of Mn–Zn ferrites: Evaluation of morphology and magnetic properties, *Journal of Alloys and Compounds* 495 (2010) 503-505.
- [14] R. V. Mangalaraja, S. Ananthakmar, P. Manohar, F. D. Gnanam, M. Awano, Characterization of  $Mn_{0.8}Zn_{0.2}Fe_2O_4$  synthesized by flash combustion technique, *Materials Science and Engineering: A* 367 (2004) 301-305.
- [15] R. Arulmurugan, G. Vaidyanathan, S. Sendhilnathan, B. Jeyadevan, Mn–Zn ferrite nanoparticles for ferrofluid preparation: Study on thermal–magnetic properties, *Journal of Magnetism and Magnetic Materials* 298 (2006) 83-94.
- [16] X. Cao, G. A. Liu, Y. M. Wang, J. H. Li, R. Y. Honga, Preparation of octahedral shaped  $Mn_{0.8}Zn_{0.2}Fe_2O_4$  ferrites via coprecipitation, *Journal of Alloys and Compounds* 497 (2010) L9-L12.
- [17] C. Rath, K. K. Sahu, S. Anand, S. K. Date, N. C. Mishra, R. P. Das, Preparation and characterization of nanosize Mn–Zn ferrite, *Journal of magnetism and magnetic materials* 202 (1999) 77-84.
- [18] L. Nalbandian, A. Delimitis, V. T. Zaspalis, E. A. Deliyanni, D. N. Bakoyannakis, E. N. Peleka, Hydrothermally prepared nanocrystalline Mn–Zn ferrites: Synthesis and characterization, *Microporous and Mesoporous Materials* 114 (2008) 465-473.
- [19] J. Wang, C. Zeng, Z. M. Peng, Q. W. Chen, Synthesis and magnetic properties of  $Zn_{1-x}Mn_xFe_2O_4$  nanoparticles, *Physica B: Condensed Matter* 349 (2004) 124-128.
- [20] D. S. Mathew, R. S. Juang, An overview of the structure and magnetism of spinel ferrite nanoparticles and their synthesis in microemulsions, *Chemical Engineering Journal* 129 (2007) 51-65.
- [21] S. Dasgupta, K. B. Kim, J. Ellrich, J. Eckert, I. Manna, Mechano-chemical synthesis and characterization of microstructure and magnetic properties of nanocrystalline  $Mn_{1-x}Zn_xFe_2O_4$ , *Journal of alloys and compounds* 424 (2006) 13-20.
- [22] Raghvendra Singh Yadav, Jaromir Havlica, Ivo Kuritka, Zuzana Kozakova, Eva Bartonickova, Jiri Masilko, Lukas Kalina, Jaromir Wasserbauer, Miroslava

Hajduchova, Vojtech Enev, Structural and Magnetic Properties of  $\text{CoFe}_{2-x}\text{Gd}_x\text{O}_4$  ( $0.0 \leq x \leq 0.1$ ) Spinel Ferrite Nanoparticles Synthesized by Starch-Assisted Sol–Gel Auto-combustion Method, *Journal of Superconductivity and Novel Magnetism* 28 (2015) 1797-1806.

[23] S. Nakayama, “LaFeO<sub>3</sub> perovskite-type oxide prepared by oxide-mixing, coprecipitation and complex synthesis methods” *Journal of materials science* 36 (2001) 5643 – 5648.

[24] P.K. Roy, J. Bera, “Enhancement of the magnetic properties of Ni–Cu–Zn ferrites with the substitution of a small fraction of lanthanum for iron” *Materials Research Bulletin* 42 (2007) 77–83.

[25] Atta ur Rahman, M.A.Rafiq, S.Karim, K.Maaz, M.Siddique, M.M.Hasan, “Reduced conductivity and enhancement of Debye orientational polarization in lanthanum doped cobalt ferrite nanoparticles” *Physica B* 406 (2011) 4393–4399.

[26] E. Rezlescu, N. Rezlescu, P.D. Popa, “Fine-grained MgCu ferrite with ionic substitutions used as humidity sensor” *Journal of Magnetism and Magnetic Materials* 290–291 (2005) 1001–1004.

[27] T. Kavetsky, O. Shpotyuk, M. Popescu, A. Lorinczi, F. Sava, FSDP-related correlations in chalcogenide glasses, *Journal of optoelectronics and advanced materials* 9 (2007) 3079-3081.

[28] Lijun Zhao, Hua Yang, Lianxiang Yu, Wei Sun, Yuming Cui, Yu Yan, Shouhua Feng, “Structure and magnetic properties of Ni<sub>0.7</sub>Mn<sub>0.3</sub>Fe<sub>2</sub>O<sub>4</sub> nanoparticles doped with La<sub>2</sub>O<sub>3</sub>” *physica status solidi (a)* 201.14 (2004): 3121-3128.

[29] A. A. Sattar, A. M. Samy, R. S. El-Ezza, and A. E. Eatah, “Effect of rare earth substitution on magnetic and electrical properties of Mn–Zn ferrites” *physica status solidi (a)* 193, No. 1, 86–93 (2002).

[30] Shahab Torkian, Ali Ghasemi, Reza Shoja Razavi, Structural and Magnetic Consequences of  $\text{Mn}_{0.6}\text{Zn}_{0.4}\text{Fe}_{2-x}\text{Gd}_x\text{O}_4$  Ferrite, *Journal of Superconductivity and Novel Magnetism* 29 (2016) 1617-1625.

[31] Mohamed Bakr Mohamed, Adel Maher Wahba, Structural, magnetic, and elastic properties of nanocrystalline Al-substituted  $\text{Mn}_{0.5}\text{Zn}_{0.5}\text{Fe}_2\text{O}_4$  ferrite, *Ceramics International* 40 (2014) 11773-11780.

[32] I. Szczygieł, K. Winiarska, A. Bien'ko, K. Suracka, D. Gaworska-Koniarek, The effect of the sol–gel autocombustion synthesis conditions on the Mn–Zn ferrite magnetic properties, *Journal of Alloys and Compounds* 604 (2014) 1–7.

- [33] Abdulhadi Baykal, Sadik Guner, Ays\_e Demir, Synthesis and magneto-optical properties of triethylene glycol stabilized  $Mn_{1-x}Zn_xFe_2O_4$  nanoparticles, *Journal of Alloys and Compounds* 619 (2015) 5–11.
- [34] Dzmitry Kotsikau, Maria Ivanovskaya, Vladimir Pankov, Yulia Fedotova, Structure and magnetic properties of manganese-zinc-ferrites prepared by spray pyrolysis method, *Solid State Sciences* 39 (2015) 69-73.
- [35] Ashok Kumar, Pawan S. Rana, M.S. Yadav, R.P. Pant, Effect of  $Gd^{3+}$  ion distribution on structural and magnetic properties in nano-sized Mn–Zn ferrite particles, *Ceramics International* 41(2015)1297–1302.

### **Chapter – 5**

- [1] P. Samoila, L. Sacarescu, A.I. Borhan, D. Timpu, M. Grigoras, N. Lupu, M. Zaltariov, V. Harabagiu, Magnetic properties of nanosized Gd doped Ni–Mn–Cr ferrites prepared using the sol–gel autocombustion technique, *Journal of Magnetism and Magnetic Materials* 378 (2015) 92-97.
- [2] Raghvendra Singh Yadav, Jaromir Havlica, Ivo Kuritka, Zuzana Kozakova, Eva Bartonickova, Jiri Masilko, Lukas Kalina, Jaromir Wasserbauer, Miroslava Hajduchova, Vojtech Enev, Structural and Magnetic Properties of  $CoFe_{2-x}Gd_xO_4$  ( $0.0 \leq x \leq 0.1$ ) Spinel Ferrite Nanoparticles Synthesized by Starch-Assisted Sol–Gel Auto-combustion Method, *Journal of Superconductivity and Novel Magnetism* 28 (2015) 1797-1806.
- [3] Seunghyun Sim, Daigo Miyajima, Tatsuya Niwa, Hideki Taguchi, Takuzo Aida, Tailoring Micrometer-Long High-Integrity 1D Array of Superparamagnetic Nanoparticles in a Nanotubular Protein Jacket and Its Lateral Magnetic Assembling Behavior, *Journal of the American Chemical Society* 137 (2015) 4658-4661.
- [4] Julie Bolley, Erwann Guenin, Nicole Lievre, Marc Lecouvey, Michael Soussan, Yoann Lalatonne, Laurence Motte, Carbodiimide versus click chemistry for nanoparticle surface functionalization: a comparative study for the elaboration of multimodal superparamagnetic nanoparticles targeting  $\alpha\beta3$  integrins, *Langmuir* 29 (2013) 14639-14647.
- [5] Sonia Gaba, Ashok Kumar, Pawan S. Rana, and Manju Arora. "Influence of  $La^{3+}$  ion doping on physical properties of magnesium nanoferrites for microwave absorption application." *Journal of Magnetism and Magnetic Materials* 460 (2018): 69-77.

- [6] Pranav P. Naik, R. B. Tangsali, S. S. Meena, and S. M. Yusuf. "Influence of rare earth ( $\text{Nd}^{3+}$ ) doping on structural and magnetic properties of nanocrystalline manganese-zinc ferrite." *Materials Chemistry and Physics* 191 (2017): 215-224.
- [7] Xiruo Zhao, Wei Wang, Yajun Zhang, Sizhu Wu, Feng Li, J. Ping Liu, Synthesis and characterization of gadolinium doped cobalt ferrite nanoparticles with enhanced adsorption capability for Congo Red, *Chemical Engineering Journal* 250 (2014) 164–174.
- [8] Gagan Dixit, Jitendra Pal Singh, R.C. Srivastava, H.M. Agrawal, Magnetic resonance study of Ce and Gd doped  $\text{NiFe}_2\text{O}_4$  nanoparticles, *Journal of Magnetism and Magnetic Materials* 324 (2012) 479–483.
- [9] Juan M. Rubio González, Carlos Otero Areán, X-Ray diffraction determination of the cation distribution and oxygen positional parameter in polycrystalline spinels, *Journal of the Chemical Society, Dalton Transactions* 10 (1985) 2155-2159.
- [10] K.A. Mohammed, A.D.Al-Rawas, A.M.Gismelseed, A.Sellai, H.M.Widatallah, A.Yousif, M.E. Elzain, M.Shongwe, Infrared and structural studies of  $\text{Mg}_{1-x}\text{Zn}_x\text{Fe}_2\text{O}_4$  ferrites, *Physica B* 407 (2012) 795–804.
- [11] H.M. Zaki, S.H. Al-Heniti, T.A. Elmosalami, Structural, magnetic and dielectric studies of copper substituted nano-crystalline spinel magnesium zinc ferrite, *Journal of Alloys and Compounds* 633 (2015) 104–114.
- [12] Gagan Kumar, Jyoti Shah, R.K. Kotnala, Virender Pratap Singh, Sarveena, Godawari Garg, Sagar E. Shirsath, Khalid M. Batoo, Mahavir Singh, Superparamagnetic behaviour and evidence of weakening in super-exchange interactions with the substitution of  $\text{Gd}^{3+}$  ions in the Mg–Mn nanoferrite matrix, *Materials Research Bulletin* 63 (2015) 216–225.
- [13] Dipali S. Nikam, Swati V. Jadhav, Vishwajeet M. Khot, R. A. Bohara, Chang K. Hong, Sawanta S. Mali, S. H. Pawar, Cation distribution, structural, morphological and magnetic properties of  $\text{Co}_{1-x}\text{Zn}_x\text{Fe}_2\text{O}_4$  ( $x= 0-1$ ) nanoparticles." *RSC Advances* 5 (2015) 2338-2345.
- [14] Vivek Chaudhari, Sagar E. Shirsath, M.L. Mane, R.H. Kadam, S.B. Shelke, D.R. Mane, Crystallographic, magnetic and electrical properties of  $\text{Ni}_{0.5}\text{Cu}_{0.25}\text{Zn}_{0.25}\text{La}_x\text{Fe}_{2-x}\text{O}_4$  nanoparticles fabricated by sol–gel method, *Journal of Alloys and Compounds* 549 (2013) 213–220.

- [15] Franco Jr, A., and M. S. Silva. "High temperature magnetic properties of magnesium ferrite nanoparticles." *Journal of Applied Physics* 109, no. 7 (2011): 07B505.
- [16] Ping Hu, Hai-boYang , De-anPan, HuaWang, Jian-junTian, Shen-genZhang, Xinfeng Wang, AlexA.Volinsky, Heat treatment effects on microstructure and magnetic properties of Mn–Zn ferrite powders, *Journal of magnetism and magnetic materials* 322 (2010) 173–177.
- [17] A. Chaudhuri, K. Mandal, Enhancement of ferromagnetic and dielectric properties of lanthanum doped bismuth ferrite nanostructures, *Materials Research Bulletin* 47 (2012) 1057–1061.
- [18] H. El Moussaoui, T. Mahfoud, M. Ben Ali, Z. Mahhouti, R. Masrour, M. Hamedoun, E. K. Hlil, and A. Benyoussef. "Experimental studies of neodymium ferrites doped with three different transition metals." *Materials Letters* 171 (2016): 142-145.
- [19] Q. A. Pankhurst, J. Connolly, S. K. Jones, J. J. Dobson, Applications of magnetic nanoparticles in biomedicine, *Journal of physics D: Applied Physics*, 36 (2003) R167.
- [20] Tobias Neuberger, Bernhard Schopf, Heinrich Hofmann, Margarete Hofmann, Brigitte von Rechenberg, Superparamagnetic nanoparticles for biomedical applications: possibilities and limitations of a new drug delivery system, *Journal of Magnetism and Magnetic Materials* 293 (2005) 483–496.
- [21] Andreas Jordan, Regina Scholz, Peter Wust, Horst Fahling, Roland Felix, Magnetic fluid hyperthermia (MFH): Cancer treatment with AC magnetic field induced excitation of biocompatible superparamagnetic nanoparticles, *Journal of Magnetism and Magnetic Materials* 201 (1999) 413-419.
- [22] Bin Liu, Dieter K. Weller, "Heat assisted magnetic recording film including superparamagnetic nanoparticles dispersed in an antiferromagnetic or ferrimagnetic matrix." U.S. Patent 7,158,346, issued January 2, 2007.
- [23] Andreas Moser, Kentaro Takano, David T Margulies, Manfred Albrecht, Yoshiaki Sonobe, Yoshihiro Ikeda, Shouheng Sun, Eric E Fullerton, Magnetic recording: advancing into the future, *Journal of Physics D: Applied Physics*, 35 (2002) R157.

